THE POWER SOURCE OF VERY LUMINOUS INFRARED GALAXIES

by

Lisa Marie Shier

A Dissertation Submitted to the Faculty of the

DEPARTMENT OF ASTRONOMY

In Partial Fulfillment of the Requirements
For the Degree of

DOCTOR OF PHILOSOPHY

In the Graduate College

THE UNIVERSITY OF ARIZONA

1995

THE UNIVERSITY OF ARIZONA
GRADUATE COLLEGE

As members of the Final Examination Committee, we certify that we have read the dissertation prepared by Lisa Marie Shier

entitled The Power Source of Very Luminous Infrared Galaxies

and recommend that it be accepted as fulfilling the dissertation requirement for the Degree of Doctor of Philosophy

John H. Black	1995 March 23 Date
Fulvio Melia	3/23/95 Date
Marcia J. Rieke	3/23/95 Date
	Date
	Date

Final approval and acceptance of this dissertation is contingent upon the candidate's submission of the final copy of the dissertation to the Graduate College.

I hereby certify that I have read this dissertation prepared under my direction and recommend that it be accepted as fulfilling the dissertation requirement.

Marcia J. Rieke — 3/27/95
Dissertation Director — Date
Marcia J. Rieke

STATEMENT BY AUTHOR

This dissertation has been submitted in partial fulfillment of requirements for an advanced degree at The University of Arizona and is deposited in the University Library to be made available to borrowers under rules of the Library.

Brief quotations from this dissertation are allowable without special permission, provided that accurate acknowledgment of source is made. Requests for permission for extended quotation from or reproduction of this manuscript in whole or in part may be granted by the head of the major department or the Dean of the Graduate College when in his or her judgment the proposed use of the material is in the interests of scholarship. In all other instances, however, permission must be obtained from the author.

SIGNED: Lisa M Sáiz

ACKNOWLEDGMENTS

Many people aided in the preparation of this dissertation. No dissertation may be completed without the guidance and advice of a faculty advisor. Marcia Rieke was the faculty advisor for this thesis. Hans-Walter Rix provided useful information on stellar dynamics and kinematic models of elliptical galaxies. John Black was a source of much useful information. The anonymous referee of the Astrophysical Journal Letters paper that became Chapter 5 wrote an exceptionally supportive and helpful report. George Rieke was tireless in the preparation of the Letters paper, and provided the stellar populations model used in Chapter 3. Bill Latter kindly obtained 0″.2 / pixel images of Zw 475.056. John Cocke was a guide through the maze of university regulations and offices. Peter Tamblyn and Crystal Martin provided useful tips on the use of online tools. Charles Liu was an excellent sounding board for ideas.

Funding for the instrumentation used in this project came from a variety of sources. NASA funded the development of the NICMOS3 arrays. FSpec was built with funds from the National Science Foundation. Zonta International, an association of professional women, provided funding for FSpec's high resolution diffraction grating. NASA, through the Graduate Student Researchers Program, provided three years of support.

DEDICATION

To my husband, David Michael Zielke

Contents

List of Figures

List of Tables

ABSTRACT

Seven very luminous galaxies were examined to determine the contribution of active nuclei to their luminosity, the nature of their stellar population, and the validity of previous measurements of their H_2 content. Spectra of the 2.3 μm bands of CO were used to measure the stellar velocity dispersion, and hence the mass in the central regions. The bolometric luminosity, ionizing continuum luminosity, CO index, and 2.2 μm luminosity were also determined.

Models of young stellar populations were compared to the observed properties of the galaxies. It was found that four of the seven galaxies have properties which are inconsistent with those of stellar populations. The active nuclei of these four galaxies produce more than half the total light of the galaxies, but less than one-third of the 2.2 μm light. The galaxies containing AGN also have young stellar populations. There is no evidence for the existence of active nuclei in the other three galaxies.

The stellar populations that dominate the starlight in the galaxies have a wide range of properties. Stellar populations range in age from 10 to 65 Myr. The timescale for star formation ranges from 5 Myr to 100 Myr. The local initial mass function is ruled out for one of the four galaxies for which stellar population analysis could be done.

The molecular gas masses for some very luminous galaxies determined from the ^{12}CO J=1$\rightarrow$0 line are in error. The previously determined molecular gas masses are larger than the dynamical masses. The I_{CO}/M_{H_2} conversion factor found for Milky Way giant molecular clouds is evidently not correct for some very luminous infrared galaxies.

Chapter 1

INTRODUCTION

1.1 Background

There exists a class of galaxies with very high bolometric luminosities and spectral energy distributions dominated by the far-infrared. Such galaxies are generally quite morphologically disturbed and contain large quantities of dust in their central regions. The nature of these galaxies, in particular their power source, stellar population, and molecular gas content is in dispute. New instrumentation and techniques have been used to explore the contents of seven very luminous infrared galaxies.

The very luminous galaxies are more important than their small space densities might suggest. Many galaxies may have been very luminous infrared galaxies at one time because the very luminous phase is short. A starburst cannot remain at high luminosity for more than about 10^8 years, due to limitations on the mass available for star formation. The very luminous phase is a time of rapid changes in the stellar population, morphology, and possibly nuclear activity of a galaxy. Very

luminous galaxies must become quiescent galaxies or active galactic nuclei (AGN). Hutchings & Neff (1991) suggest that some of the very luminous infrared galaxies take each evolutionary path.

Very luminous infrared galaxies are known to harbor different types of AGN, principally Seyfert 1 and Seyfert 2 nuclei. Under current AGN unification theories, the principle difference between Seyfert 1 and Seyfert 2 galaxies is the degree of obscuration of the nucleus, with the Seyfert 2 nuclei being the more heavily obscured (Antonucci 1993). The very luminous infrared galaxies have very high extinction generally and may harbor AGN so obscured that they are not even optically selected Seyfert 2 galaxies. Detecting such obscured AGN is very difficult, especially in the presence of a starburst which produces strong emission lines.

The principal observational signatures of Seyfert nuclei include a lack of stellar absorption features in the spectrum, hot dust emission in the 2 to 60 μm region of the spectrum, lack of silicate absorption at 10 μm, and X-ray emission. Many infrared galaxies with luminosities in excess of $2.5 \times 10^{11} L_{\odot}$ have not been found to have these signatures of Seyfert nuclei. However, a deeply buried Seyfert nucleus may not be visible in the well-studied optical part of the spectrum. A deeply buried AGN will have very strong far-infrared emission created by reprocessing by dust of the soft X-ray, ultraviolet, and optical emission of the central engine. Starbursts are also known to create strong far-infrared emission, so a large far-infrared flux alone is insufficient evidence to invoke the existence of an unseen AGN. Other possible observational signatures include very compact mid-infrared or radio emission, weak broad or high excitation emission lines, warm far-infrared colors, or hard X-ray emission.

The idea that very luminous infrared galaxies must evolve into optically

selected AGN was suggested by Sanders et al. (1988). Not all of the progenitors of luminous infrared galaxies need to contain an AGN. A mechanism by which massive starbursts may create supermassive black holes has been proposed (Norman & Scoville 1988). The large amounts of disk gas falling into the centers of the galaxies provide ample fuel for an AGN (Barnes & Hernquist 1991). The very luminous infrared galaxies destined to become optically selected AGN would contain luminous AGN in their infrared phase in the Sanders et al. (1988) scenario. Finding evidence for deeply buried AGN in very luminous galaxies that could evolve into Seyfert 2 galaxies like NGC 1068, and possibly later into Seyfert 1 galaxies would provide additional support for the Sanders et al. (1988) picture of AGN evolution.

Hard evidence for the ongoing creation of AGN and the link between AGN and merging galaxies would advance the state of knowledge of AGN evolution. Since galaxy merger rates are directly related to galaxy densities, the merger rate of large disk galaxies as a function of redshift is relatively easy to compute. A good estimate of the AGN birth rate could aid in resolving the current uncertainty over whether number evolution or luminosity evolution is most important in determining the evolution of the AGN luminosity function. It could also lead to an understanding of why the era of quasars was at a redshift of about 2.5, and not earlier or later in the history of the universe.

The stellar populations in many of the very luminous infrared galaxies are known to be quite different from those in the solar neighborhood. Such galaxies have very young stellar populations, and may have initial mass functions (IMF) unlike the local IMF, as was suggested for M 82 (Rieke et al. 1993). Detailed stellar population analysis allows the age, mass and star formation rate to be measured. Some limits may be placed on the IMF in very luminous infrared galaxies. NGC

1614 must have a stellar population with a higher proportion of high mass stars than is seen in local star forming regions. However, strong limits on the IMF in the other galaxies require reliable determinations of mass of the pre-starburst stellar population and non-stellar components. The maximal luminosities of starburst populations, and the range in star formation rates and mass fractions involved in star formation in massive starbursts may be determined. The variation of the star formation rate in merger induced star formation may be examined. Since merging gas-rich galaxies, including the very luminous infrared galaxies, are believed to produce elliptical galaxies (Toomre & Toomre 1972; Hernquist 1993), studies of the stellar population in very luminous infrared galaxies may shed light on the star formation history of elliptical galaxies. Since many of the very luminous galaxies do have AGN, and these may later become quite visible at many wavelengths, the nature of star formation in the very luminous infrared galaxies may provide information on the type of host galaxies that should be found around AGN at high redshift. Such information could aid in searches for these host galaxies, or show that high redshift AGN were created in a different manner than low redshift Seyfert galaxies.

^{12}CO J=1$\rightarrow$0 maps of very luminous galaxies made with interferometers suggest that many of these galaxy have large concentrations of gas near their centers. The amount of gas in the regions of strong ^{12}CO J=1$\rightarrow$0 emission has been determined using a conversion factor between the ^{12}CO J=1$\rightarrow$0 luminosity and H_2 mass determined from observations of Milky Way giant molecular clouds (Young & Scoville 1991). There have been challenges to the validity of this method for measuring the mass of molecular gas in the centers of very luminous infrared galaxies, where the state of the gas is quite different from that in local giant molecular clouds (Maloney & Black 1988; Aalto et al. 1991, 1994; Downes, Solomon

& Radford 1993). Measurements of the dynamical mass place an upper limit on the mass of the molecular gas. The dynamical mass has a large uncertainty, but it is shown in Chapter 2 to be free from large systematic errors. The comparison of the dynamical mass and the claimed H_2 mass allow the universality of the I_{CO}/M_{H_2} conversion factor to be tested.

1.2 Overview

New methods for addressing the existence of AGN in very luminous infrared galaxies, the nature of their stellar population and their molecular gas content are presented here. Searches for AGN, even in very dusty galaxies, generally rely on detecting emission from the central source. Other workers have looked for optical emission line ratios and far-infrared spectra energy distributions indicative of a non-thermal ultraviolet continuum (Armus, Heckman, & Miley 1989, Rowan-Robinson & Crawford 1989, Veilleux, et al. 1995), broad hydrogen recombination lines (Depoy, Becklin, & Geballe 1987), weak 2.3 μm CO bands (Ridgway et al. 1994), point radio sources (Lonsdale, Smith, & Lonsdale 1993), X-ray emission (Rieke 1988). The methods developed in Chapter 3 can detect an AGN that is not directly detectable at any wavelength, and determine the degree to which it contributes to the bolometric luminosity of the galaxy. Examination of the stellar population in galaxies has frequently relied on the details of the emission in the visible part of the spectrum. Such methods are unusable in the very luminous infrared galaxies due to their large and variable extinction. In Chapters 2 and 3 enough data are extracted from infrared observations, which are less affected by dust extinction than visible light observations, to determine the properties of the stellar populations of the galaxies. The methods used in Chapter 5 to examine

the molecular gas content of three very luminous infrared galaxies are particularly robust in that no assumptions must be made about the temperature, density or kinematics of the gas.

The power source of the very luminous infrared galaxies has been determined by comparing the properties of the galaxies to those of starburst populations models. These comparisons reveal what kind of stellar population, if any, has properties like those of a particular galaxy. The age, star formation rate, and possibly initial mass function (IMF) of the starburst population can be determined. In the cases where no stellar population model matches the properties of the galaxy, an active nucleus may be invoked The relative contributions of the starburst and AGN to the total and near-infrared light can be determined. In some galaxies with AGN, the properties of the stellar population can be determined as well.

Seven bright galaxies with bolometric luminosities in excess of 2.5×10^{11} $L_{\odot}$ were observed. Galaxies known to have strong Seyfert nuclei were excluded from the sample. The high dust content of very luminous infrared galaxies requires that observations at infrared wavelengths be used to study such galaxies. The properties of the galaxies that were compared to stellar population models are the mass, CO index, 2.2 μm luminosity, bolometric luminosity and ionizing continuum luminosity. Each galaxy mass was derived from measurements of the dispersion of the 2.3 μm overtone bands of CO. New techniques, based partially on traditional optical spectroscopic techniques, were developed and used for determining each galaxy's mass from the CO bands. These methods are detailed in Chapter 2. Near-infrared photometry provided the 2.2 μm luminosities. The determination of the bolometric and ionizing continuum luminosity was performed with the aid of previously published data.

The predictions of models of stellar populations were compared to the observed properties of the galaxies. The contribution of an AGN to the bolometric luminosity was determined for all seven galaxies. The models require the existence of an AGN in only four galaxies. Stellar populations with exponentially declining star formation rates were found to be consistent with the properties of some of the galaxies, while other galaxies seem to have had a very short burst of star formation. Ages of the stellar populations were found to range between 10 and 65 Myr. No single age or star formation rate was found which could produce the observed properties of all the stellar populations. The local IMF, as described by Basu & Rana (1992), is allowed for all but one of the galaxies in the sample if H_o = 75 km/s/Mpc. The mass-to-light ratio in NGC 1614 is incompatible with the local IMF.

The dynamical masses derived from the stellar velocity dispersions were compared to the molecular gas masses in three galaxies, as described in Chapter 5. It was found that the molecular gas masses claimed for these galaxies are too large, especially if the fraction of the mass that must be in the form of young stars is considered.

Chapter 2

OBSERVATIONS AND DATA REDUCTION

2.1 Introduction

New observations of seven luminous infrared galaxies were used to examine the power source, stellar population and molecular gas content of these galaxies. It is difficult to obtain information on the nature of infrared galaxies from optical observations because infrared galaxies generally contain large amounts of interstellar dust, which obscures their centers at visible wavelengths. Observations at near-infrared wavelengths are less affected by interstellar dust (Rieke & Lebofsky 1985). A combination of near-infrared spectroscopy and imaging provided the data necessary for the determination of the nuclear mass, CO index, and 2.2 μm luminosity.

The mass of a galaxy is generally determined by sampling the gravitational field of the galaxy. The velocities of any class of objects within the galaxy may

be used to determine the strength of the gravitational potential if the velocities of those objects are unaffected by nongravitational forces. In the centers of luminous infrared galaxies, supernovae, gas infall, and massive stellar winds are likely to affect the kinematics of the ionized gas, so the widths of optical and near-infrared emission lines may not be good indicators of the mass of a galaxy. In some merging galaxies, the gas and stars are known to have very different kinematics (Lake & Dressler 1986; Gaffney, Lester & Telesco 1993). However, the orbits of stars are not changed directly by gas dynamical processes. The masses derived here were obtained from stellar kinematics. The masses are computed for the central region of each galaxy.

The best near-infrared spectral lines for measuring stellar kinematics in galaxies are the 2.3 μm overtone bands of CO. These bands are the strongest absorption features in the near-infrared spectra of red giant and red supergiant stars (Kleinmann & Hall 1986), which dominate the near-infrared light of galaxies. The CO absorption bands are asymmetric, and have a sharp edge at the short wavelength end of the band which allows velocity information to be extracted from the band shape (Gaffney, Lester, & Telesco, 1993; Doyon et al. 1994; Gaffney, Lester, & Doppmann 1995). The nuclear velocity dispersion was measured for all six galaxies for which spectra were obtained. The small size of the galaxy nuclei (2-3″) did not permit a rotation curve to be determined.

Models of the kinematic structure of the galaxies were constructed which allowed the mass to be inferred from the velocity dispersion. The model galaxies included both kinematically hot and kinematically cold galaxies. All of the models have a length scale of the galaxy as a parameter. K band images were used to measure the scale radii of the galaxies.

The CO index is classically determined from filter photometry, but it may also be determined from high-resolution spectroscopy (Kleinmann & Hall 1986). The same spectra may be used for determinations of both the stellar velocity dispersion and the CO index. Measurements of the CO index are required for the selection of proper template stars for the determination of the velocity dispersion.

The absolute K magnitude is determined from the observed K magnitude and the distance. Corrections were made to the K magnitude to account for extinction and hot dust emission. The distance may be computed from the galaxy redshifts, after a value of the Hubble constant is chosen. The near-infrared colors of the galaxies were used to determine the amount of extinction and hot dust emission in the K band.

2.2 Sample

Seven galaxies were observed to investigate the nature of luminous infrared galaxies. All seven galaxies – NGC 1614, NGC 2623, NGC 3690, IC 694, NGC 6240, Arp 220 and Zw 475.056 – have bolometric luminosities in excess of $2.5 \times 10^{11} L_{\odot}$. Very luminous galaxies whose bolometric luminosity is obviously dominated by an active nucleus (Mrk 231, for example) were not observed. The observing techniques placed some constraints on the selection of galaxies to be observed. Galaxies with redshifts greater than 12,000 km/s were not observed because the redshifted CO bands of such objects fall in a region of strong telluric water absorption, making ground-based observations of their CO bands impractical. Galaxies below -10^{o} declination were also excluded from the sample since they may not be observed for long periods in Arizona. Galaxies with K fluxes below 15 mJy in a 5" aperture (NGC 695, for example) were excluded from the sample due to the excessive time

required to obtain a spectrum with sufficient signal-to-noise at Steward Observatory telescopes.

The galaxies in the sample all have disturbed morphologies and spectral energy distributions dominated by their far-infrared radiation. Arp 299 (NGC 3690 + IC 694) has several regions of intense star formation and NGC 6240 and Arp 220 have two nuclei each (Gehrz, Sramek, & Weedman 1983; Eales et al. 1990). Tidal tails or bridges may be seen in deep images of NGC 1614, NGC 2623 and IC 694.

Spectra and images were not obtained for all the galaxies in the sample due to weather problems. The only spectrum of Arp 220 created with FSpec data was of too low signal-to-noise to be used for determination of the velocity dispersion of this galaxy. Doyon et al. (1994) used methods similar to those described here to obtain a nuclear velocity dispersion of Arp 220, and their dispersion was used in the analysis of Arp 220. Spectra with sufficient signal-to-noise for cross-correlation analysis were obtained for the other six galaxies in the sample. Images were obtained for all galaxies except NGC 6240. Photometry and contour maps from the literature (Eales et al. 1990; Thronson et al. 1990; Zenner & Lenzen 1993) were used to derive the structure and 2.2 μm luminosity of this galaxy.

2.3 Observations

Spectroscopic observations were made at the Steward 2.3 m telescope on Kitt Peak with FSpec, a new near-infrared spectrometer (Williams et al. 1993). Table 2.1 lists the dates of the observations and the integration times of these observations. FSpec is a long-slit ($2''.4 \times 90''$) spectrometer with NICMOS3 HgCdTe detector array. In the high-resolution mode, FSpec has a resolving power of $\frac{\lambda}{\Delta\lambda} = 3700 = 80$ km/s. During observations of the galaxies, the telescope

was beam-switched at an interval of no more than four minutes so that the sky background could be monitored. The terrestrial absorption spectrum was sampled by observing a star of spectral type A V - G V every half hour. Stars of type K5 III - M2 III were observed as templates for cross-correlation.

The reduction of the spectra required several steps. Temporally adjacent images were subtracted to remove the terrestrial background emission and the dark current. Dome flats were used to flat-field the images. The spectrograph was set to the same wavelength when observing the flat-field screen as when observing the galaxies to minimize the effects of fringing. Before flat-fielding, the fringes have an amplitude of about 1%. The flat-fielding procedure described above reduces the amplitude of the fringes below the measurement errors of the flat-field frames. All of the images from each half hour between observations of the dwarf star were combined. A one dimensional spectrum was extracted from a 4″.8 wide section of the final image, thus the aperture size for all of the galaxy spectra is 2″.4 × 4″.8. The dwarf star spectra were reduced in a similar manner. The galaxy spectrum was then divided by the dwarf spectrum to remove terrestrial absorption effects. It was not possible calibrate the wavelength a scale of the spectra with atmospheric lines because there are no strong OH air glow lines in the region 2.27 μm $< \lambda <$ 2.34 μm. Xenon lamp spectra were used for the April and May 1993 data and NeKr lamp spectra for the later data for wavelength calibration. No attempt was made to flux-calibrate the spectra. Figures 2.1, 2.2, and 2.3 show the spectra of all the galaxies observed.

Near-infrared images were obtained at the Steward Observatory 2.3 telescope. A NICMOS3 camera (Rieke et al. 1993) was used. The filters and plate scales used are listed in Table 2.2. Two different filters were used for 2.2 μm imaging. The K filter has an effective wavelength of 2.22 μm and a width of 0.42 μm, while the K_s

Table 2.1: Log of Spectroscopic Observations

Galaxy	Date	Time
NGC 1614	9/30-10/1/93	4.2h
NGC 2623	3/29/94	2.6h
NGC 3690	4/2/93	1.1h
NGC 6240	3/31/93	1.4h
IC 694	5/8/93	2.1h
Zw 475.056	9/30-10/1/93	3h

Fig. 2.1.— Spectra of NGC 1614 and NGC 2623 Near 2.3 μm

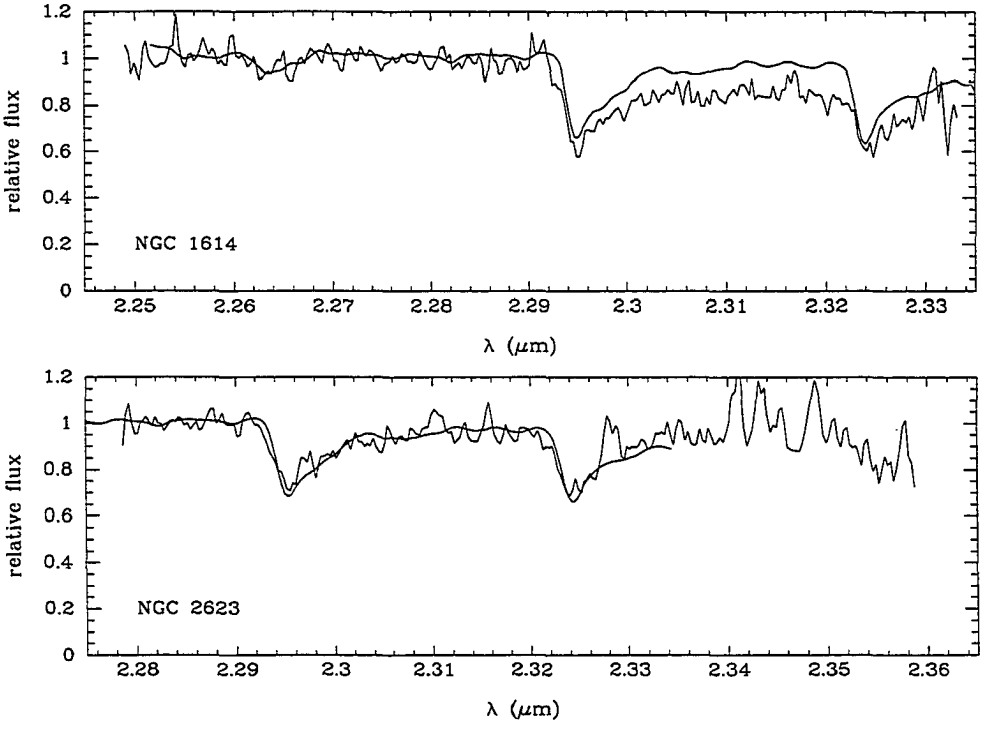

The spectra of NGC 1614 and NGC 2623 near the CO(2,0) band. Also shown is a spectrum of HR 7800 broadened by a Gaussian of the same width as the velocity dispersions listed in Table 2.5.

Fig. 2.2.— Spectra of NGC 3690 and NGC 6240 Near 2.3 μm

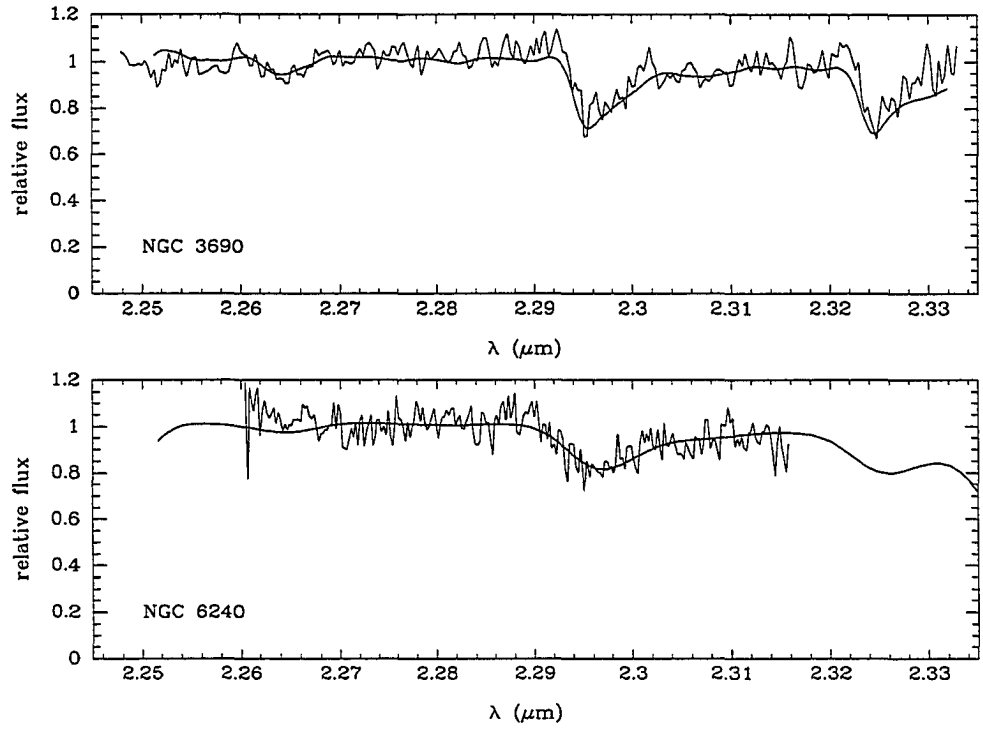

The spectra of NGC 3690 and NGC 6240 near the CO(2,0) band. Also shown is a spectrum of HR 7800 broadened by a Gaussian of the same width as the velocity dispersions listed in Table 2.5.

Fig. 2.3.— Spectra of IC 694 and Zw 475.056 Near 2.3 μm

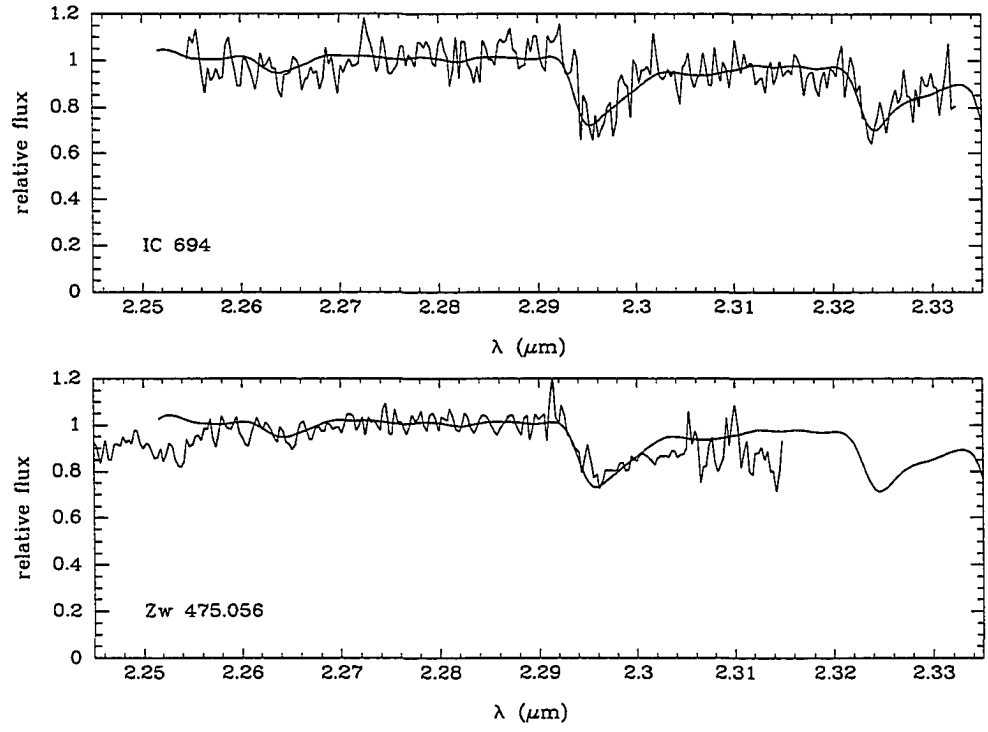

The spectra IC 694 and Zw 475.056 near the CO(2,0) band. Also shown is a spectrum of HR 7800 broadened by a Gaussian of the same width as the velocity dispersions listed in Table 2.5.

filter has an effective wavelength of 2.16 μm and a width of 0.3 μm. The telescope was beam-switched once per minute to monitor sky-brightness changes. Blank sky images were subtracted from galaxy images to remove the sky background and dark current. The data were flat-fielded with flats constructed from blank sky images. None of the imaging was done under photometric conditions. The aperture photometry of Carico et al. (1990) was used to calibrate the images of all the galaxies except NGC 3690 and IC 694 which were calibrated using photometry from Nakagawa et al. (1989). Figures 2.4 through 2.9 show contour maps of the K images.

2.4 CO index

The CO index is a measure of the strength of the 2.3 μm CO absorption bands. It provides information on the source of the 2.2 μm light. The CO index is largest in supergiant stars, especially cool supergiants. Giant stars have weaker CO bands than supergiants, and dwarf stars have the weakest CO bands of all. In galaxies, the CO index is sensitive to the red giant to red supergiant ratio. The spectrum of hot dust does not have CO absorption, so if a significant amount of the 2.3 μm light is emitted by hot dust, the CO index will be reduced. Synchrotron radiation

Table 2.2: Log of Photometric Observations

Galaxy	Date	Filters	Plate Scale
NGC 1614	11/4/92	J, H, K_s	0″.6/pixel
NGC 2623	3/17/92	J, H, K	0″.2/pixel
NGC 3690/IC 694	3/17/92	J, H, K	0″.2/pixel
Arp 220	3/17/92	J, H, K	0″.2/pixel
Zw 475.056	11/4/92	J, H, K_s	0″.6/pixel
Zw 475.056	10/28/93	K_s	0″.2/pixel

Fig. 2.4.— Contour Map of NGC 1614 at K_s Band

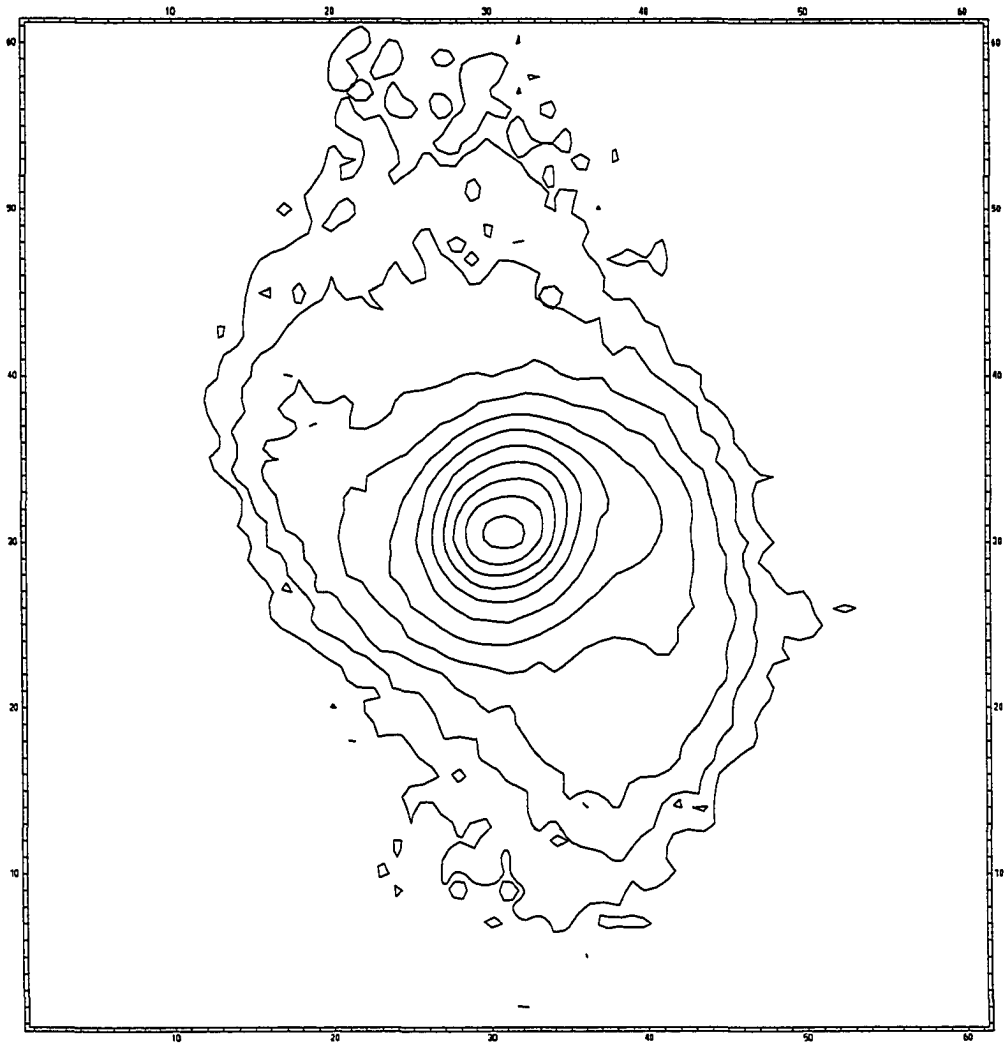

Contour map of μ_{K_s} in NGC 1614. North is at the top, east is to the left. This map is 40″ on a side. The lowest contour is at $\mu_{K_s} = 18$ mag/arcsec^2. The contour interval is 0.5 mag/arcsec^2. The brightest pixel is at 12.8 mag/arcsec^2.

Fig. 2.5.— Contour Map of NGC 2623 at K Band

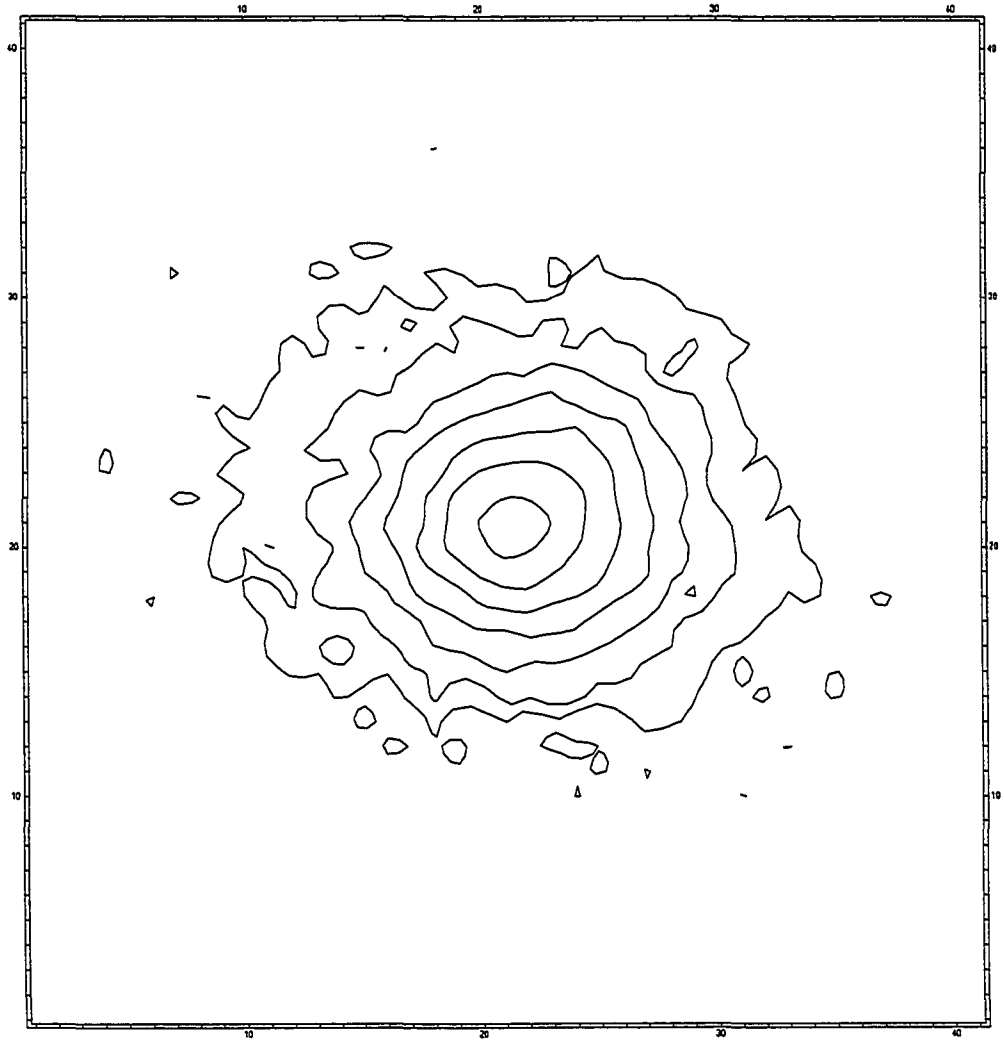

Contour map of μ_K in NGC 2623. North is at the top, east is to the left. This map is 10″ on a side. The lowest contour is at $\mu_K = 16$ mag/arcsec^2. The contour interval is 0.5 mag/arcsec^2. The brightest pixel is at 12.8 mag/arcsec^2.

Fig. 2.6.— Contour Map of NGC 3690 at K Band

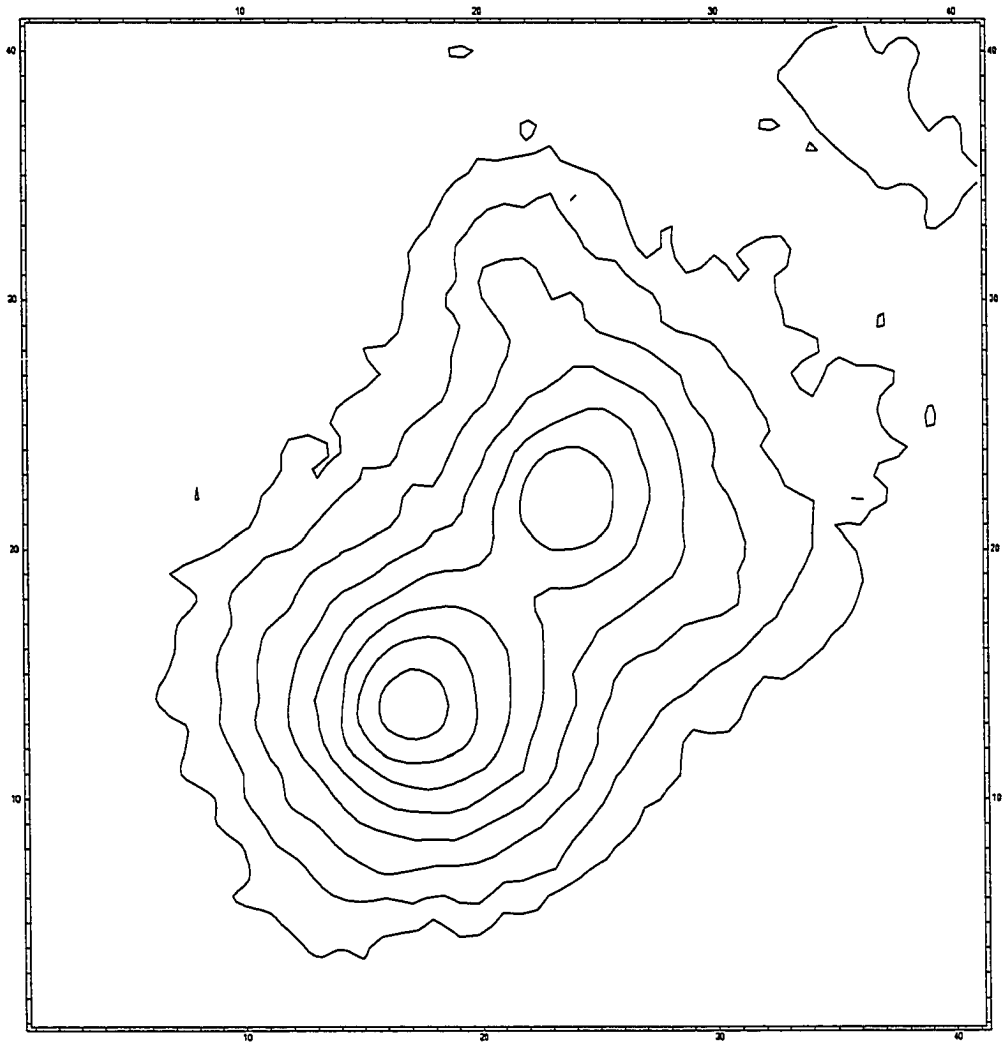

Contour map of μ_K in NGC 3690. North is at the top, east is to the left. The northern source is NGC 3690B_2 and the southern source is NGC 3690B_1. This map is 10″ on a side. The lowest contour is at μ_K = 16 mag/arcsec^2. The contour interval is 0.5 mag/arcsec^2. The brightest pixel is at 12.2 mag/arcsec^2.

Fig. 2.7.— Contour Map of IC 694 at K Band

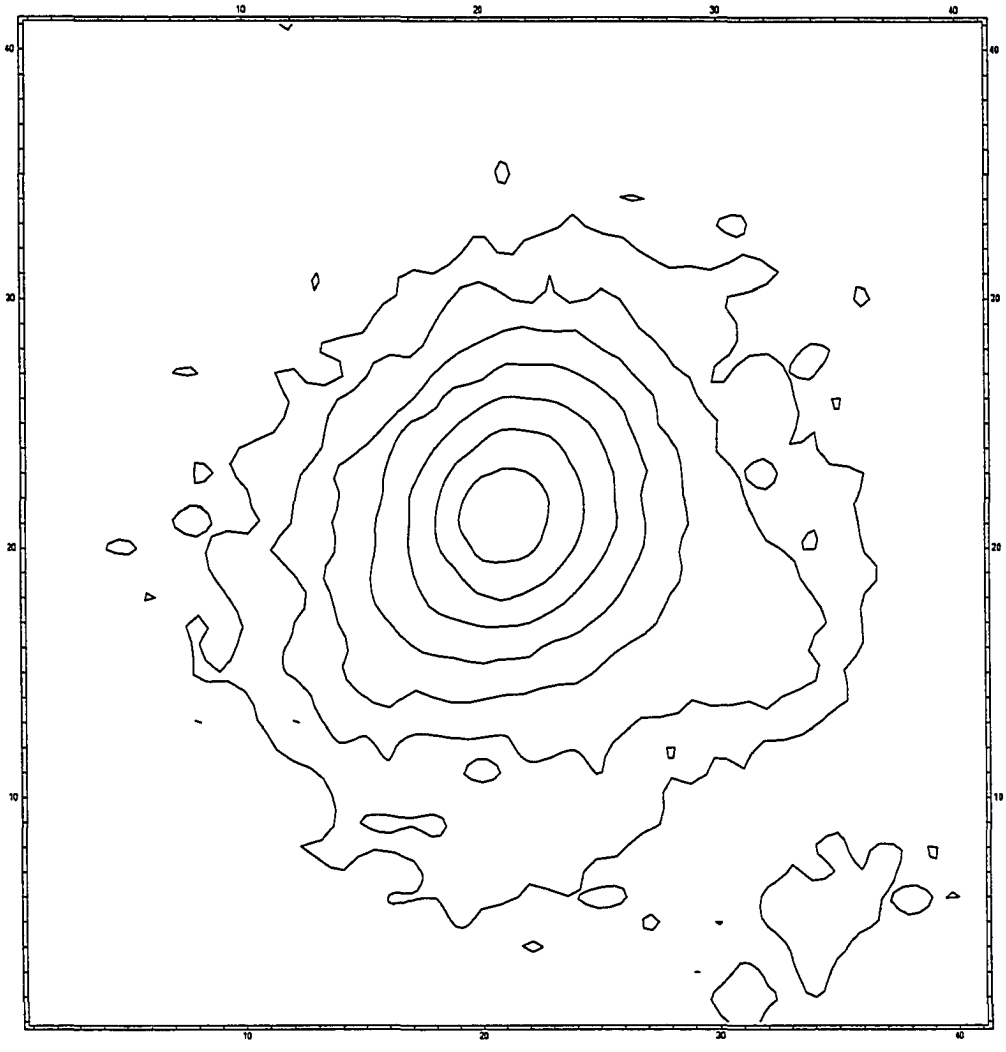

Contour map of μ_K in IC 694. North is at the top, east is to the left. This map is 10″ on a side. The lowest contour is at $\mu_K = 16$ mag/arcsec^2. The contour interval is 0.5 mag/arcsec^2. The brightest pixel is at 12.6 mag/arcsec^2.

Fig. 2.8.— Contour Map of Arp 220 at K Band

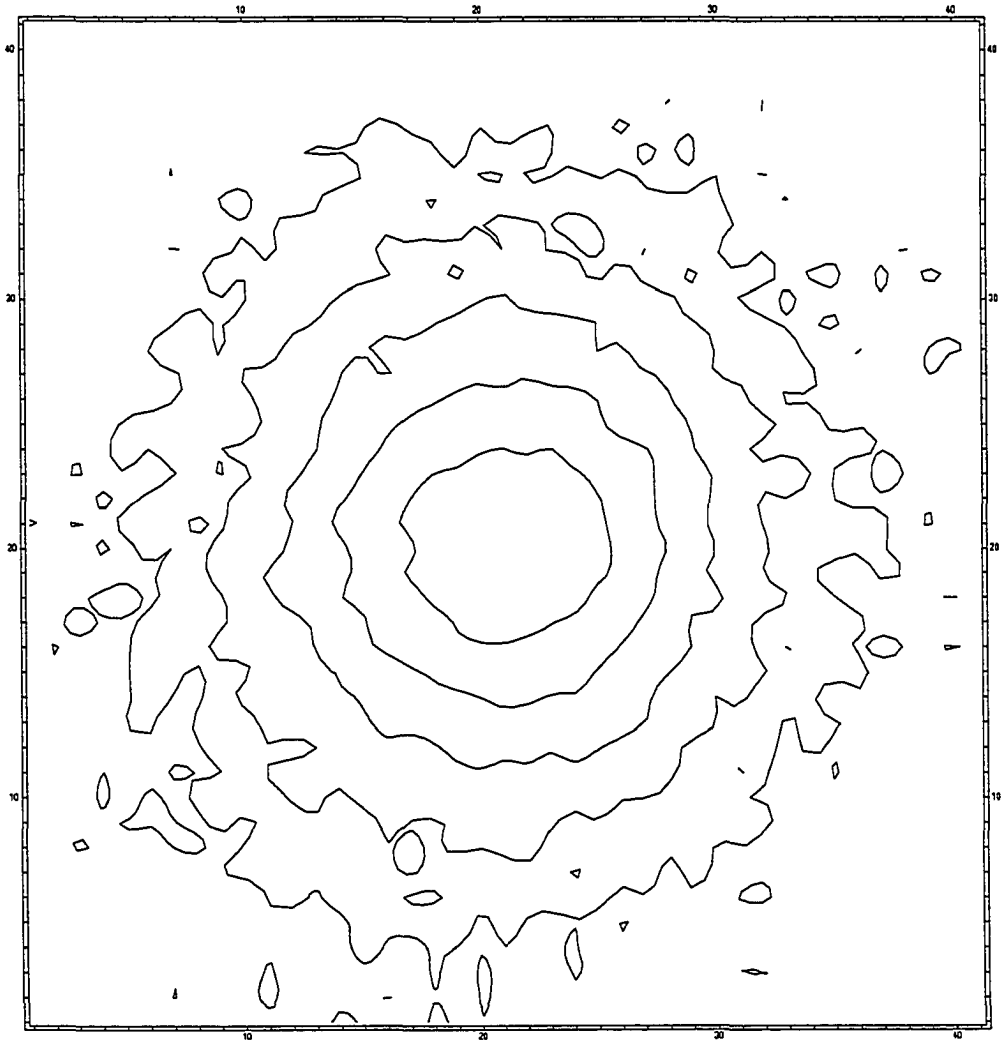

Contour map of μ_K in Arp 220. North at the top, east is to the left. This map is 10″ on a side. The lowest contour is at $\mu_K = 16$ mag/arcsec^2. The contour interval is 0.5 mag/arcsec^2. The brightest pixel is at 13.6 mag/arcsec^2.

Fig. 2.9.— Contour Map of Zw 475.056 at K_s Band

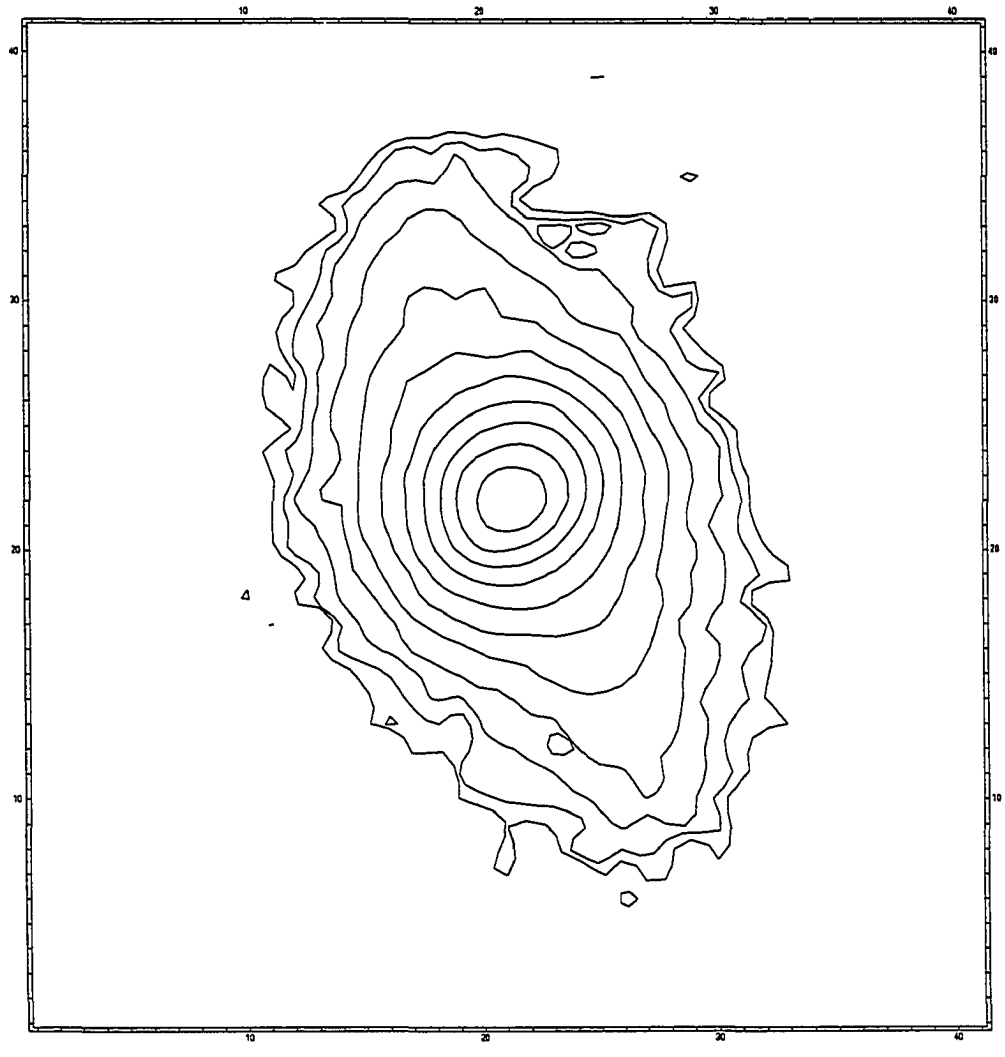

Contour map of μ_{K_s} in Zw 475.056. North is at the top, east is to the left. This map is 27″ on a side. The lowest contour is at $\mu_{K_s} = 19$ mag/arcsec^2. The contour interval is 0.5 mag/arcsec^2. The brightest pixel is at 13.6 mag/arcsec^2.

likewise does not have any features at 2.3 μm, and will reduce the CO index if present.

The CO index as originally defined (Frogel et al. 1978) is the difference, in magnitudes, between the flux density in two narrow filters, one at 2.22 μm and the other centered in the region of strong absorption by CO around 2.3 μm. A spectroscopic CO index was defined by Kleinmann & Hall (1986) for their Fourier transform spectra of bright red stars. This spectroscopic CO index samples two regions, one in the continuum shortward of the CO(2,0) bandhead at 2.293 μm, and one in the deepest part of the CO(2,0) band. A conversion between the spectroscopic CO index and the photometric CO index was computed by Kleinmann & Hall (1986). Doyon et al. (1994) defined a different spectroscopic CO index which is based on the flux between 2.31 and 2.4 μm. The Doyon et al. (1994) spectroscopic CO index was not used on the FSpec spectra because the spectra have insufficient spectral coverage.

The Kleinmann & Hall (1986) method was used to measure the CO index of all the galaxies and template stars. The spectroscopic CO index is slightly affected by line broadening due to the velocity dispersion of the galaxies. A correction for velocity dispersion was calculated and applied to all of the galaxy CO indices. The spectroscopic CO indices were converted to photometric CO indices so that they could be compared with the models in Chapter 3. The CO indices for all the galaxies is presented in Table 2.3. Ridgway et al. (1994) used the Doyon et al. (1994) method to measure the CO indices of six of the galaxies in the sample. Their CO indices agree with the CO indices derived from the FSpec spectra. The CO index after correction for hot dust emission as described in Section 2.5 is also listed in Table 2.3.

2.5 Absolute K Magnitude

The 2.2 μm luminosity is an important constraint on the stellar populations models described in Chapter 3. The observed K magnitude is not sufficient to determine the 2.2 μm luminosity of the stars. Neglecting extinction can cause the 2.2 μm luminosity of the stars to be underestimated. The 2.2 μm luminosity of the stars could be overestimated if non-stellar emission, e.g. thermal radiation from hot dust or synchrotron radiation, is not subtracted from the observed K band flux density. J-H and H-K colors were used to calculate the amount of extinction and non-stellar emission in the K band.

J, H, and K or K_s magnitudes were determined for the starburst region of each galaxy. The starburst region of the galaxies was determined to be the central kiloparsec for all of the galaxies in the sample except NGC 3690, as described in Section 3.2.1. NGC 3690 has two bright condensations in the center, (B_1 and B_2) separated by 2.4" = 450 pc. B_1 is the brighter of the pair at 2.2 μm and lies to the south of B_2. The colors of NGC 3690 B_1 and B_2 were measured separately through a 2.4" = 450 pc aperture. The photometry of Zw 475.056 was derived from analysis of the 0".6 / pixel images. The near- infrared photometry of Thronson et al. (1990) was used to determine the colors and K magnitude of the central 1 kpc region of NGC 6240. It was assumed that the flux aperture relation is a power law and the J, H, and K magnitudes were obtained through interpolation. The K magnitudes and colors of the galaxies are listed in Table 2.4 and plotted in Figures 2.10 and 2.11.

The observed color of a galaxy depends on the amount and distribution of interstellar dust. Two models for the distribution of stars and dust were examined. The first model is the foreground screen model, in which it is assumed that the

Table 2.3: CO Index

Galaxy	Observed CO Index	Corrected CO Index
NGC 1614	0.20 ± 0.01	0.24
NGC 2623	0.145 ± 0.005	0.17
NGC 3690B_1	0.18 ± 0.01[a]	0.24
NGC 3690B_2	0.18 ± 0.01[a]	0.24
NGC 6240	0.22 ± 0.02	0.22
IC 694	0.20 ± 0.02	0.23
Arp 220	0.20 ± 0.05[b]	0.21
Zw 475.056	0.15 ± 0.01	0.17

[a]CO index of composite spectrum

[b]Rieke et al. 1985

Table 2.4: Near Infrared Photometry

Galaxy	Distance Mpc	K	J-H	H-K	% Dust[a]	A_V	M_K[b]
NGC 1614	63	10.87	1.14	0.68	15	4.9	-23.5
NGC 2623	74	12.14	1.16	0.67	16	3.8	-22.4
NGC 3690 B_1	41	11.83	1.14	1.08	23	8.8	-22.0
NGC 3690 B_2	41	11.96	0.88	0.32	0	1.2	-21.3
NGC 6240	97	11.48[c]	1.46[c]	0.52[c]	0	4.4	-24.0
IC 694	41	11.13	1.11	0.68	11	4.6	-22.3
Arp 220	73	11.94	1.34	0.71	6	6.4	-23.0
Zw 475.056	110	13.30	0.78	0.33	9	0.3	-21.8

[a]maximum possible contribution of dust to 2.2 μm flux

[b]absolute magnitude of stellar component

[c]see text

dust lies in a uniform screen in front of all the stars. The second model assumes a uniform mixture of dust and stars in a spherical galaxy of the type described in Section 2.6.1. The intrinsic colors of the stellar population were taken to be: J-H=0.75, H-K=0.24, and H-K_s=0.21. Changes of 0.04 magnitudes in the assumed H-K colors affect the calculated stellar bolometric luminosity by less than 0.1 magnitudes. The reddening law of Rieke & Lebofsky (1985) was used to compute the colors for the model distributions. Colors of galaxies with both model dust distributions are plotted in Figures 2.10 and 2.11. Extinction corrections based on the H-K color are not particularly sensitive to the dust distribution model. As Figure 2.12 shows, the effective extinction, defined as

$$A_K(\text{effective}) = -2.5 \log_{10} \left(\frac{\text{f}_\nu(\text{K})}{\text{f}_\nu(\text{K, no extinction})} \right), \qquad (2.1)$$

is not much different for the screen model and the uniform mix model at the same H-K color. The use of the foreground screen model may cause estimates of the stellar 2.2 μm luminosity to be slightly too small.

The luminosity sources contributing to the near-infrared continua of the very luminous infrared galaxies may include stars, hot dust and synchrotron radiation. The amount of non-stellar emission seen in the near-infrared affects not only the near-infrared colors, but also the CO index. Accurate calculation of the 2.2 μm luminosity of the stars requires that the fraction of the 2.2 μm flux attributable to non-stellar sources be determined. The corrections to the colors and CO indices of the stellar populations galaxies were computed with the assumption that the observed fluxes were a mixture of reddened starlight and either emission from 750 K dust or synchrotron emission with $f_\nu \sim \nu^{-0.85}$. Examination of the spectral energy distributions of Seyfert 1 galaxies show that they often have a non-thermal component with an index of 0.6 to 1.3 (Rieke 1978, McAlary & Rieke 1988). The

Fig. 2.10.— J-H and H-K Colors of Galaxies and Dust Models

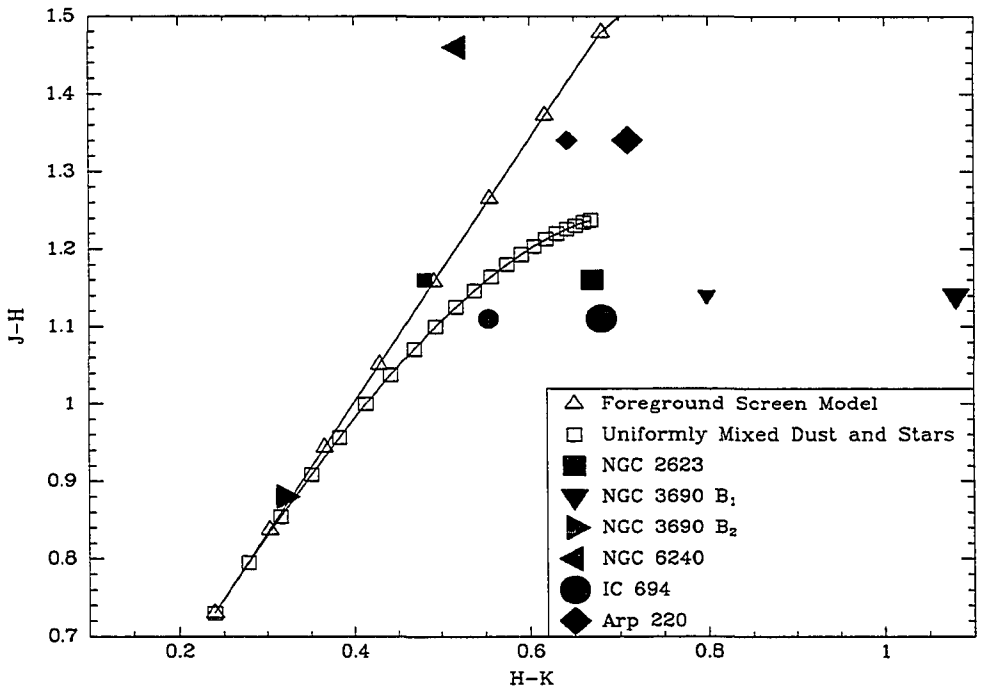

J-H and H-K colors of the galaxies and two dust distribution models. Symbols on the tracks for the dust models are plotted every A_V(center)=1 for A_V(center) = 0 to 20. The large solid symbols are the observed colors of the galaxies. The small solid symbols are the colors of the galaxies after hot dust emission (750 K) has been removed as described in the text.

Fig. 2.11.— J-H and H-K_s Colors of Galaxies and Dust Models

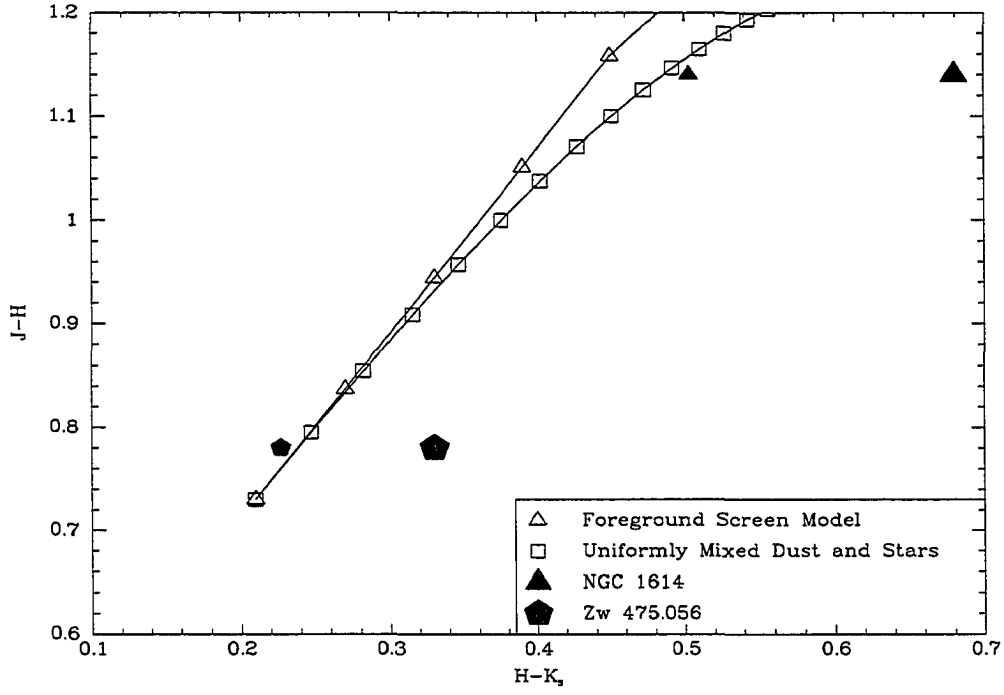

J-H and H-K colors of the galaxies and two dust distribution models. Symbols on the tracks for the dust models are plotted every A_V(center)=1 for A_V(center) = 0 to 20. The large solid symbols are the observed colors of the galaxies. The small solid symbols are the colors of the galaxies after hot dust emission (750 K) has been removed as described in the text.

Fig. 2.12.— H-K Colors of Models and Effective Extinction

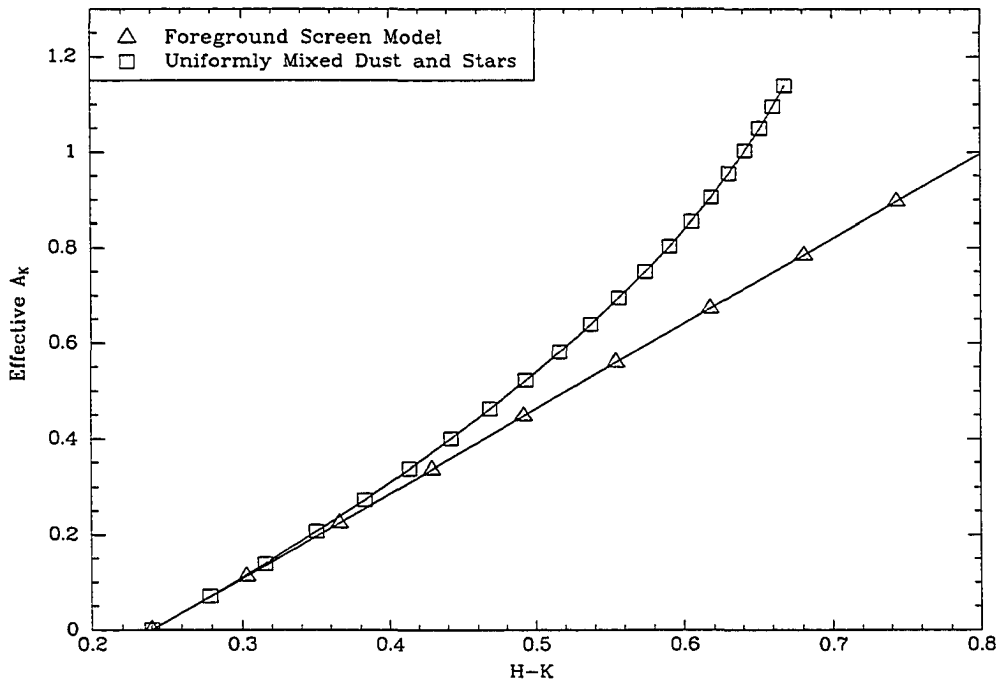

The effective extinction at K as a function of H-K color for the two dust distribution models. Symbols on the tracks for the dust models are plotted every A_V(center)=1 for A_V(center) = 0 to 20. Two model galaxies with the same H-K color but different dust distributions have similar effective extinctions even though the extinction to the center of the galaxy may be very different.

non-stellar source of emission was assumed to lie behind a screen of dust with $A_V = 10$. A mixture of stars and hot dust is a better fit to the colors of the galaxies than mixtures of stars and synchrotron radiation. An upper limit to the amount of 2.2 μm emission from hot dust was set by requiring that the corrected CO index for the stellar population not exceed 0.24. The starburst models in Chapter 3 models generally have a CO index no greater than 0.24. The correction for hot dust emission was never permitted to be larger than the amount required to place the galaxy on the foreground screen reddening curve for a stellar population. The nuclear K-L colors of NGC 3690 B_1, NGC 3690 B_2, NGC 6240, IC 694 and Arp 220 were measured by Zhou, Wynn-Williams, & Sanders (1993). The K-L color of the stars and hot dust was computed, assuming that the intrinsic K-L color of the stars is 0.20. The amount of hot dust emission was required to be small enough that the K-L color of the stars and hot dust was no redder than the observed nuclear K-L color. Nuclear 10 μm fluxes for NGC 1614, NGC 2623, and NGC 6240 and Arp 220 were measured by Wynn-Williams & Becklin (1993). The observed 10 μm flux density of the galaxies was always more than the 10 μm flux predicted on the basis of the hot dust emission seen at 2.3 μm. The corrected colors of the stellar populations in the galaxies have been plotted in Figures 2.10 and 2.11. Both NGC 3690 B_1 and NGC 3690 B_2 lie in the spectroscopic aperture for NGC 3690 and the spatial resolution is insufficient to separate them, so it is not possible to determine the CO index of the sources separately. It was assumed that each source has the same CO index.

The K band flux was corrected for distance, hot dust emission, and extinction to obtain the 2.2 μm luminosity of the stars. The distances were obtained from the redshifts of the galaxies, assuming $H_o = 75$ km/s/Mpc. The hot dust emission corrections were set such that the corrected CO index of the stellar population is

0.24, or the corrected colors of the galaxy lie on the foreground screen reddening curve, whichever requires less hot dust emission. The extinction was determined from the H-K color of the galaxy after the hot dust correction was made. The foreground screen model was used to make the extinction corrections. The absolute K magnitudes of each galaxy's stellar populations are listed in Table 2.4. The corrected CO indices are given in Table 2.3.

2.6 Nuclear Masses

The relationship between the aperture velocity dispersion and the nuclear mass depends on the kinematic and density structure of a galaxy. It is not obvious whether the nuclei of luminous infrared galaxies most closely resemble kinematically hot spherical systems or kinematically cold disk systems. Three independent lines of reasoning suggest that a kinematically hot model is appropriate for the centers of the galaxies: the centers of spiral galaxies are often dominated by kinematically hot bulges, numerical simulations of merging galaxies produce remnants that are much like elliptical galaxies (Toomre & Toomre 1972; Hernquist 1993), and the light profiles of all but the very disturbed galaxies in the sample are better fit by an $r^{1/4}$ law than by an exponential law. However, a disk model may be a better description of the young stars with strong CO lines than a spherical model. The young stars are born in the gas which falls to the center the luminous infrared galaxies and settles into a ring configuration (Barnes & Hernquist 1991). Therefore, the mass-aperture dispersion relation has been calculated for both spherical and disk systems. The effects of extinction and radially dependent mass-to-light ratios are considered in Section 2.6.6, and found to be negligible.

2.6.1 Spherical Models

For the spherical models, the galaxy is assumed to have no rotation and an isotropic velocity tensor. In such a system, the hydrostatic equilibrium equation becomes

$$\frac{d(\rho\sigma_{los}^2)}{dr} = -\rho\frac{d\Phi}{dr}, \tag{2.2}$$

where ρ is the mass density, σ_{los}^2 is the one-dimensional velocity dispersion and Φ is the gravitational potential (Binney & Tremaine 1990). An integral form of Equation 2.2 is

$$\sigma_{los}^2(r) = \frac{G}{\rho(r)}\int_r^\infty \frac{M(r)\rho(r)dr}{r^2}. \tag{2.3}$$

Stars at many different radii contribute to the observed spectrum of a galaxy. The velocity dispersion measured from the spectrum is an average of the dispersions in the volume included in the aperture of the spectrograph. This average of the velocity dispersions is weighted by the flux detected from each volume element. The observed 2.3 μm flux is a function of the density, ρ, mass-to-2.3 μm luminosity ratio, γ, and extinction along the line-of-sight, $e^{-\tau}$. If scattering of light by seeing is neglected, the observed velocity dispersion is given by

$$\sigma_a^2 = \frac{\int_a \sigma_{los}^2(r)\rho/\gamma e^{-\tau}dV}{\int_a \rho/\gamma e^{-\tau}dV}. \tag{2.4}$$

The integrals in Equation 2.4 are volume integrals that run over the portion of the galaxy seen through the spectroscopic aperture. For the spectra presented in Section 2.3 the integral runs over the volume described by

$$-2.4/206265 \times \mathrm{D} \leq \quad x \quad \leq 2.4/206265 \times \mathrm{D} \tag{2.5}$$

$$-1.2/206265 \times \mathrm{D} \leq \quad y \quad \leq 1.2/206265 \times \mathrm{D} \tag{2.6}$$

$$-\infty < \quad z \quad < \infty \tag{2.7}$$

where the origin of the coordinate system is at the center of the galaxy, and D is the distance to the galaxy.

The mass density distributions in the spherical models are taken from the analytic η-models of Tremaine et al. (1994). These models have central density cusps of variable strength described by the parameter η. Only two of the η-models are considered here: the $\eta = 3$ model, in which the density tends to a constant value at small radii, and the $\eta = 2$ model, where $\rho \sim 1/r$ at small radii. To describe the density in physical units, it necessary to introduce a second parameter, the scale radius, r_s. The scale radius describes the physical size of the model galaxy and the radius where the density power law changes. The mass density in the η-models may be written in physical units as

$$\rho(r) = \frac{\rho_o}{(r/r_s)^{\eta-3}(1+r/r_s)^{\eta+1}}. \tag{2.8}$$

The mass interior to a radius r is given by

$$M(r) = \frac{r_s\sigma_a^2}{G}\frac{(r/r_s)^\eta}{(1+r/r_s)^\eta}\frac{\int_a \rho/\gamma e^{-\tau}dV}{\int_a \bar{v^2}_{r,\eta}(r)\rho/\gamma e^{-\tau}dV}, \tag{2.9}$$

where $\bar{v^2}_{r,\eta}(r)$ is the dimensionless velocity dispersion calculated by Tremaine et al. (1994). The relationship between the dimensionless velocity dispersion and the velocity dispersion in physical units is given by

$$\bar{v^2}_{r,\eta}(r) = GM_T/r_s\sigma(r), \tag{2.10}$$

where M_T is the total mass of the galaxy. A normalized form of $\sigma(r)$ is shown in Figure 2.13 for $\eta = 2$ and $\eta = 3$.

In the case of no extinction, and a constant mass-to-light ratio, the mass-aperture dispersion of the $\eta = 3$ model reduces to

$$M(r) = \frac{r_s\sigma_a^2}{G}\frac{(r/r_s)^3}{(1+r/r_s)^3}\frac{\int_a(1+2/r_s)^{-4}dV}{\int_a \frac{6r/r_s+1}{30(1+r/r_s)^6}dV}. \tag{2.11}$$

Fig. 2.13.— Normalized Velocity Dispersions for $\eta = 2$ and $\eta = 3$

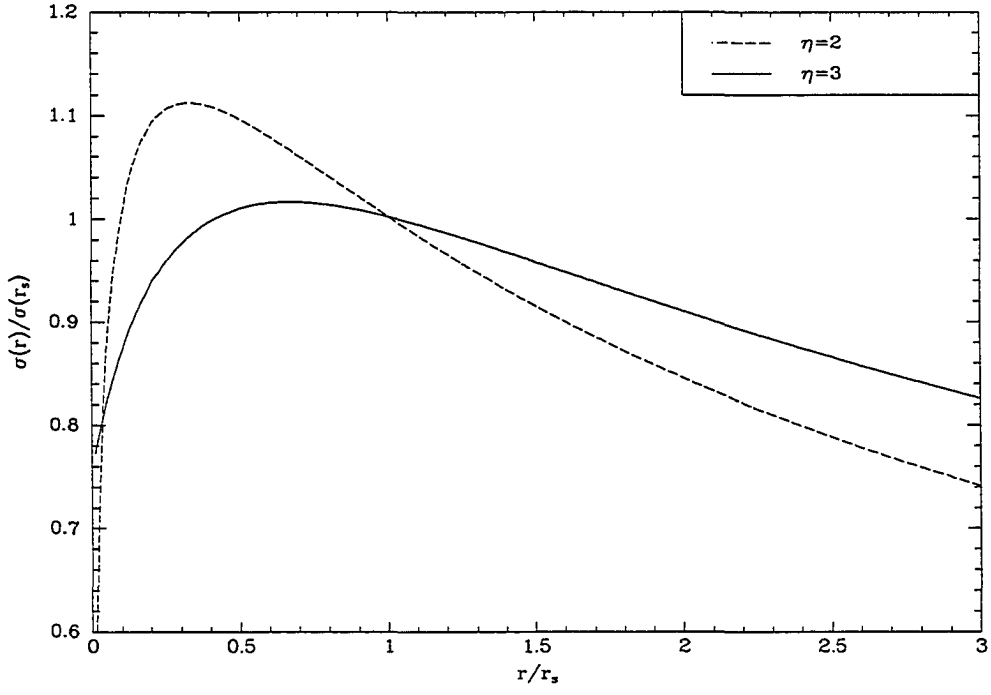

The velocity dispersion as a function of radius. The velocity dispersion has been normalized by the velocity dispersion at the scale radius.

2.6.2 Disk Models

If a galaxy has disk-like kinematics and structure, then a substantial velocity dispersion will still be measured for the galaxy due to unresolved rotation within the aperture. In disks, nearly all stars are on circular orbits, and the local velocity dispersion is very small in comparison to the circular velocity. In a cold disk, the circular velocity is given by

$$v_c^2(r) = \frac{GM(r)}{r}. \tag{2.12}$$

The line-of-sight velocity is generally smaller than the circular velocity. The inclination of the galaxy reduces the line-of-sight velocity by the cosine of the inclination, i. Stars that are not on the observed major axis have motions that are partially in the plane of the sky. The observed velocity is given by

$$v_{los}(r,\theta) = v_c \cos i \sin\theta, \tag{2.13}$$

where θ is the azimuthal coordinate within the galaxy.

The observed velocity dispersion is the standard deviation of the velocities of stars within the aperture of the spectrograph. As in the case of the spherical models, the standard deviation is weighted by the flux received from each point within the aperture. The observed velocity dispersion is given by

$$\sigma_a^2 = \frac{\int_a \frac{GM(r)}{r} \cos^2 i \sin^2\theta \rho/\gamma dA}{\int_a \rho/\gamma dA}. \tag{2.14}$$

where the integrals run over the surface portion of the disk seen in the spectroscopic aperture. For the spectra presented in Section 2.3, the integral runs over the surface described by

$$-2.4/206265 \times \mathrm{D} \leq \quad x \quad \leq 2.4/206265 \times \mathrm{D} \tag{2.15}$$

$$-1.2/206265/\cos i \times \mathrm{D} \leq \quad y \quad \leq 1.2/206264/\cos i \times \mathrm{D} \tag{2.16}$$

where the origin or the coordinate system is at the center of the galaxy, the x-axis runs along the apparent major axis of the galaxy, and D is the distance to the galaxy.

For a galaxy with a surface mass density given by

$$\Sigma = \Sigma_o e^{r/r_e}, \tag{2.17}$$

the mass interior to a radius r is given by

$$M(r) = \frac{r_e \sigma_a^2}{G \cos^2 i}(1 - e^{-r/r_e}(1 + r/r_e)) \frac{\int_a \Sigma/\gamma dA}{\int_a \frac{1-e^{-r/r_e}(1+r/r_e)}{r/r_e} \sin^2\theta \Sigma/\gamma dA}. \tag{2.18}$$

2.6.3 Velocity Dispersion

Previous kinematic studies using the CO(2,0) band (Lester & Gaffney 1993; Doyon et al. 1994) had very restricted wavelength coverage. FSpec in the high-resolution mode has a wavelength coverage of 0.075 μm which allows traditional techniques for the determination of the velocity dispersion to be applied. The cross-correlation technique described by Tonry & Davis (1979) and the Fourier quotient technique of Sargent et al. (1978) are used for measuring the redshift and velocity dispersion of galaxies from optical spectra. The cross-correlation method was used in this study because it produces more accurate results in cases where the velocity dispersion is less than 150 km/s (Larsen et al. 1983). In the cross-correlation method, the velocity dispersion of a galaxy is deduced from the width of the peak in the correlation function of the galaxy spectrum and that of a template star. The stellar template must have a spectrum similar to that of the galaxy. The method also requires that the continuum be accurately subtracted from each spectrum.

The CO index was used to select template stars with a band strength close to that of the galaxies. Stars of type K5 - M2 III were chosen as templates. The strengths of the CO bands of these stars are similar to those observed in the spectra of the galaxies. At least two template stars were observed on each run. The measured velocity dispersion proved insensitive to the choice of template star so long as the star has a CO index similar to that of the galaxy and the template spectrum has a signal-to-noise ratio in excess of 100.

Neither polynomial fitting nor Fourier methods for continuum subtraction proved satisfactory for use on the galaxy spectra in this study. The true continuum is not seen longward of 2.29 μm because of CO absorption. However, it is possible to define a pseudocontinuum for regions in the wings of the CO bands. The shape of this pseudocontinuum is not well described by a low-order polynomial. A polynomial of sufficiently high order to match the shape of the pseudocontinuum cannot be fit to the galaxy spectra due to the noise in the spectra. Tonry & Davis (1979) used a different approach to remove some of the continuum: they removed low frequency Fourier components from their spectra. Unfortunately, the CO bands are sufficiently broad that they contribute power to the low frequency terms so that removal of the low frequency terms from the spectra does not reliably remove the continuum. A method was developed which takes advantage of the possibility of fitting polynomials to the stellar spectra which have high signal-to-noise ratios. All spectra were divided by the spectrum of HR 7405 (MO III). The quotient spectra are nearly flat and could be fit with a fourth order polynomial. The region near the CO(2,0) band was excluded from the fit. The original spectra were then multiplied by the fit so that their continuum shapes were the same as that of HR 7405. The tenth-order polynomial fit to the spectrum of HR 7405 was then subtracted from each galaxy or template spectrum. The spectrum of HR 7405 and

the pseudocontinuum fit to it are shown in Figure 2.14.

The relationship between the width of the cross-correlation peak and the velocity dispersion of the galaxies was measured using the template stars. One of the templates from each run was broadened by a Gaussian. The second template and the broadened template were cross-correlated, and the width of the cross-correlation peak determined. The peak width was measured for Gaussian widths of 0 to 400 km/s at intervals of 30 km/s. The velocity dispersion as a function of width was fit to a parabola.

The uncertainties for the velocity dispersions were obtained from Monte Carlo simulations. A template star was used to create 100 realizations of a spectrum with the same velocity dispersion, line strength, and signal-to-noise ratio as the observed galaxy. The stellar spectra were broadened with a Gaussian function. The quoted uncertainty for all the galaxies except NGC 6240 is the standard deviation of the Monte Carlo values. NGC 6240 has such a high velocity dispersion that the distribution of dispersions from the Monte Carlo simulations is significantly non-Gaussian, with a tail at high velocity dispersions. The uncertainty listed for the velocity dispersion of this galaxy is the 67% confidence limit.

The velocity dispersions and uncertainties of each galaxy are listed in Table 2.5. The velocity dispersion listed for Arp 220 is taken from Doyon et al. (1994), and was obtained with a $2.''2 \times 2.''2$ aperture. The velocity dispersion of NGC 6240 has been measured by others, who also used the CO bands. Doyon et al. (1994) obtained a velocity dispersion of 350 ± 30 km/s in an aperture of $2.''2 \times 2.''2$. Lester & Gaffney (1994) also measured a velocity dispersion of 350 ± 40 km/s for this galaxy.

Fig. 2.14.— HR 7405 and the Pseudocontinuum

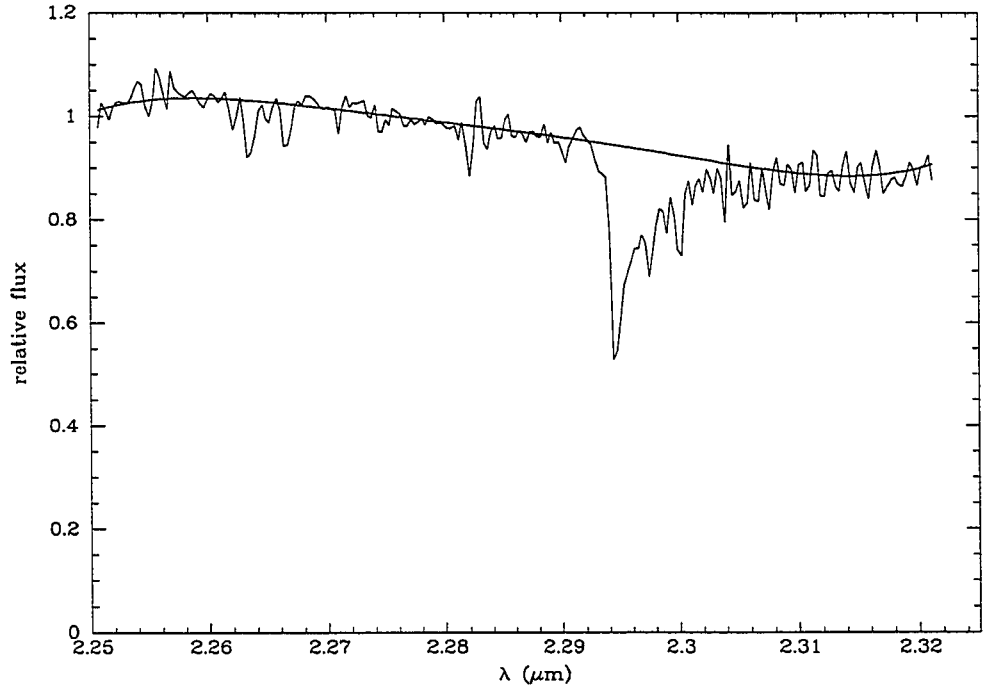

The spectrum of HR 7504 (MO III) and its pseudocontinuum. The pseudocontinuum was constructed by fitting a tenth-order polynomial to the stellar spectrum in the regions $\lambda < 2.29$ μm and $\lambda > 2.31$ μm.

Table 2.5: Observed Velocity Dispersion

Galaxy	Velocity Dispersion km/s
NGC 1614	75 ± 12
NGC 2623	95 ± 13
NGC 3690	124 ± 23
NGC 6240	360 ± 75
IC 694	135 ± 21
Arp 220	150 ± 21[a]
Zw 475.056	151 ± 28

[a]Doyon et al. 1993

2.6.4 Scale Radii

Light profiles were extracted from K or K_s band images because the K band light is less affected by extinction than light at shorter wavelengths and is a better tracer of the mass distribution (Rix 1993). Since stellar populations of all ages have significant CO absorption, the stars which dominate the CO absorption must also be major contributors to the broadband 2.2 μm light. For most of the galaxies, the light profile was obtained by applying the IRAF ellipse-fitting routine isophote.ellipse to K or K_s band images. The light profiles of NGC 3690 and Zw 475.056 had to be obtained from major and minor axis cuts due to the double nucleus in NGC 3690, and the unusual light profile of Zw 475.056. The light profile of NGC 6240 was obtained from the contour plots of Eales et al. (1990) and Zenner & Lenzen (1993).

The scale radii, r_s, of the spherical models were found by fitting seeing convolved projections of the $\eta = 3$ model density functions to the light profiles. It was not possible to distinguish between different values of η because the galaxy cores were within the seeing disk. Because the galaxy cores were within the seeing disk, the value of r_s derived from the light profiles was independent of whether $\eta = 2$ or $\eta = 3$ models were used for the fitting. The seeing FWHM was approximately 1".2 for images of NGC 1614 and Zw 475.056, and 0".8 for the other galaxies. The uncertainty in the scale radii is 0.1 - 0.2 ". The scale radii for the spherical models are given in Table 2.6. The scale radius of Arp 220 implies a half-light radius in good agreement with that found by Wright et al. (1990). The half-light radius for NGC 1614 is 12% larger than that found by Forbes et al. (1992). The effects of extinction in a uniform mixture of dust and stars were calculated. The portion of the light profile significantly affected by extinction is within the seeing disk for the

light profiles considered here. The region within the seeing disk was not used to determine the scale radii, so extinction does not affect the measured scale radii.

The exponential scale radii, r_e, for the disk models were determined by fitting exponentials to the galaxy light profiles. The seeing FWHM used in fitting the exponential profiles were the same as in the case of the spherical models. The exponential scale radii of the galaxies are listed in Table 2.7.

The light profiles of the galaxies and the best fitting model light profiles are shown in Figures 2.15 through 2.22.

2.6.5 Calculation of the Masses

The kinematic models in Sections 2.6.1 and 2.6.2 were combined with the velocity dispersions and scale radii determined in Sections 2.6.3 and 2.6.4 to estimate the mass within the central kiloparsec of all the galaxies except NGC 3690, which is discussed below.

Three models are considered here: a spherical model with $\eta = 3$, a spherical model with $\eta = 2$, and a disk model with an inclination of 30°. In a collection of randomly oriented disks, 30° is the median inclination. It is assumed here that the mass-to-2.2 μm light ratio is constant, and that extinction is negligible. In Section 2.6.6, it is shown that these assumptions do not significantly affect the derived masses. The masses are listed in Tables 2.6 and 2.7. The uncertainties quoted for the masses are those derived from the uncertainties in the velocity dispersions. Examination of Table 2.6 and Table 2.7 shows that the values for the mass in all three models are the same within the errors imposed by the uncertainties of the velocity dispersions.

Fig. 2.15.— Light Profile of NGC 1614 and Model Fits

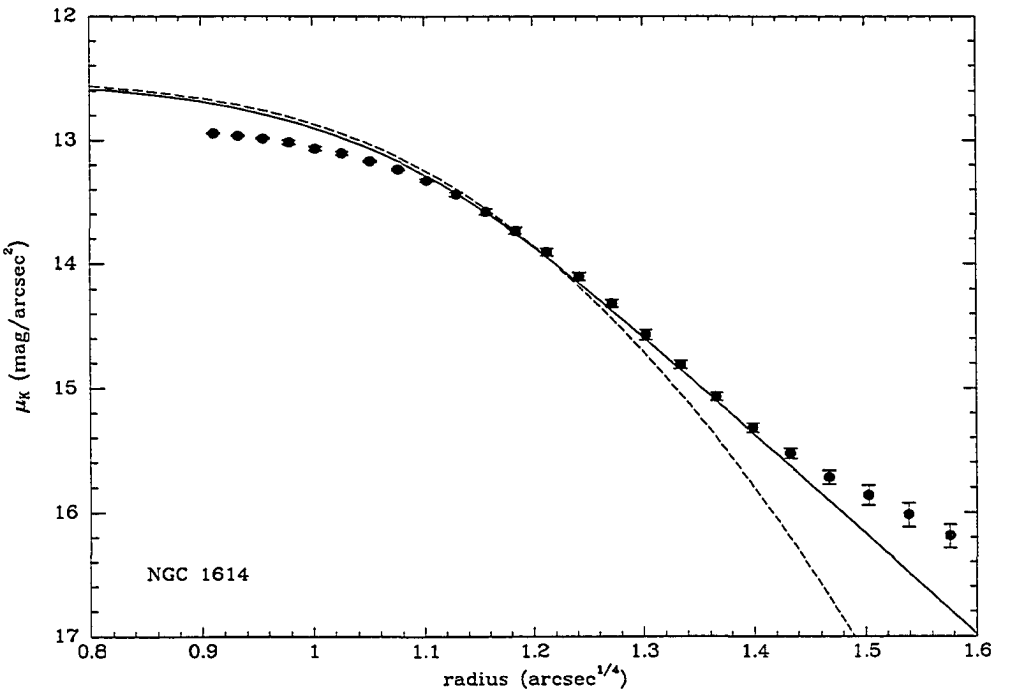

K_s band light profile of NGC 1614. The projection of the $\eta = 3$ model is drawn in a solid line, an exponential light profile is drawn in a dashed line.

Table 2.6: Nuclear Masses for Galaxies Assuming Spherical Geometry

Galaxy	Scale Radius	Mass $\eta = 3$	Mass $\eta = 2$
	pc	$10^9 M_\odot$	$10^9 M_\odot$
NGC 1614	460	1.5 ± 0.5	1.8 ± 0.6
NGC 2623	340	2.8 ± 0.8	3.0 ± 0.8
NGC 3690 B_1	125	2.7 ± 0.4	2.6 ± 0.4
NGC 3690 B_2	200	1.1 ± 0.2	1.3 ± 0.2
NGC 6240	620	30 ± 12	41 ± 17
IC 694	220	5.8 ± 1.8	5.8 ± 1.8
Arp 220	700	4.6 ± 1.3	6.6 ± 1.3
Zw 475.056	600	7 ± 3	5 ± 2

Fig. 2.16.— Light Profile of NGC 2623 and Model Fits

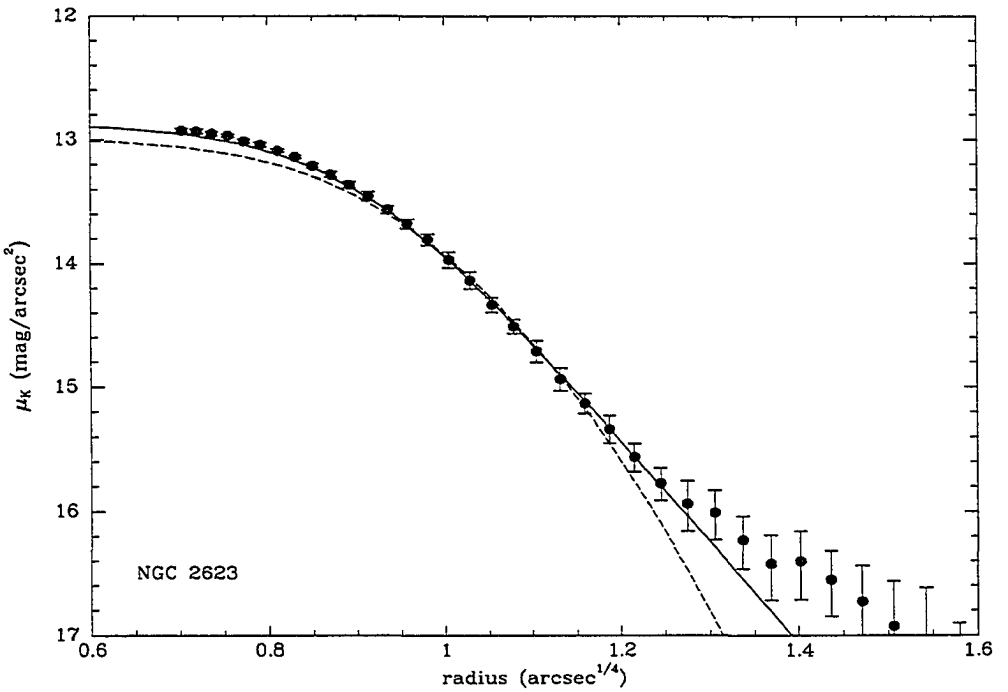

K band light profile of NGC 2623. The projection of the $\eta = 3$ model is drawn in a solid line, an exponential light profile is drawn in a dashed line.

Table 2.7: Nuclear Masses for Galaxies Assuming Disk Geometry

Galaxy	Scale Radius	Mass
	pc	$10^9 M_\odot$
NGC 1614	300	1.8 ± 0.6
NGC 2623	250	2.9 ± 0.8
NGC 3690 B_1	125	2.7 ± 0.4
NGC 3690 B_2	200	1.3 ± 0.2
NGC 6240	550	31 ± 12
IC 694	150	5.6 ± 1.8
Arp 220	600	4.5 ± 1.2
Zw 475.056	700	7 ± 3

Fig. 2.17.— Light Profile of NGC 3690 B_1 and Model Fits

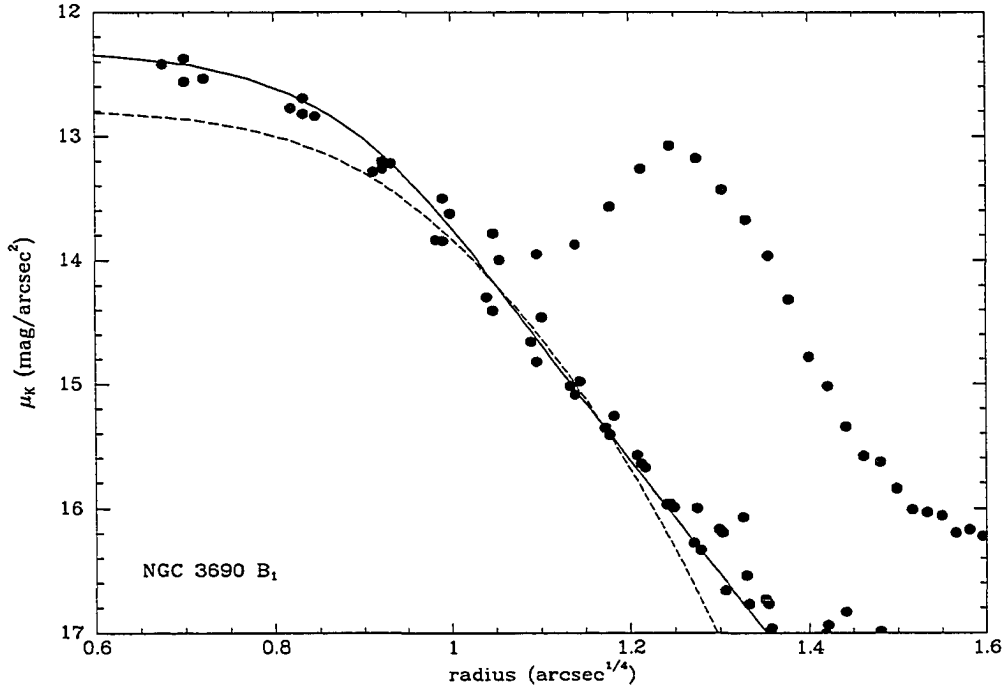

K band light profile of NGC 3690 B_1. The projection of the $\eta = 3$ model is drawn in a solid line, an exponential light profile is drawn in a dashed line.

Fig. 2.18.— Light Profile of NGC 3690 B_2 and Model Fits

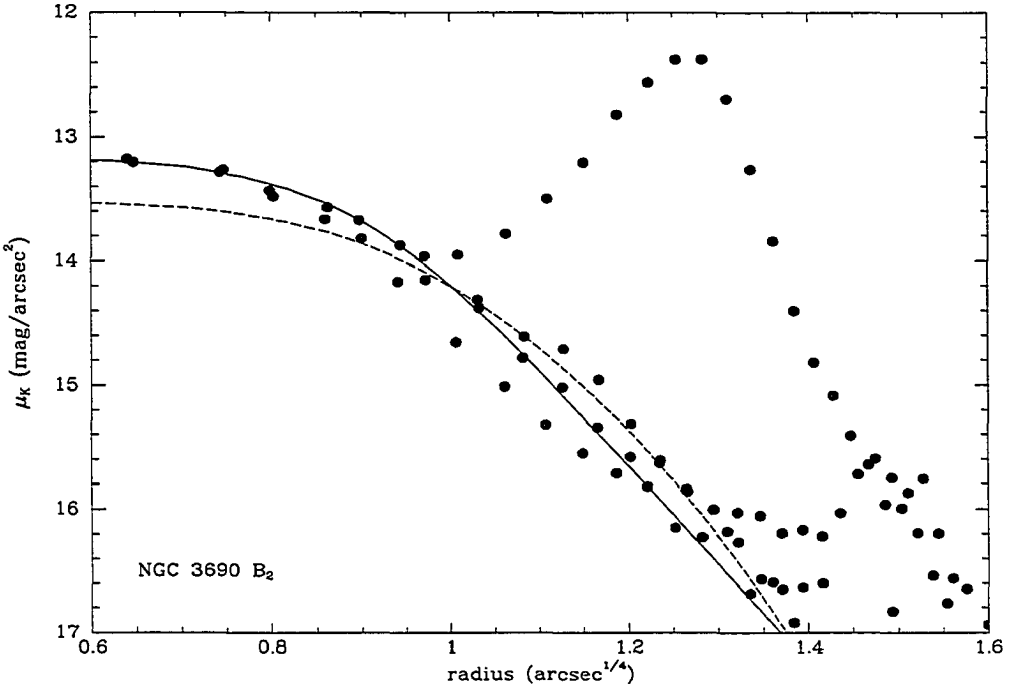

K band light profile of NGC 3690 B_2. The projection of the $\eta = 3$ model is drawn in a solid line, an exponential light profile is drawn in a dashed line.

Fig. 2.19.— Light Profile of NGC 6240 and Model Fits

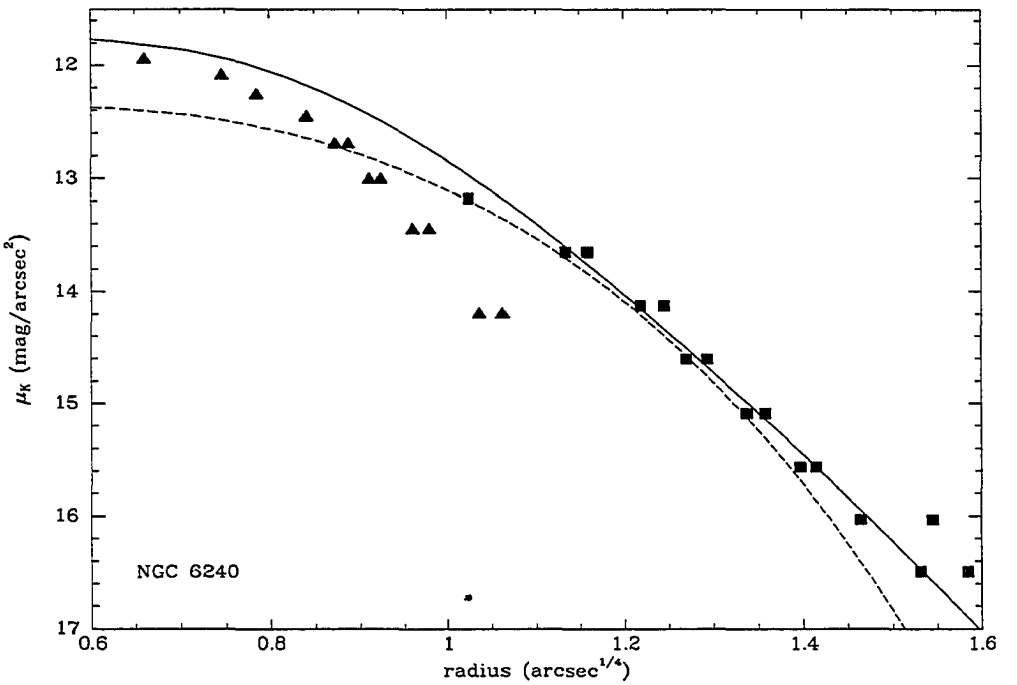

K band light profile of NGC 6240. The projection of the $\eta = 3$ model is drawn in a solid line, an exponential light profile is drawn in a dashed line. The points marked with a triangle are taken from the contour map of Eales et al. (1990), and the points marked a square are from the contour plot of Zenner & Lenzen (1993).

Fig. 2.20.— Light Profile of IC 694 and Model Fits

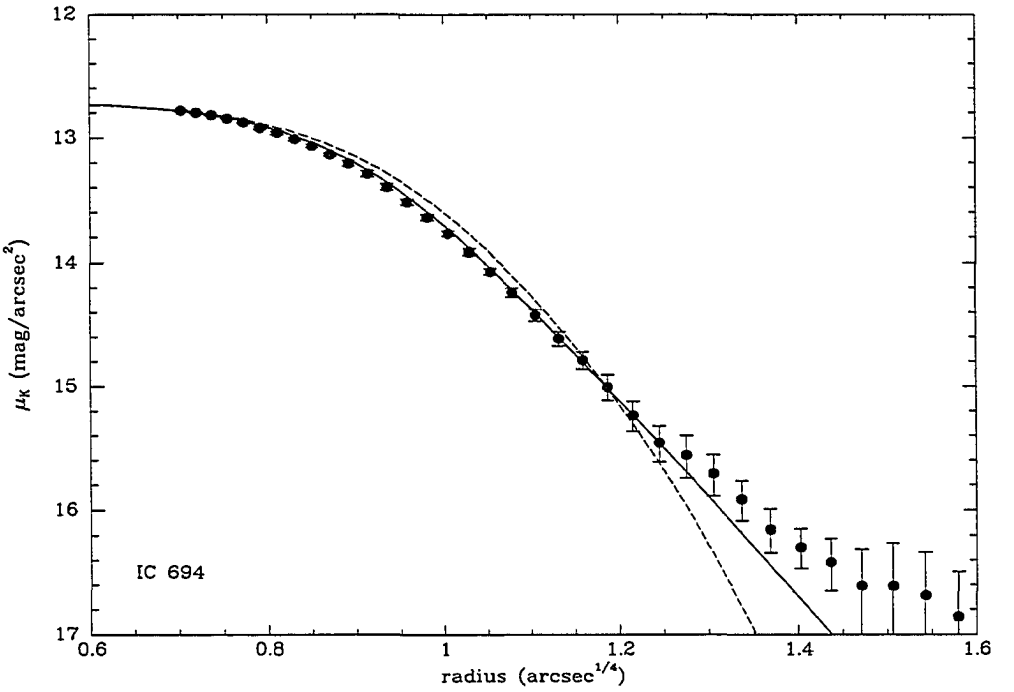

K band light profile of IC 694. The projection of the $\eta = 3$ model is drawn in a solid line, an exponential light profile is drawn in a dashed line.

Fig. 2.21.— Light Profile of Arp 220 and Model Fits

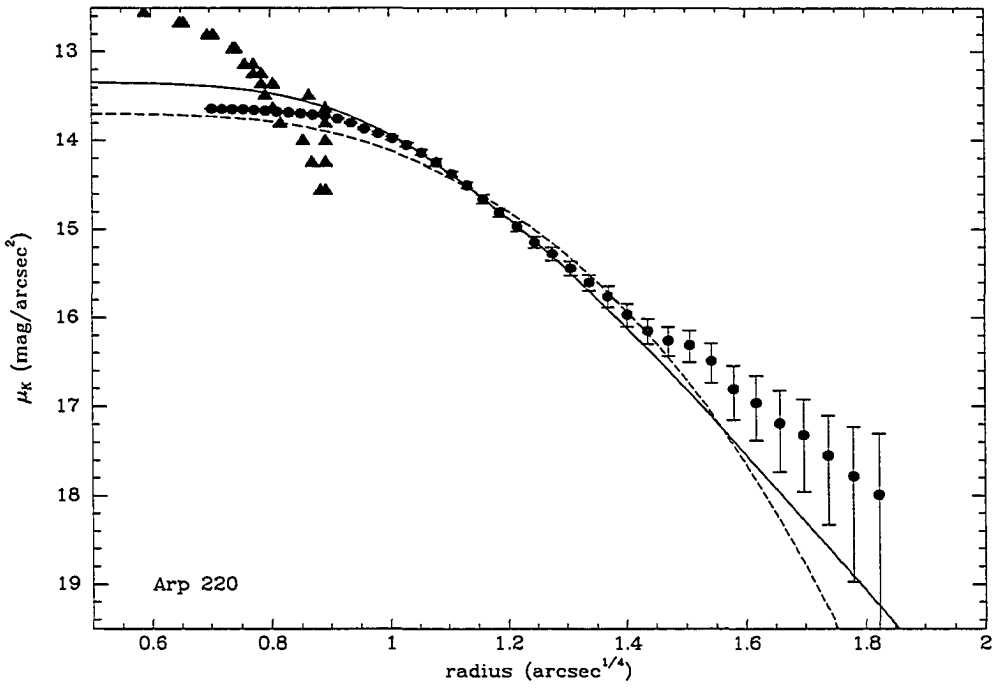

K band light profile of Arp 220. The projection of the $\eta = 3$ model is drawn in a solid line, an exponential light profile is drawn in a dashed line. The points marked with triangles are from Graham et al. (1990).

Fig. 2.22.— Light Profile of Zw 475.056 and Model Fits

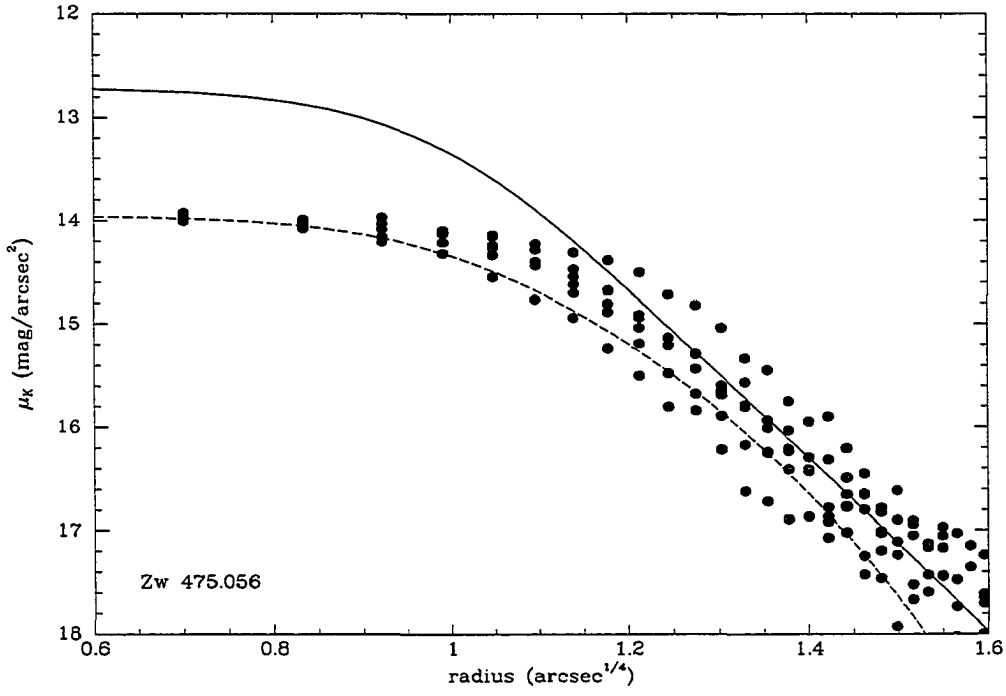

K_s band light profile of Zw 475.056. The projection of the $\eta = 3$ model is drawn in a solid line, an exponential light profile is drawn in a dashed line. This light profile is taken from the 0″.2 / pixel image.

NGC 3690 has a very disturbed morphology, and cannot be modeled as either a spheroid or a disk. Both NGC 3690B_1 and B_2 lie in the spectroscopic aperture, so the observed spectrum is a combination of the spectra of both sources. The H-K color map of the center of NGC 3690, shown in Figure 2.23, shows that B_1 and B_2 are redder than the region between them, indicating that they are two separate objects, and not a single elongated nucleus cut by a dust lane. The two sources were fit separately with spherical and disk models.

This system was modeled as two galaxies orbiting each other. The tidal interactions of the mass distributions were neglected. The mass distributions were truncated at r = 250 pc. The orbit was assumed to be circular. The velocity dispersions of the two sources and their relative velocity may be computed from the masses and physical separation of the centers of mass. The apparent separation of 450 pc may be smaller that the true separation. The median apparent separation of two objects on circular orbits viewed at random angles is about 80% of the physical separation, so the physical separation was taken to be 570 pc. The observed relative velocity of the sources may also be affected by projection effects. The observed relative velocity was assumed to be 60% of the actual relative velocity, based on the median value for the ratio between the actual and observed relative velocities in randomly oriented binary systems. The ratio of the masses of the two sources was chosen to be 2, the ratio of their stellar 2.2 μm luminosity in a 2$''$.4 aperture. Using these two assumptions, the relationships between the velocity dispersions of each nucleus and the relative velocity between them is completely determined. Synthetic spectra of this system were created by adding two spectra with different velocity dispersions and redshifts. The effective velocity dispersion of the model spectra was determined through the use of the cross-correlation program described in Section 2.6.3. If the CO index of the two sources is the same, the relative velocity of the

Fig. 2.23.— H-K Color Map of NGC 3690

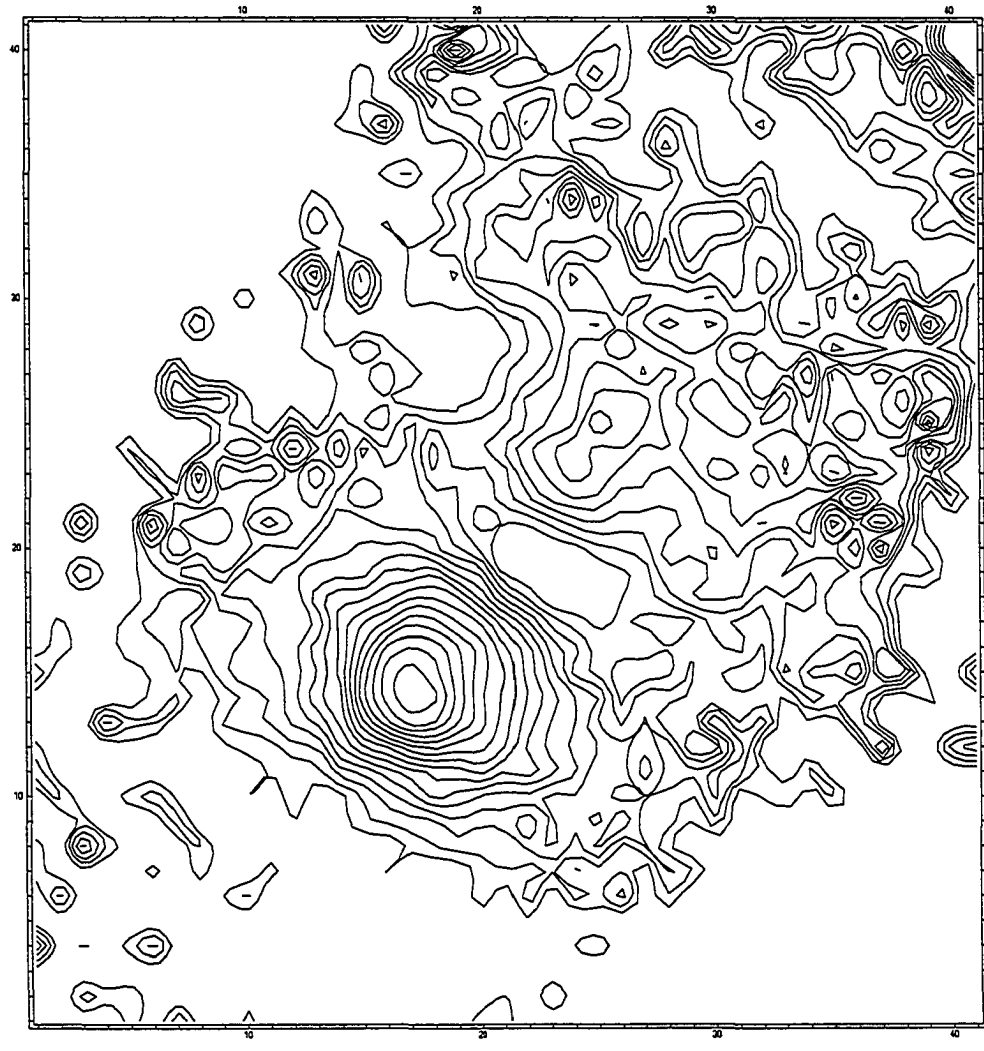

A H-K color map of the center of NGC 3690. The scale and field of view of this map is the same as the contour map of the K band image in Figure 2.6. The lowest contour is at H-K = 0.1. The contour interval is 0.1. The peak value is H-K = 1.7.

two sources is 140 ± 20 km/s, the velocity dispersion of B_1 is 135 ± 10 km/s and the velocity dispersion of B_2 is 90 ± 10 km/s. Relaxation of the assumption that the CO indices are equal does not change the derived masses by a significant amount. If the CO index of B_1 is 0.145, the smallest value permitted by the observations, the best fitting values for the masses of B_1 and B_2 are well within 1-σ of the values derived for the equal CO index case. An upper limit to the mass of source B_1 can be set by finding the mass ratio that maximizes the value of the velocity dispersion of B_1 allowed by the observations. If the CO index of the sources is equal, then the mass within 250 pc of source B_1 is not greater than $3.0 \pm 0.5 \times 10^9 M_\odot$.

2.6.6 Nonuniform M/L_K and Extinction

The models in Section 2.6.1 and 2.6.2 explicitly contain the mass-to-K light ratio. In the kinematically hot models, the flux is dominated by light originating at radii near $r = r_s(\eta - 1)/2$. As shown in Figure 2.13, the line-of-sight velocity dispersion is weakly dependent on the radius at which most of the light is generated. For this reason, variations in the mass-to-light ratio with radius do not strongly affect the derived mass.

The effect of a radially dependent mass-to-light ratio was tested for the extreme case where the mass distribution is unrelated to the K band light distribution. The mass and light distributions were assumed to have the same functional form, but the mass distribution was permitted to be more extended than the K band light distribution. Such a situation could arise if the mass is dominated by a spatially extended old stellar population and the K band light is dominated by young stars born in centrally condensed molecular gas. The mass-to-K band light ratio, γ, in the spherical models is related to the scale radius of the K band light, r_K, and the

scale radius of the mass distribution, r_M, by

$$\gamma(r) = \gamma(r = \infty)\frac{(r + r_K)^{1+\eta}}{(r + r_M)^{1+\eta}}. \tag{2.19}$$

In the disk models, γ is given by

$$\gamma(r) = \gamma(r = 0)e^{-r(r_K - r_M)/(r_K r_M)}, \tag{2.20}$$

where r_K is the exponential scale length of the K band light distribution and r_M is the exponential scale radius of the mass distribution. For $1 < r_M/r_K < 2$ the effect of mass-to-light ratio variations is never significantly larger than the 1-σ uncertainties in the masses imposed by the uncertainty in the velocity dispersions. The effect of radially dependent mass-to-K band light ratios on the mass derived for the central kiloparsec of NGC 1614 is shown in Figure 2.24.

The extinction of 2.3 μm photons does occur in the very luminous infrared galaxies, but it has a minimal effect on the observed velocity dispersion, and hence on the estimated mass, provided that stars near the scale radius are not completely obscured. Extinction was considered for the case of the spherical models only. If the extinction is best described by a uniform screen model, then the light of all of the stars in the galaxy is uniformly absorbed, and the spectrum is unaffected by the extinction. In the case of uniformly mixed stars and dust, extinction causes the flux to be dominated by stars slightly more distant from the galactic center than those that dominate the light if there is no extinction. Examination of the models reveals that the velocity dispersion is not a strong function of radius at the radii generating most of the observed flux in either the case of no extinction, or the case of moderate extinction at 2.3 μm (A_V = 0 - 20), so the observed velocity dispersion is not significantly effected by extinction. If the stars and dust are evenly mixed, extinctions of less than $A_V = 20$ to the center will affect the derived masses by less than 5%.

Fig. 2.24.— Effect of a Variable Mass-to-Light Ratio

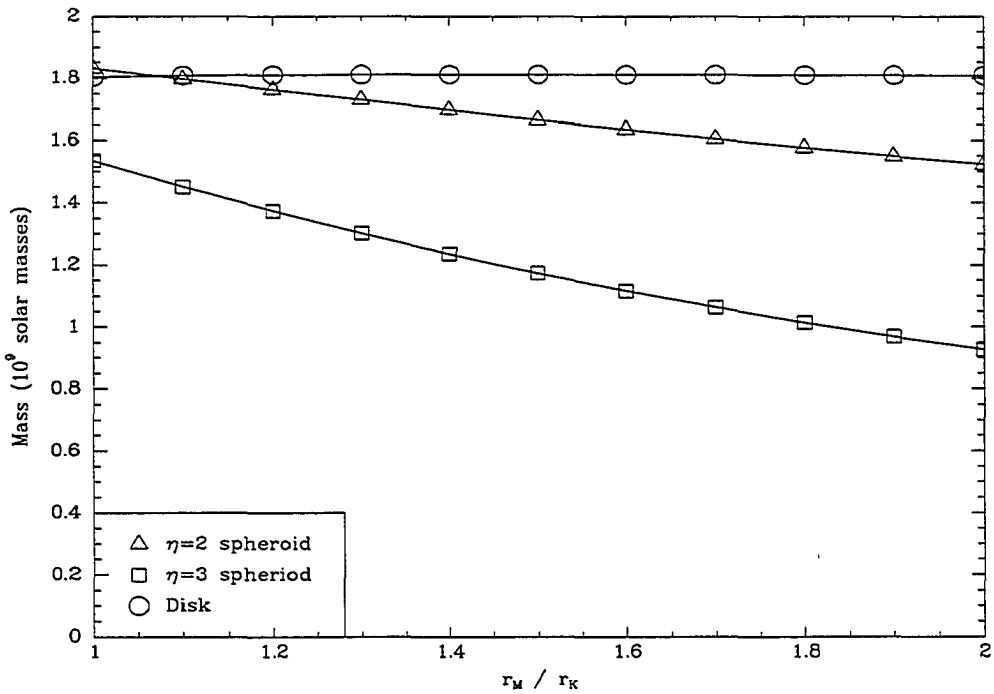

Masses for the central kiloparsec of NGC 1614 if the K band light is more centrally condensed than the mass. The mass and K band light are assumed to have distributions with the same functional form, but the scale radius of the K band light, r_K, is smaller than the scale radius of the mass, r_M. Masses have been computed for both the η-models described in Section 2.6.1 and the disk models of Section 2.6.2. The uncertainty in the velocity dispersion causes an uncertainty of 30% in the masses.

Chapter 3

POWER SOURCES

3.1 Introduction

The nature of a galaxy's power source affects the observable properties of the galaxy. Thus, the observed properties may be used to determine if the bolometric luminosity of a galaxy is produced entirely by stars, or if it contains a luminous AGN. In this Chapter, the relations between observable parameters that can be attained by stellar populations are calculated. By comparing the observations of a sample of seven very luminous infrared galaxies with the calculated relations for stellar populations, the seven galaxies can be sorted into two groups: for three, the energetics could be completely derived from starbursts, while four appear to require an additional (AGN) source.

Careful consideration must be given to the large interstellar dust content of very luminous infrared galaxies, and the extinction it causes, when selecting properties for comparison between the galaxies and the stellar population models. As was demonstrated in Section 2.5, the optical depths in most of the galaxies

observed significantly exceed unity in the V band, but not in the K band. Therefore, the properties of the galaxies and starburst models chosen for comparison must be derived from infrared observations, so that a fair sample of the stars in each galaxy are observed. This consideration led to the selection of five galaxy properties for comparison to the starburst models – the bolometric luminosity, ionizing continuum flux, 2.2 μm luminosity, mass, and CO index. All of these properties of the galaxies can be determined from infrared observations. The mass, CO index and 2.2 μm luminosity of the galaxies were determined in Chapter 2. The bolometric luminosity and ionizing continuum flux of the galaxies were determined from previously published data, as discussed below.

The mass-to-bolometric luminosity ratios, as discussed in Section 3.3, indicate that the dominant source of the luminosity of the galaxies, if stellar, must be very young stars. The large flux of ionizing photons (Section 3.2.2) and the strong CO index (Section 2.4) seen in many of the galaxies are further indicators of a large young component to the stellar population. Models created for the study of young populations are thus the most appropriate for comparison to the very luminous infrared galaxies. Models used for the examination of M 82 are used in Section 3.4 (Rieke et al. 1993).

3.2 Hydrogen Recombination Lines

A literature search was performed to find hydrogen recombination line fluxes for the galaxies. The hydrogen recombination line fluxes in different sized apertures were used in the determination of the size of the starburst region in the galaxies. The ionizing continuum flux was generally determined from near-infrared hydrogen recombination line fluxes. Optical recombination line fluxes were used when

near-infrared data were not available. Estimates of the ionizing continuum made from the 12.8 μm Ne II line and H92α were also considered. Table 3.1 lists the near-infrared hydrogen recombination line fluxes, while Table 3.2 lists the optical hydrogen recombination line fluxes.

3.2.1 Size of the Starburst Region

The starburst activity is confined to the central regions of the very luminous infrared galaxies. The size of the starburst region varies between galaxies. The size of the starburst region may be determined from recombination line fluxes as a function of aperture size, or mid-infrared imaging and photometry.

The comparison of emission line fluxes in different sized apertures may be used to determine the size of the emission line region and hence the size of the region of starburst activity. Examination of Tables 3.1 and 3.2 shows that line fluxes in different sized apertures are available for many of the galaxies in the sample. Other information on the size of the line emitting region is available for some of the galaxies.

Examination of the Brγ fluxes of NGC 1614 in Table 3.1 reveals that nearly all of the Brγ emission originates in the inner 5″. Joy & Harvey (1987) claim that all of the emission line flux of NGC 2623 is contained within an 5″= 1.8 kpc aperture on the basis of the optical spectra in 5″ and 22″apertures. The Hα line fluxes in Table 3.1 also suggest that nearly all of the recombination line flux is within the central 5″. The Brγ line imaging of Arp 299 by Fischer, Smith, & Glaccum (1991) demonstrates that the Brackett line emission originates in three small regions: a very small (3″) region centered on the source B_1, a source smaller than 5″ = 1 kpc in IC 694, and a region centered on source C. The Brγ line fluxes support a small

Table 3.1: Near Infrared Hydrogen Recombination Line Fluxes

Aperture arcsec	Line	Flux W/m^2	Reference
NGC 1614			
5	Brγ	$6.0 \pm 0.2 \times 10^{-17}$	5
6×6	Brγ	$5.9 \pm 0.5 \times 10^{-17}$	9
7.2	Brγ	$7.2 \pm 0.5 \times 10^{-17}$	2
7.2	Brα	$5.5 \pm 0.5 \times 10^{-16}$	2
NGC 2623			
5.5	Brγ	$1.2 \pm 0.5 \times 10^{-17}$	11
NGC 3690			
2.7	Brγ	$< 1.7 \times 10^{-17}$	10
5.5×7.0	Brγ	$3.2 \pm 0.6 \times 10^{-17}$	7
7.2	Brγ	$< 4.6 \times 10^{-17}$	1
7.2	Brα	$4.0 \pm 1.1 \times 10^{-16}$	1
NGC 6240			
5.5	Paα	$6.8 \pm 1.3 \times 10^{-17}$	4
3.5	Brγ	$6 \pm 1.5 \times 10^{-18}$	8
2×9	Brγ	$1.8 \pm .4 \times 10^{-17}$	6
5.5	Brγ	$< 3.3 \times 10^{-17}$	2
6×6	Brγ	$< 6 \times 10^{-17}$	9
8.7	Brγ	3.1×10^{-17}	12
5.5	Brα	$< 1.5 \times 10^{-16}$	4
IC 694			
2.7	Brγ	$1.9 \pm 0.7 \times 10^{-17}$	10
5.5×5.5	Brγ	$4.1 \pm 0.7 \times 10^{-17}$	7
7.2	Brγ	$6.1 \pm 1.6 \times 10^{-17}$	1
7.2	Brα	$4.8 \pm 1.1 \times 10^{-16}$	1
Arp 220			
8.7	Brγ	3×10^{-17}	12
5	Brα	$3.8 \pm 0.5 \times 10^{-17}$[a]	3
7.2	Brα	$< 2.8 \times 10^{-16}$	1

[a] one component fit

References: 1 = Beck et al. 1986, 2 = Beck, Turner, & Ho 1990, 3 = Depoy, Becklin, & Geballe 1987 4 = DePoy, Beckin, & Wynn-Williams 1986, 5 = Doyon, R., Puxley, & Joseph 1992, 6 = Elston & Maloney 1990, 7 = Fischer, Smith, & Glaccum 1991, 8 = Lester et al. 1988, 9 = Moorwood & Oliva 1988, 10 = Nakagawa et al. 1989, 11 = Prestwich, Joseph, & Wright 1994, 12 = Rieke et al. 1985

Table 3.2: Optical Hydrogen Recombination Line Fluxes

Aperture arcsec	Line	Flux W/m^2	Reference
NGC 1614			
2×4.5	Hβ	6.05×10^{-17}	1
5	Hβ	9.28×10^{-17}	2
2×4.5	Hα	5.2×10^{-16}	1
5	Hα	8.11×10^{-16}	2
NGC 2623			
2×4.5	Hα	5.7×10^{-18}	1
5	Hα	1.85×10^{-17}	2
8.1	Hα	2.2×10^{-17}	4
NGC 3690			
4.7	Hβ	4.4×10^{-17}	5
5	Hβ	7.43×10^{-17}	3
4.7	Hα	2.71×10^{-16}	5
8.1	Hα	1.636×10^{-15}	4
NGC 6240			
1.5×4.2	Hβ	5.0×10^{-18}	6
1.5×4.2	Hα	8.0×10^{-17}	6
8.1	Hα	3.50×10^{-16}	4
IC 694			
2×4.5	Hβ	3×10^{-17}	1
5	Hβ	7.43×10^{-17}	2
2×4.5	Hα	1.9×10^{-16}	1
4.7	Hα	4.42×10^{-16}	5
8.1	Hα	4.15×10^{-16}	4
Zw 475.056			
1.5×3.8	Hα	5.4×10^{-17}	6
1.5×3.8	Hβ	5.6×10^{-18}	6

References: 1 = Armus et al. 1989, 2 = Bushouse 1986, 3 = Bushouse & Gallager 1984, 4 = Keel 1984, 5 = Keel et al. 1985, 6 = Veilleux et al. 1994

size for NGC 3690 and IC 694. The Hα line fluxes suggest that the emission line region of NGC 6240 is larger than 1".5×4".2. The reported Brγ fluxes for NGC 6240 should not be used to deduce the emission line region size of this galaxy. Lester, Harvey & Carr (1988) claimed that the Brγ line of NGC 6240 was blended with a H_2 line of greater strength in low resolution spectra. Multiaperture high resolution spectroscopy of this galaxy is not available.

Spatially resolved mid-infrared observations have been made of many of the galaxies in the sample. The 10 μm map of Arp 299 shows that the emission is concentrated near three sources (A, B_1 and C), which are less than 500 pc in size (Wynn-Williams et al. 1991). Wynn-Williams & Becklin (1993) examined the 12 and 25 μm compactness of several galaxies, including NGC 1614, NGC 2623, NGC 6240 and Arp 220. They found that most of the 10 μm emission of NGC 1614 is within the central kpc. Their data for NGC 2623 are consistent with all of the mid-infrared emission originating in a region less than 2 kpc across. In the case of NGC 6240, Wynn-Williams & Becklin (1993) found no evidence that the mid-infrared emission is more extended than 1.3 kpc. The 32 μm diameter of Arp 220 is 700 pc or less, and the 12 μm emission appears to originate in a region of size 1000 pc or less. (Wynn-Williams & Becklin 1993). Deconvolution of 10 μm images showed that the size of the starburst region of Arp 220 is smaller than 320 × 530 pc (Keto et al. 1992).

On the basis of the multiaperture emission line fluxes and mid-infrared data, the size of the starburst region was chosen to be 1 kpc in all of the galaxies except NGC 3690. The sources B_1 and B_2 in NGC 3690 were treated separately. They were assumed to be 250 pc in radius, which is half their projected separation.

3.2.2 Ionizing Continuum Luminosity

The ionizing continuum of the very luminous infrared galaxies is absorbed by dust or gas near where it is emitted. Ionizing photons absorbed by hydrogen atoms will eventually cause the emission of one or more lower energy photons in the recombination lines. The luminous infrared galaxies have strong recombination lines at optical, near-infrared and radio wavelengths. The extinction in the galaxies results in large errors when determining the ionizing continuum luminosity from optical recombination lines, so that near-infrared lines such as Brγ and Brα are better determinants of the ionizing continuum flux.

The extinction to the hot blue stars producing the ionizing continuum may be different than the extinction to the red stars dominating the near-infrared flux, so extinctions to the gas must be calculated from the recombination line ratios where possible. The ratio A_λ / A_V of each of the hydrogen recombination lines except Brα was computed from the formula given by Cardelli, Clayton & Mathis (1989). $A_{Br\alpha}$ / A_V was computed from by linear interpolation of the values of Rieke & Lebofsky (1985).

The temperatures of the H II regions affect both the relation between the Brγ flux and the ionizing continuum and the intrinsic line ratios. Attempts have been made to measure the electron temperature of the H II in two of the galaxies in the sample. Veilleux et al. (1994) determined that the electron temperature, T_e, in NGC 1614 is between 8,000 and 14,000 K, depending on the electron density. Anantharamaiah et al. (1993) determined that $T_e = 10,000$ K in IC 694. It was assumed that $T_e = 10,000$ K in all of the galaxies in the sample. The recombination coefficients and the intrinsic line ratios were taken from Osterbrock (1989). Case B recombination was assumed.

Both Hα / Hβ and Hα / Brγ of NGC 1614 suggest that the extinction to the gas is about $A_V = 3.3$. The 5″ Brγ flux corrected for extinction was used to obtain an ionizing continuum flux of 3×10^{54} photon/sec. This result is quite consistent with the estimate of the ionizing continuum of Roche et al. (1991) from the 12.8 μm fine structure line of Ne II.

The spectrum of NGC 2623 is unusual for a luminous infrared galaxy: Hβ and all of the higher Balmer lines appear in absorption. By adopting the mean of the two larger aperture Hα fluxes, and comparing that value to the Brγ flux, the A_V of the line emitting gas can be calculated to be 6.3. This may be an overestimate of the extinction, since the observed Hα line flux may be affected by underlying stellar absorption. The Brγ flux combined with the extinction estimate yield a value for the ionizing continuum luminosity of 1×10^{54} photons/sec.

The Brγ images of the central region of NGC 3690 by Fischer, Smith, & Glaccum (1991) suggest that nearly all the line flux originates in source B_1. The Brα/Brγ ratio suggests an extinction to the ionized gas of A_V=23. From the Brα flux and the extinction, an ionizing continuum luminosity of 2×10^{54} was computed.

The strong lines of H_2 and the relatively weak hydrogen recombination lines make determination of the ionizing continuum luminosity in NGC 6240 difficult. In low resolution spectra, Brγ is blended with the 2-1 S(2) line of H_2, a line of comparable strength (Lester et al. 1988). An upper limit to the ionizing continuum luminosity may be obtained from the Brγ flux of Rieke et al. (1985). This flux was measured from low resolution spectra, so the line is a blend of Brγ and H_2 2-1 S(2). Using the extinction derived from the near-infrared colors in Section 2.5i, the ionizing continuum flux can be calculated to be is less than 4×10^{54} photons/sec. This estimate is in good agreement with the upper limit

to the ionizing continuum derived from the upper limit on the Brα flux found by DePoy, Beckin, & Wynn-Williams (1986). A lower limit to the ionizing continuum luminosity of 8×10^{53} photons/sec may be set by considering the small aperture Brγ flux of Lester et al. (1988).

In IC 694, the 7".2 Brackett line fluxes of Beck, Turner, & Ho (1986) were used to derive an extinction to the ionized gas of A_V=16. The Brα flux, corrected for this amount of extinction, implies a ionizing continuum luminosity of 5×10^{54} photon/sec. The ionizing continuum flux was determined to be 1×10^{54} photons/sec by Anantharamaiah et al. (1993) on the basis of their measurement of the flux in the H92α line.

The Brα line of Arp 220 has a broad and a narrow component (Depoy, Becklin, & Geballe 1987), suggesting that part of the Brα flux may originate in an active nucleus. The Brα / Brγ line ratio is inconsistent with recombination case B for any value of A_V. The ionizing continuum luminosity was computed from the Brα flux in the narrow component, assuming that $A_V = 4.2$, which was determined from the J-H color. The ionizing continuum in this galaxy is approximately 9×10^{53} photons/sec.

There are no published near-infrared line fluxes for Zw 475.056. The Hα/Hβ line ratio may be used to compute an extinction of $A_V = 4$. However, optical depth effects may cause this extinction to be an underestimate. Using the Hα flux of Veilleux et al. (1994) a lower limit of 1×10^{54} photon/sec may be placed on the ionizing continuum of Zw 475.056.

3.3 Bolometric Luminosity

The bolometric luminosity of the very luminous infrared galaxies is nearly equal to their combined mid- and far-infrared luminosity. The infrared fluxes of all the galaxies in this study were measured by IRAS (Soifer et al. 1987; Lester & Gaffney 1994). IC 694 and NGC 3690 are in the same IRAS beam. Joy et al. (1989) determined that 60% of their combined far infrared luminosity could be attributed to IC 694 and 40% to the combination of NGC 3690 and Arp 299 C. Wynn-Williams et al. (1991) used 25 μm photometry to determine that 10% of the total luminosity of the Arp 299 system originates in source C. The bolometric luminosities of NGC 3690 B_1 and NGC 3690 B_2 cannot be determined from currently available data. It has been assumed that both sources have the same 2.2 μm -to-bolometric luminosity ratio. The far-infrared luminosities and mass-to-light ratios are listed in Table 3.3.

The far-infrared luminosities are not sufficient to determine the power source of the galaxies; however, they do provide useful information. None of the galaxies has a mass-to-light ratio so low as to preclude the possibility of a stellar origin for all of the observed luminosity. However, if any significant fraction of the bolometric luminosity of the galaxies is provided by stars, the stellar population must include large numbers of short-lived, high-mass stars.

3.4 Comparison of Galaxies and Stellar Population Models

The direct comparison of properties between the galaxies and models of stellar populations allows the nature of the power source of the galaxies to be examined. The properties of the very luminous infrared galaxies indicate that they all have

large populations of young stars created in a short burst of star formation. The mass-to-light ratios in Table 3.3 are inconsistent with an intermediate age or old stellar population. The CO indices of the stellar populations in the galaxies are stronger than those of normal galaxies, suggesting that supergiants are contributing to the 2.2 μm light. The ionizing continuum luminosities are also larger than those seen in normal galaxies with moderate star formation, so there must be high levels of star formation. The 8.4 GHz images of these galaxies are extended, providing further evidence of starburst activity (Condon et al. 1991). In addition, the existence of luminous AGN can be demonstrated in some of the galaxies.

Table 3.4 summarizes the properties of the galaxies derived in Sections 2.4, 2.6.5, 2.5, 3.2.2, and 3.3. This form of the galaxy properties is not the most useful for comparison to the stellar population models . Table 3.5 has the properties of all the galaxies normalized to $L_{BOL} = 1\ L_{\odot}$.

The most appropriate models for the stellar populations in the very luminous galaxies are starburst models. Models of populations of solar metallicity stars are more likely to approximate the properties of the young stellar populations in in very luminous galaxies than low metallicity models developed for the study

Table 3.3: Bolometric Luminosity and Mass-to-Light Ratios

Galaxy	L_{FIR} $10^{11}L_{\odot}$	M/L_{BOL} $M_{\odot}/L_{\odot}$
NGC 1614	3.8	0.003
NGC 2623	2.9	0.01
NGC 3690 $B_1 + B_2$	2.1	0.02
NGC 6240	3	0.1
IC 694	3.2	0.02
Arp 220	13	0.007
Zw 475.056	2.6	0.02

Table 3.4: Summary of Stellar Modeling Data

Galaxy	L_{BOL} $10^{11}L_{\odot}$	Log(UV) photons/s	M_K magnitudes	CO index magnitudes	M $10^9 M_{\odot}$
NGC 1614	3.8	54.5	-23.5	0.24	1.5
NGC 2623	2.9	54.3	-22.4	0.17	2.8
NGC 3690 B_1	1.1	54.3	-22.0	...	2.7
NGC 6240	5	53.9-54.6	-24.0	0.22	30
IC 694	3.2	54.7	-22.3	0.23	5.8
Arp 220	13	53.9	-23.0	0.21	4.6
Zw 475.056	2.6	> 54.0	-21.8	0.17	6.2

Table 3.5: Normalized Galaxy Properties

Galaxy	Log(UV) photons/s	M_K magnitudes	CO index magnitudes	M $M_{\odot}$
NGC 1614	42.9	5.5	0.24	0.004
NGC 2623	42.8	6.3	0.17	0.01
NGC 3690 B_1	43.3	5.5	...	0.02
NGC 6240	42.4-43.1	4.7	0.22	0.1
IC 694	43.2	6.5	0.23	0.02
Arp 220	41.8	7.2	0.21	0.004
Zw 475.056	> 42.6	6.7	0.17	0.02

of globular clusters. The kind of gravitational disturbances caused by the close proximity of another galaxy, which produce the disturbed morphology of the very luminous infrared galaxies, also causes a large fraction of the gas in disk of the galaxy to fall into the center of the galaxy (Barnes & Hernquist 1991). In the galaxies where star formation occurs over 10^7 years or more, the supernovae from the earliest generation of stars will enrich the gas from which later stars are formed. The models developed by Rieke et al. (1993) for the study of the young stellar population in M 82 were used here. These models include the recent treatments of stellar evolution by Maeder & Meynet (1988). Models with two different initial mass functions (IMF), denoted # 3 and # 8 by Rieke et al. (1993), were compared to the galaxy observations. IMF # 3 is a power law approximation to the local IMF, and IMF # 8 is the initial mass function found to describe the stellar population in M 82. IMF # 8 is more heavily weighted toward high mass stars than IMF # 3. Both IMF # 3 and IMF # 8 are shown in Figure 3.1. A variety of star formation rates were considered including a short burst lasting 5×10^6 years, constant star formation, and exponentially declining star formation rates.

The properties of the stellar population models, normalized at each timestep to $L_{BOL} = 1\ L_{\odot}$ are shown in Figures 3.2 through 3.9. The properties of models with five different star formation rates are considered: a short burst, exponentially declining star formation rates with time constants of 20, 50 and 100 Myr, and constant star formation. All of the models assume that star formation began suddenly, so the values for the observational parameters may not be physcially reasonable for model ages less than 5 Myr. With the exception of the masses, the properties of the IMF # 3 and IMF # 8 models are quite similar, as might be expected because the high mass parts of the IMFs are similar. Models with star formation rate time constants in excess of 50 Myr have very similar properties, so

Fig. 3.1.— Model Initial Mass Functions

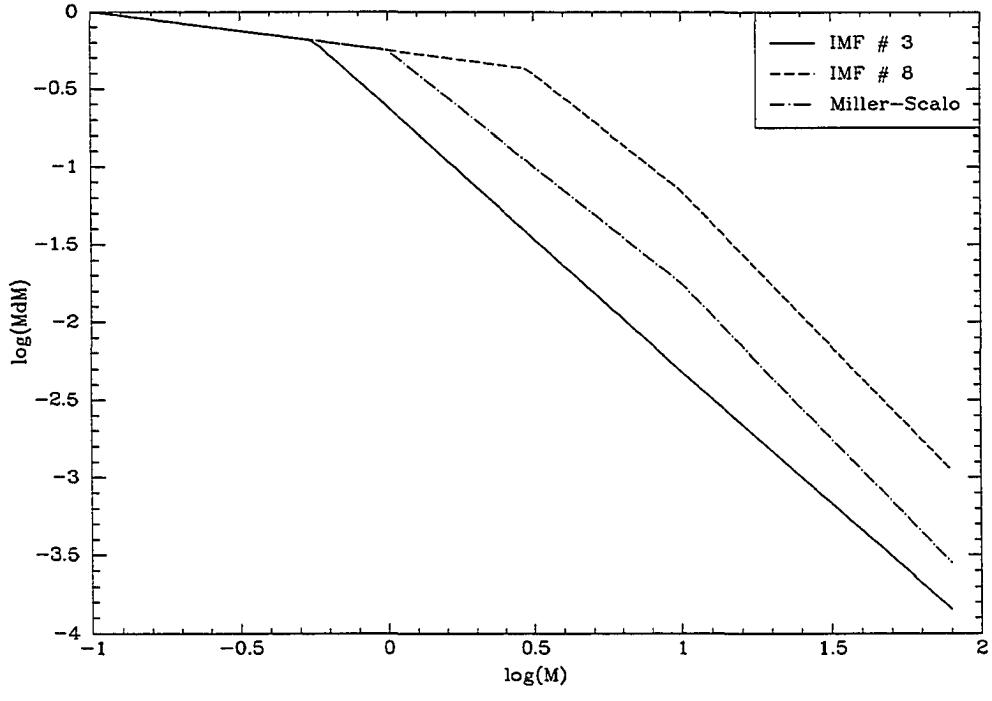

Three model initial mass functions from Rieke et al. (1993). IMF # 3 is a fit to some of the IMFs considered by Basu & Rana (1992). This IMF is a recent estimate of the local IMF. IMF # 8 was found to be a plausible description of the IMF in M 82 by Rieke et al. (1993). A power law fit to the Miller-Scalo IMF (Miller & Scalo 1979) is included for reference.

observationally distinguishing between them is nearly impossible.

The properties of the models and the galaxies are compared in Figures 3.10 through 3.13. It can be seen immediately in Figures 3.10 and 3.11 that three galaxies, Arp 220, NGC 2623 and Zw 475.056 have properties that are inconsistent with any of the stellar populations considered. These galaxies must contain AGN which contribute to the bolometric luminosity of the galaxies. Figures 3.12 and 3.13 provide additional information on the possible stellar populations of the galaxies. The CO bands of IC 694 are stronger than those of the 10 Myr old stellar population which Figures 3.10 and 3.11 suggest might be the principal source of luminosity in this galaxy. IC 694 must also contain a luminous AGN. Combinations of young and old or intermediate-age stellar populations are inconsistent with the observed properties of Arp 220, IC 694, NGC 2623, and Zw 475.056. The other three galaxies in the sample, NGC 1614, NGC 3690 B_1, and NGC 6240 have properties that are entirely consistent with a young stellar population. The details of the stellar populations in the galaxies will be discussed further in Chapter 4.

A unique contribution that stellar population modeling can make to the study of the very luminous infrared galaxies is that the relative contribution of the AGN and the stellar population to the energetics of the galaxy can be assessed. The strong CO bands seen in all of the galaxies demonstrates that most of the K band flux of the galaxies is from stars. The stellar population cannot possibly produce more than 100% of the observed ionizing continuum flux. The most luminous stellar population allowed by the observations is one with the same ratio of 2.2 μm luminosity to ionizing continuum luminosity as the galaxy. The luminosity of this stellar population is smaller than that of the galaxy. The difference between the total luminosity and the stellar luminosity must be from a non-stellar source, i.e., an AGN. If the AGN is contributing to the hydrogen recombination lines used

Fig. 3.2.— Ionizing Continuum Luminosity of IMF # 3 Models

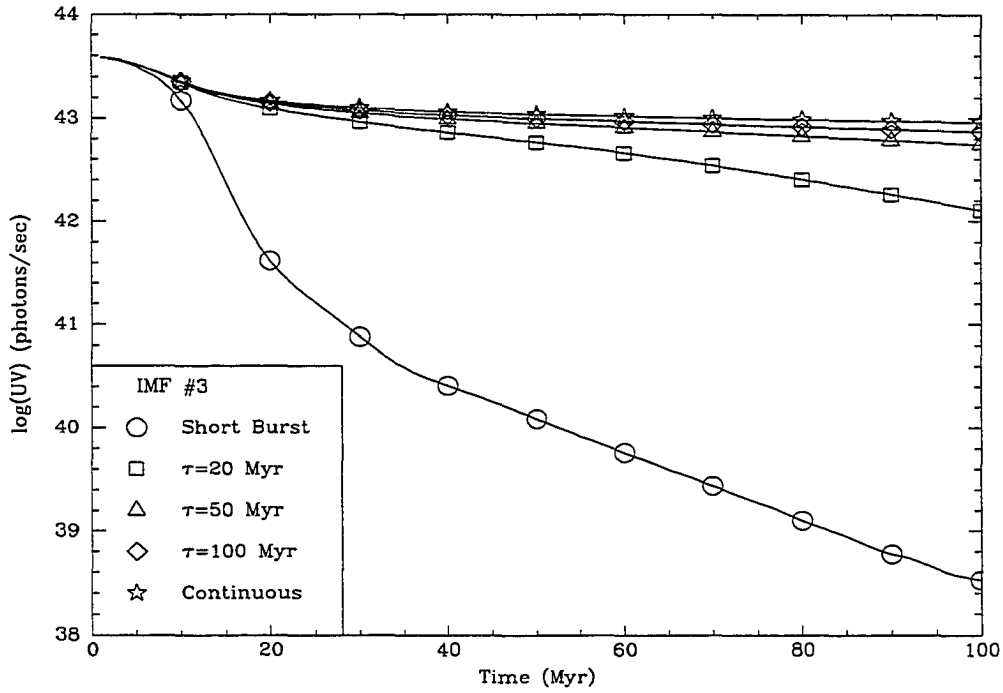

Log of the ionizing continuum luminosity in photons/ sec. This luminosity has been normalized to $L_{BOL} = 1\ L_{\odot}$. Models with five star formation rates are shown: a short burst of star formation, lasting 5×10^6 yr, exponentially declining star formation with time constant, τ, equal to 20, 50, or 100 Myr, and a constant star formation rate.

Fig. 3.3.— Ionizing Continuum Luminosity of IMF # 8 Models

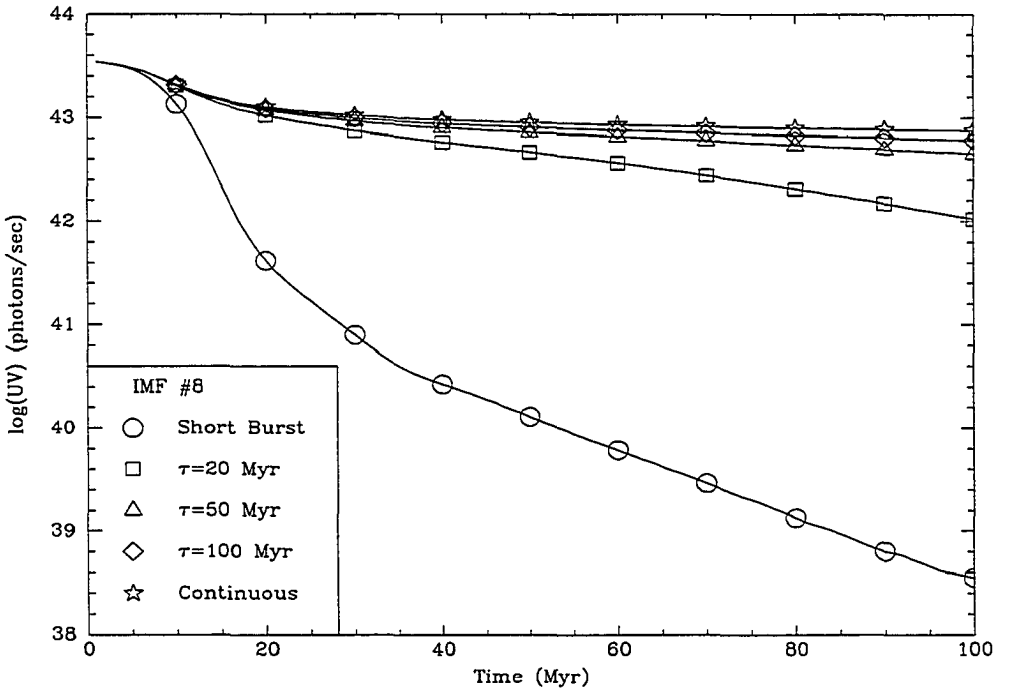

Log of the ionizing continuum luminosity in photons/ sec. This luminosity has been normalized to $L_{BOL} = 1\ L_{\odot}$. Models with five star formation rates are shown: a short burst of star formation, lasting 5×10^6 yr, exponentially declining star formation with time constant, τ, equal to 20, 50, or 100 Myr, and a constant star formation rate.

Fig. 3.4.— K magnitude of IMF # 3 Models

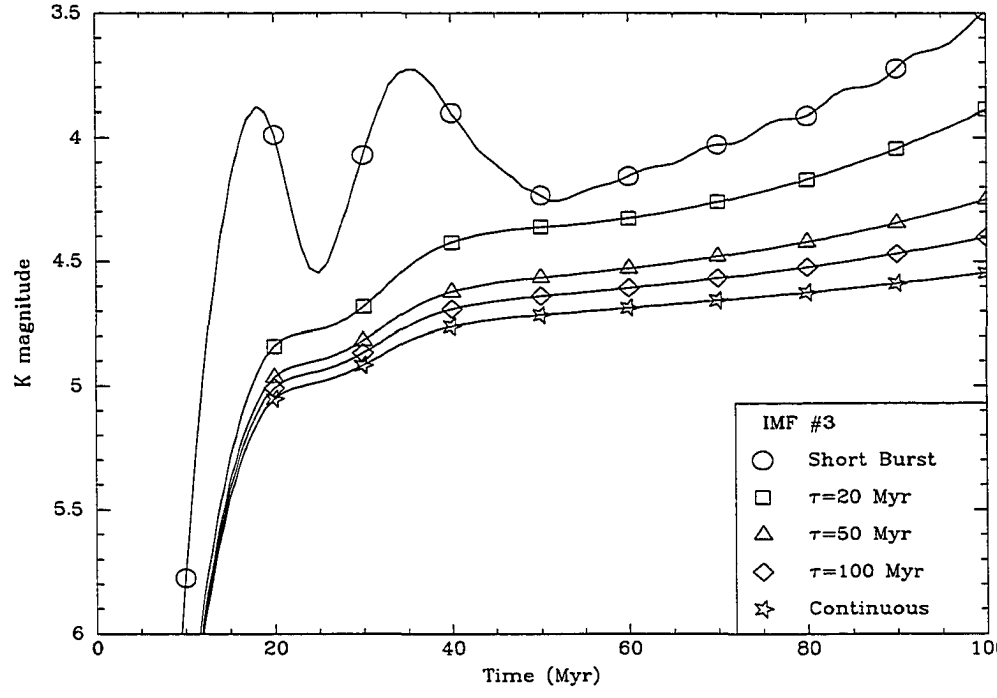

The K magnitude of the stellar populations models, scaled to $L_{BOL} = 1\ L_{\odot}$. Models with five star formation rates are shown: a short burst of star formation, lasting 5×10^6 yr, exponentially declining star formation with time constant, τ, equal to 20, 50, or 100 Myr, and a constant star formation rate.

Fig. 3.5.— K magnitude of IMF # 8 Models

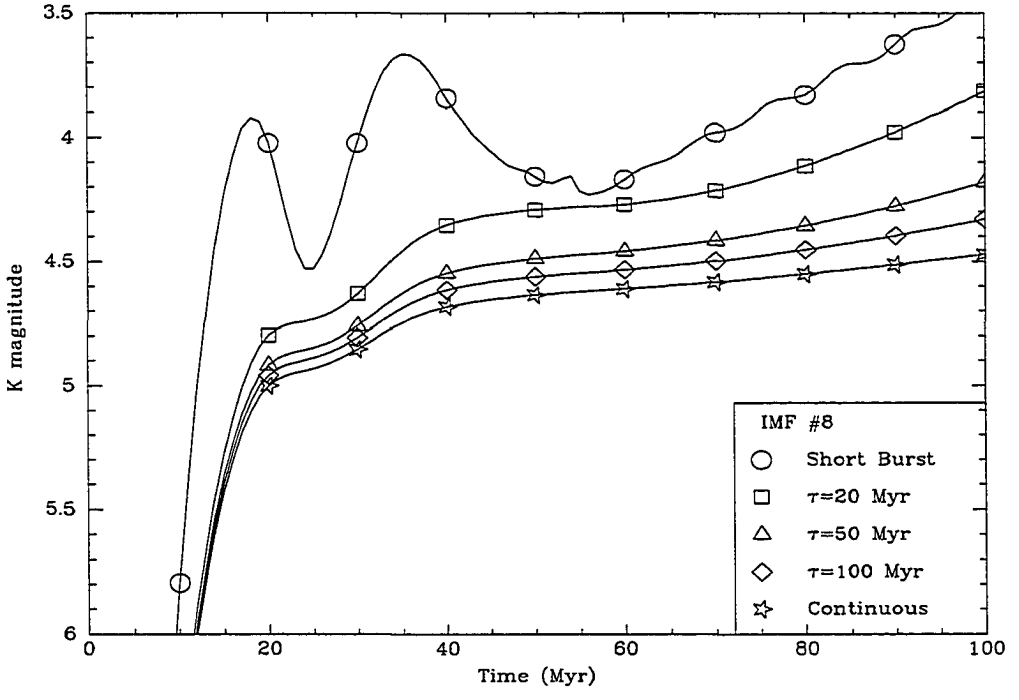

The K magnitude of the stellar populations models, scaled to $L_{BOL} = 1\ L_{\odot}$. Models with five star formation rates are shown: a short burst of star formation, lasting 5×10^6 yr, exponentially declining star formation with time constant, τ, equal to 20, 50, or 100 Myr, and a constant star formation rate.

Fig. 3.6.— CO Index of IMF # 3 Models

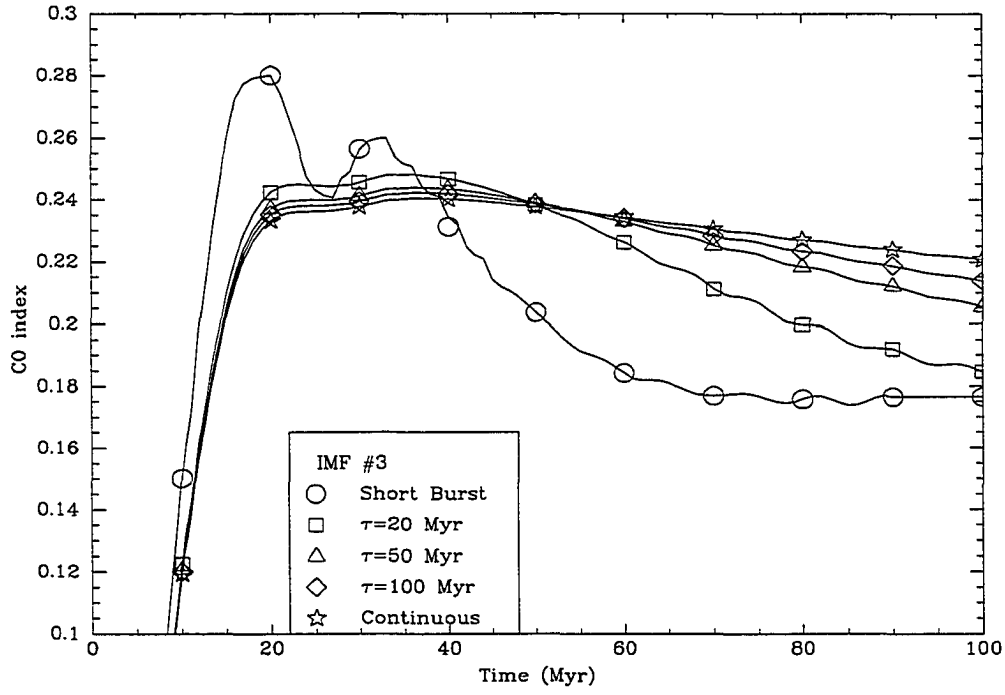

The CO index of the IMF # 3 models. Models with five star formation rates are shown: a short burst of star formation, lasting 5×10^6 yr, exponentially declining star formation with time constant, τ, equal to 20, 50, or 100 Myr, and a constant star formation rate.

Fig. 3.7.— CO Index of IMF # 8 Models

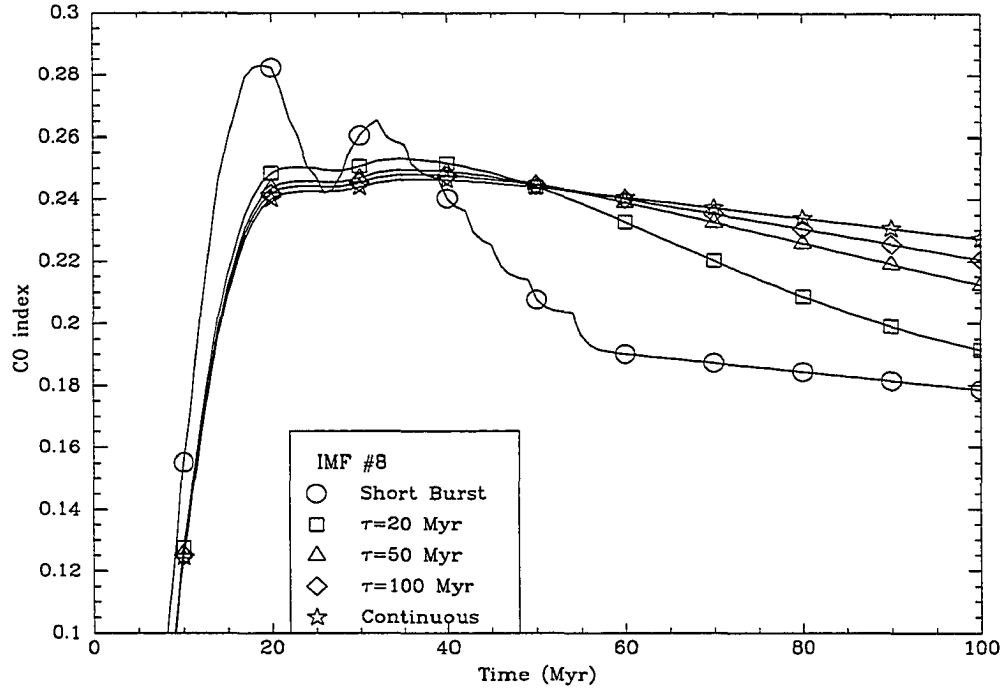

The CO index of the IMF # 8 models. Models with five star formation rates are shown: a short burst of star formation, lasting 5×10^6 yr, exponentially declining star formation with time constant, τ, equal to 20, 50, or 100 Myr, and a constant star formation rate.

Fig. 3.8.— Mass-to-Light Ratio of the IMF # 3 Models

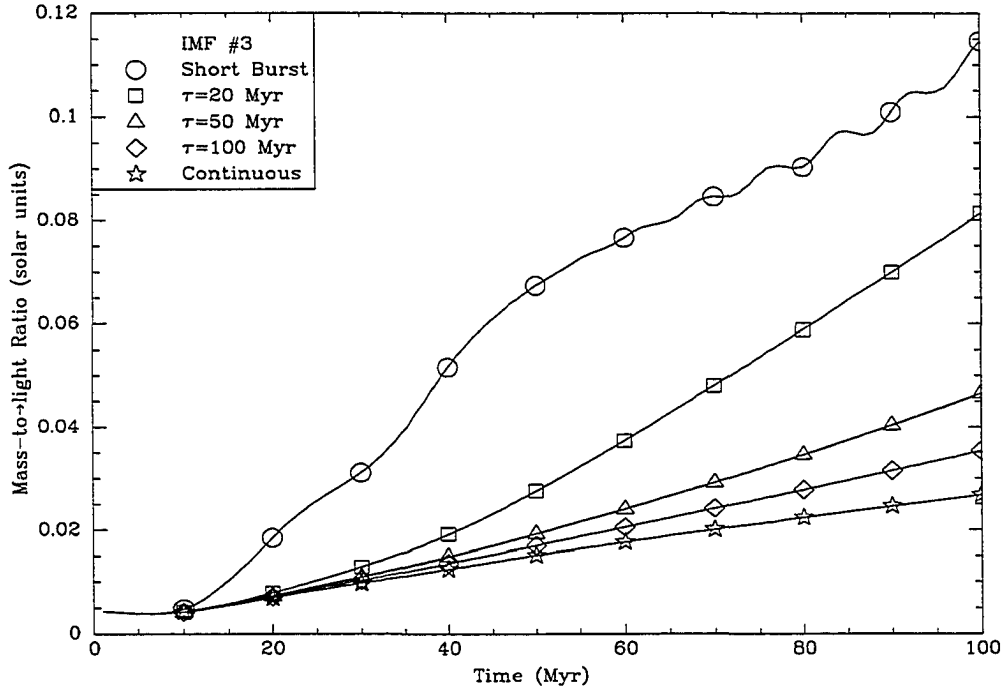

The mass-to-light ratio in $M_\odot/L_\odot$ of the IMF # 3 models. Models with five star formation rates are shown: a short burst of star formation, lasting 5×10^6 yr, exponentially declining star formation with time constant, τ equal to 20, 50, or 100 Myr, and a constant star formation rate.

Fig. 3.9.— Mass-to-Light Ratio of the IMF # 8 Models

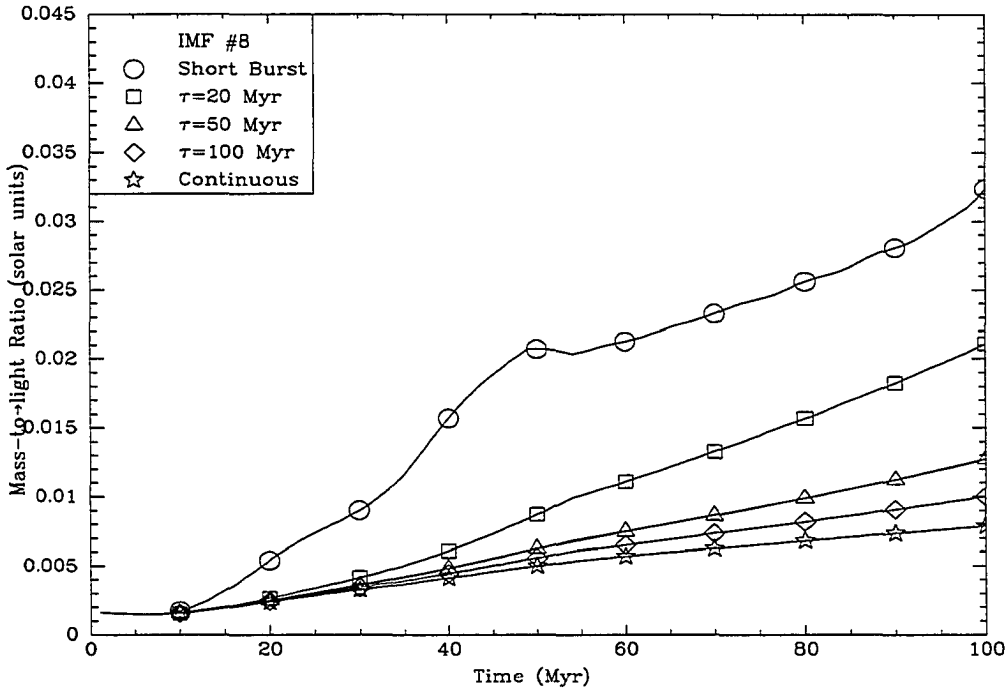

The mass-to-light ratio in $M_\odot/L_\odot$ of the IMF # 8 models. Models with five star formation rates are shown: a short burst of star formation, lasting 5×10^6 yr, exponentially declining star formation with time constant, τ, equal to 20, 50, or 100 Myr, and a constant star formation rate.

Fig. 3.10.— Galaxies in the log(UV) - M_K Plane and the IMF # 3 Models

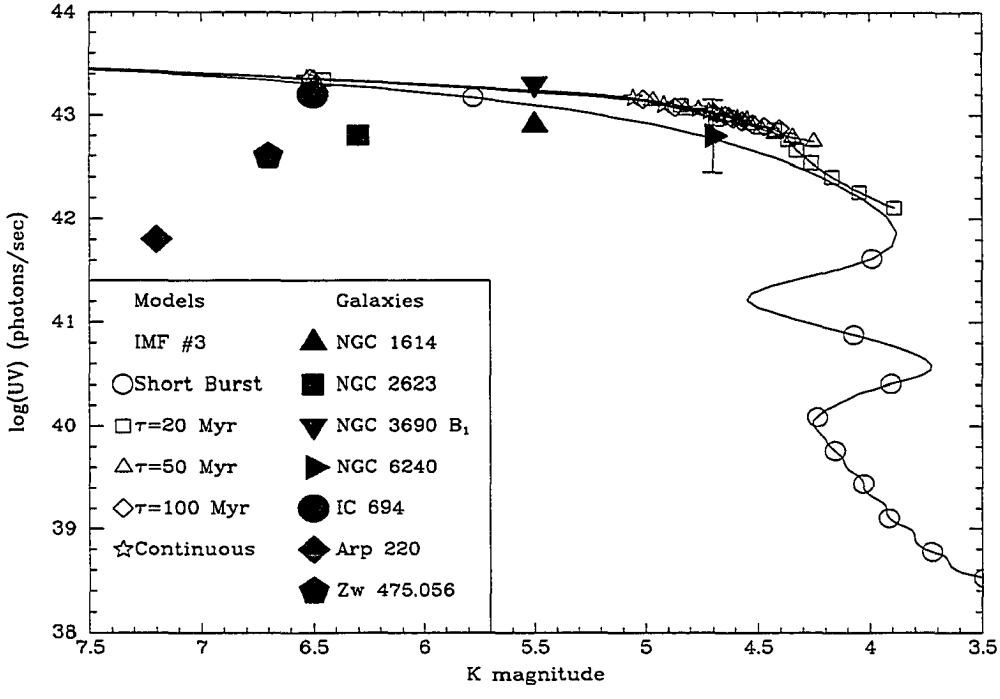

Comparison of the ionizing continuum luminosity and 2.2 μm luminosity of the galaxies and the IMF # 3 models. All luminosities have been normalized to L_{BOL} = 1 $L_{\odot}$. Models with five star formation rates are shown: a short burst of star formation, lasting 5×10^6 yr, exponentially declining star formation with time constant, τ, equal to 20, 50, or 100 Myr, and a constant star formation rate. Symbols appear every 10 Myr on the model tracks.

Fig. 3.11.— Galaxies in the log(UV) - M_K Plane and the IMF # 8 Models

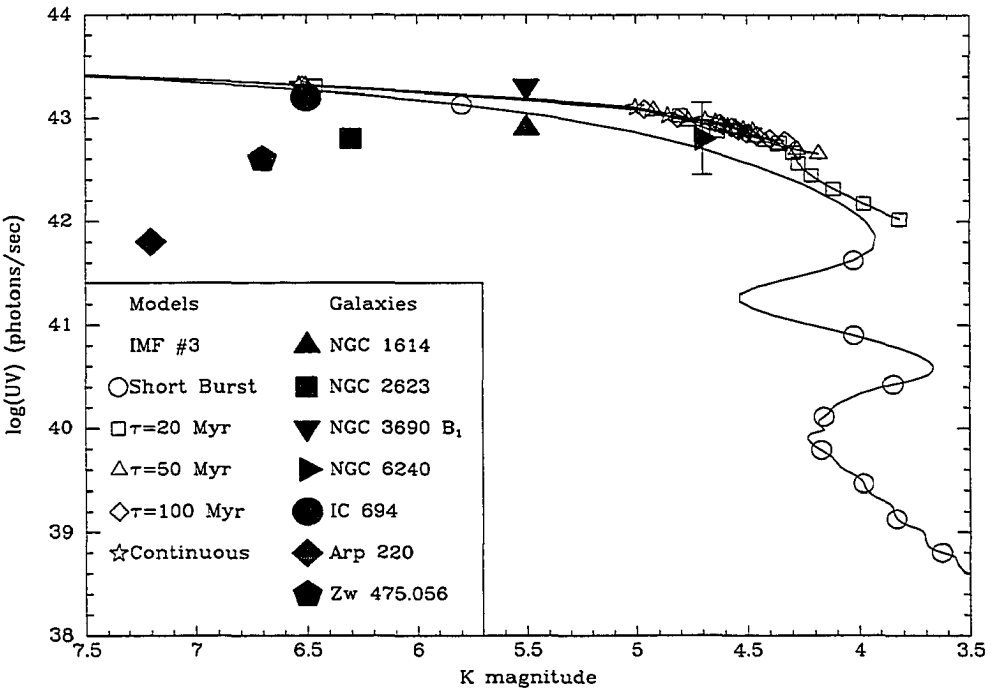

Comparison of the ionizing continuum luminosity and 2.2 μm luminosity of the galaxies and the IMF # 8 models. All luminosities have been normalized to L_{BOL} = 1 $L_{\odot}$. Models with five star formation rates are shown: a short burst of star formation, lasting 5×10^6 yr, exponentially declining star formation with time constant, τ, equal to 20, 50, or 100 Myr, and a constant star formation rate. Symbols appear every 10 Myr on the model tracks.

Fig. 3.12.— Galaxies in the CO Index - M/L Plane and the IMF # 3 Models

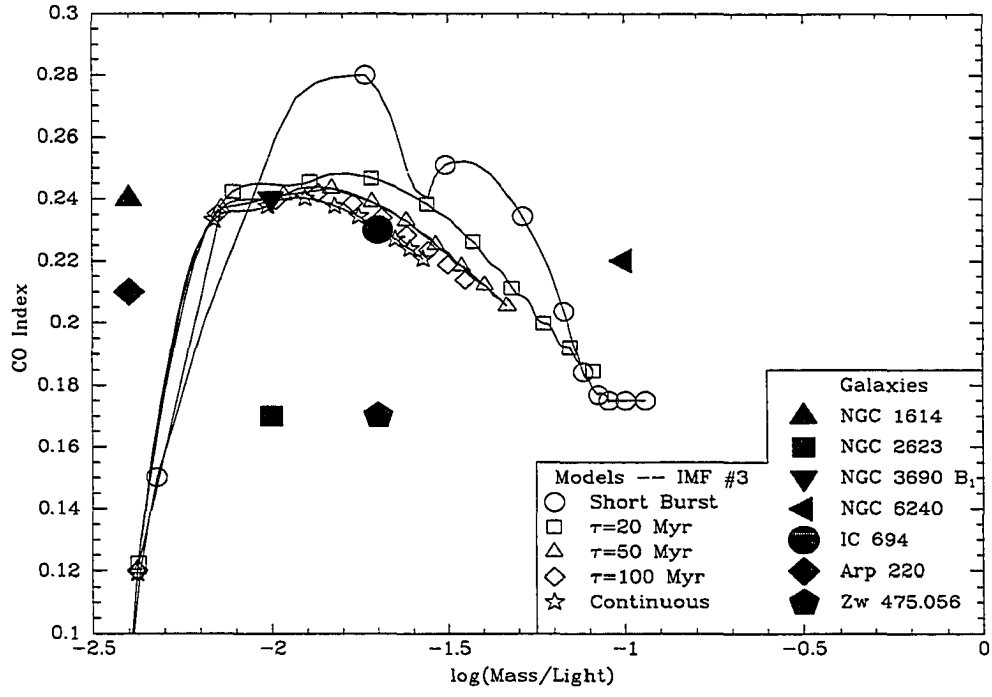

Comparison of the CO index and mass-to-light ratio of the galaxies and the IMF # 3 models. Models with five star formation rates are shown: a short burst of star formation, lasting 5×10^6 yr, exponentially declining star formation with time constant, τ, equal to 20, 50, or 100 Myr, and a constant star formation rate. Symbols appear every 10 Myr on the model tracks.

Fig. 3.13.— Galaxies in the CO Index - M/L Plane and the IMF # 8 Models

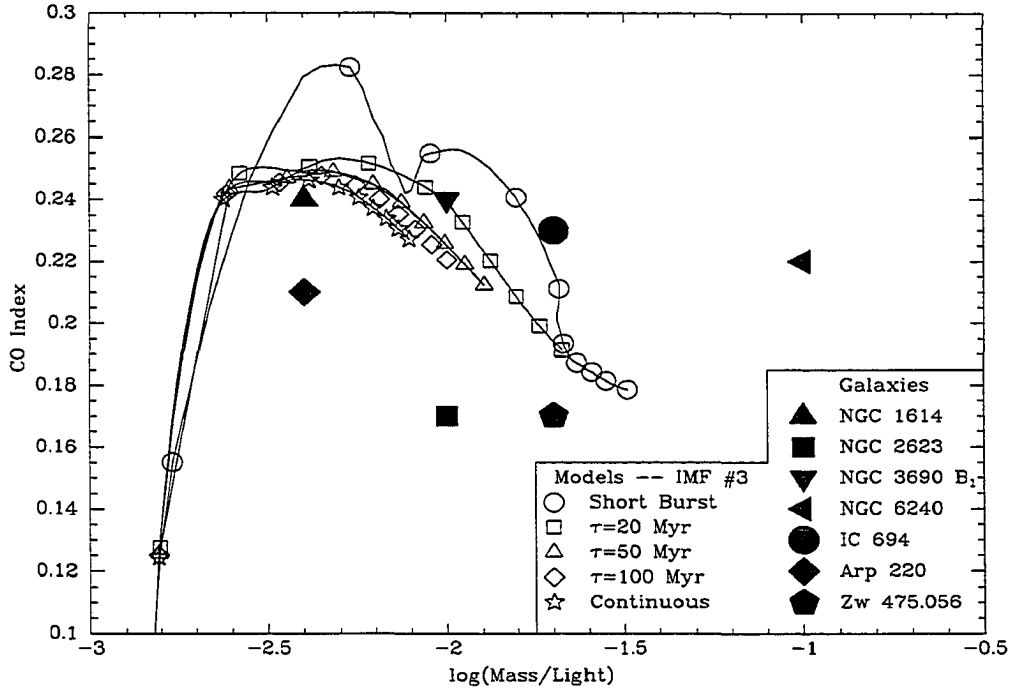

Comparison of the CO index and mass-to-light ratio of the galaxies and the IMF # 8 models. Models with five star formation rates are shown: a short burst of star formation, lasting 5×10^6 yr, exponentially declining star formation with time constant, τ, equal to 20, 50, or 100 Myr, and a constant star formation rate. Symbols appear every 10 Myr on the model tracks.

to calculate the ionizing continuum luminosity, then the stellar population is less luminous than the most luminous possible stellar population.

The above procedure can be refined by placing an upper limit on contribution of non-stellar sources to the 2.2 μm luminosity. Observations of the CO index allow limits to be placed on the fraction of the observed 2.2 μm luminosity which has a non-stellar origin. As discussed in Section 2.4, hot dust and synchrotron spectra do not have CO absorption bands. The addition of non-stellar flux to the K band weakens the CO bands. As shown in Figures 3.6 and 3.7, the CO index of a stellar population rarely exceeds 0.24. The maximum possible amount of non-stellar emission in the K band is thus found by determining how much non-stellar emission would reduce the CO index from 0.24 to the observed value. The nuclear K-L color and 10 μm flux density place additional constraints on the amount of hot dust emission at K. The fraction of the bolometric and 2.2 μm luminosities attributable to active nuclei is discussed below for Arp 220, IC 694, NGC 2623, and Zw 475. This information is summarized in Table 3.6.

As Table 3.6 indicates, the near-infrared light of all the galaxies identified as AGN is dominated by starlight. Searches for AGN based on the weakness of the CO index, such as that conducted by Ridgway et al. (1994), cannot identify any of the galaxies in the sample as AGN.

Table 3.6: Luminosity from an AGN

	% from AGN	
Galaxy	Bolometric	2.2 μm
Arp 220	92	6
IC 694	≥ 70	11
NGC 2623	≥ 60	16
Zw 475.056	≥ 75	9

The strong CO bands in Arp 220 require that at least 90% of the observed 2.3 μm flux of this galaxy be generated by stars. If the non-stellar emission at 2.3 μm is from hot dust, then dust can provide no more than 6% of the total K band luminosity. If it is assumed that a hidden active nucleus is contributing to the bolometric luminosity, but not the 2.2 μm luminosity, then it is possible to find stellar populations model which fit this galaxy. The stars produce 8% of the bolometric luminosity. The stellar population of this galaxy is discussed in detail in Chapter 4.

In IC 694, the CO index provides the strongest constraint on the age and luminosity of the stellar population. The population must be older than 12 Myr if the burst of star formation was very short, and older than 15 Myr if the star formation rate has an exponential decay time of 50 Myr or more. If the burst of star formation was quite short, the stars produce 20% or less of the bolometric luminosity, and 10% or less of the observed Brα luminosity. The more temporally extended star formation burst allows the stars to produce up to 30% of the bolometric luminosity and 20% of the observed Brα.

NGC 2623 must have an active nucleus, and it may not be completely hidden at near-infrared wavelengths, unlike the case of Arp 220. The arguments of Section 2.5 suggest that the stars contribute about 84% of the K band light. A stellar population like that in NGC 1614 is permitted for this galaxy. Such a population would produce 85% the 2.2 μm luminosity, 40% of the bolometric luminosity, and all of the observed Brγ flux. Such a scenario seems unlikely in view of the estimate that 15% of the K band continuum is nonstellar in origin. A combination of an AGN and a stellar population model older than 10 Myr is permitted by the observations if a large fraction of the Brγ flux is produced by the AGN.

Many models in which an AGN is combined with a stellar population are consistent with the observed properties of Zw 475.056. It is not possible to determine the exact nature of the stellar population, but some limits may be placed on its properties. stellar population of the galaxy has a CO index near 0.24, which is typical of the younger starburst models, then the stars produce about two-thirds of the observed 2.2 μm flux. If the stellar population produces 90% of the 2.2 μm light, 25% of the bolometric luminosity, and all of the observed recombination line flux, then this galaxy's stellar population could be very similar to that of NGC 1614. If the observed Balmer line flux is not entirely produced by stars, then starburst models older than 11 Myr are consistent with the observations.

3.5 Other Evidence

Under AGN unification schemes like that of Antonucci (1993), the AGN found here would be classed as extreme examples of Seyfert 2 galaxies. The broad line region is unseen, the narrow line region is barely detectable at best, and the near-infrared hot dust emission may be largely obscured or much weaker than the starburst-enhanced stellar continuum. A large fraction of the bolometric luminosity of the AGN is reprocessed by dust. This dust will reradiate isotropically, as it is believed to be optically thin in the far-infrared. There are few ways to look for the AGN directly, but searches at various wavelengths have provided some evidence for AGN in NGC 2623, Arp 220, and Zw 475.056.

The identification of some of the galaxies as AGN is supported by emission line studies, radio imaging data, and work on the far-infrared spectral energy distributions. The optical emission line ratios of the galaxies have been used to distinguish between AGN-like and H II region-like galaxies. Bushouse (1986) claims

that the [N II] / Hα ratio in NGC 2623 indicates that this galaxy is a LINER. Armus et al. (1989) used the methods of Veilleux & Osterbrock (1987) to classify the optical emission line spectra of six galaxies in the present sample. NGC 2623, Arp 220, and NGC 6240 have LINER-like emission line ratios. NGC 3690 is clearly an H II region-like galaxy and NGC 1614 and IC 694 have line ratios that are inconclusive. Veilleux et al. (1994) used similar methods to classify NGC 1614 as H II region-like, Arp 220 and Zw 475.056 as Seyfert 2 and NGC 6240 as a LINER. They note that the H II in many LINER galaxies may be ionized by shocks or very hot stars in dense environments. Broad Brα emission at 4μm was found in Arp 220 by Depoy et al. (1987), indicating that this galaxy does have an energetic, if heavily obscured, nucleus.

There have been searches for clues to the power source of very luminous galaxies in the radio region of the spectrum. Extended radio emission is seen by the VLA in many of the galaxies in the sample (Condon et al. 1991). Supernovae can produce strong extended radio emission in starburst galaxies. Three galaxies in the Condon et al. sample could contain radio point sources detectable with VLBI (Lonsdale, Smith & Lonsdale 1993). NGC 2623, Arp 220 and Zw 475.056 were observed with VLBI. In NGC 2623 a radio core with a brightness temperature exceeding 10^7 K was found. The core has a complex structure, but the data are consistent with an unresolved point source. A radio core was also found in Arp 220, but the structure is not consistent with a single high brightness temperature core. No VLBI core was found in Zw 475.056.

The far infrared spectral energy distributions of three sample galaxies were examined by Rowan-Robinson et al. (1989). On the basis of the fluxes in the four IRAS bands, they determined the contribution of a starburst, a normal stellar population, and an AGN to the radiation field heating the dust. They found the

dust in NGC 1614 to be heated almost entirely by a starburst. Both a starburst and a normal stellar population appear to be heating the dust in NGC 6240. They could not determine the nature of the central source in Arp 220, but concluded that it must be highly extincted.

Additional evidence for AGN in very luminous galaxies could come from space-based telescopes. Detection of gamma-rays or very small mid-infrared sources would provide additional support for the conclusion that Arp 220, IC 694, Zw 475.056, and NGC 2623 contain luminous AGN.

3.6 Summary

The comparison of the properties of seven very luminous infrared galaxies with stellar populations models allowed four of the galaxies to be identified as containing AGN. The remaining three galaxies have properties which are consistent with young stellar populations. The properties of Arp 220, IC 694, NGC 2623, and Zw 475.056 cannot be modeled with pure stellar populations. An AGN must be present to provide some of the bolometric luminosity. This AGN may also contribute to the 2.2 μm flux or the observed hydrogen recombination line flux. The active nucleus in these galaxies is producing at least 60% of the bolometric luminosity. The hot dust is contributing at least 6% of the of the 2.2 μm luminosity of these galaxies.

Chapter 4

STELLAR POPULATIONS

4.1 Introduction

In the previous Chapter, it was determined that three of the galaxies have observed properties that are consistent with those of stellar populations. Here the properties of the stellar populations of those galaxies are explored in detail. The mass, age, IMF and star formation history of the populations are examined. The stellar populations of the active galaxies are investigated, and limits placed on the ages of their stellar populations. It proved possible to obtain detailed information on the stellar population in Arp 220 because the active nucleus is obscured even in the near-infrared.

The very luminous infrared galaxies prove to be a highly nonuniform group. NGC 1614 cannot have a starburst with an IMF like that of the solar neighborhood. The local IMF requires less than 10% of the mass in NGC 6240. The possible ages of the stellar populations are 10 - 73 Myr. There is evidence for bursts of star formation, and also star formation on more extended time scales. An attempt was

made to determine the nature of the IMF of the starburst population. The stellar populations of the galaxies are discussed below.

4.2 Starburst Galaxies

4.2.1 NGC 1614

A few stellar population models were found which reproduce the observed properties of NGC 1614. None of the models with the local IMF could reproduce the luminosity of this galaxy, given the constraint on the total mass. Even for the IMF # 8 models, the mass-to-light ratio of this galaxy requires that the stellar population be less than $\approx$ 16 Myr old, as shown in Figure 3.13. The ionizing continuum is too high and the 2.2 μm luminosity too small for models younger than 11 Myr in the case of a short burst, and 15 Myr for any exponentially declining star formation rate model, as seen in Figures 3.10 and 3.11.

The best fit stellar population models feature a short, but quite intense, burst of star formation that occurred about 12 Myr ago. The properties of the model stellar population are compared to those of NGC 1614 in Figure 4.1. This figure demonstrates that the stellar population model and the galaxy have similar properties for only a short time. Stellar populations with continuing star formation are not allowed by the observations.

4.2.2 NGC 3690 B_1

The exact properties of NGC 3690 B_1 are difficult to determine, since many observations have insufficient spatial resolution to separate B_1 and B_2. If the

Fig. 4.1.— Stellar Population Model for NGC 1614

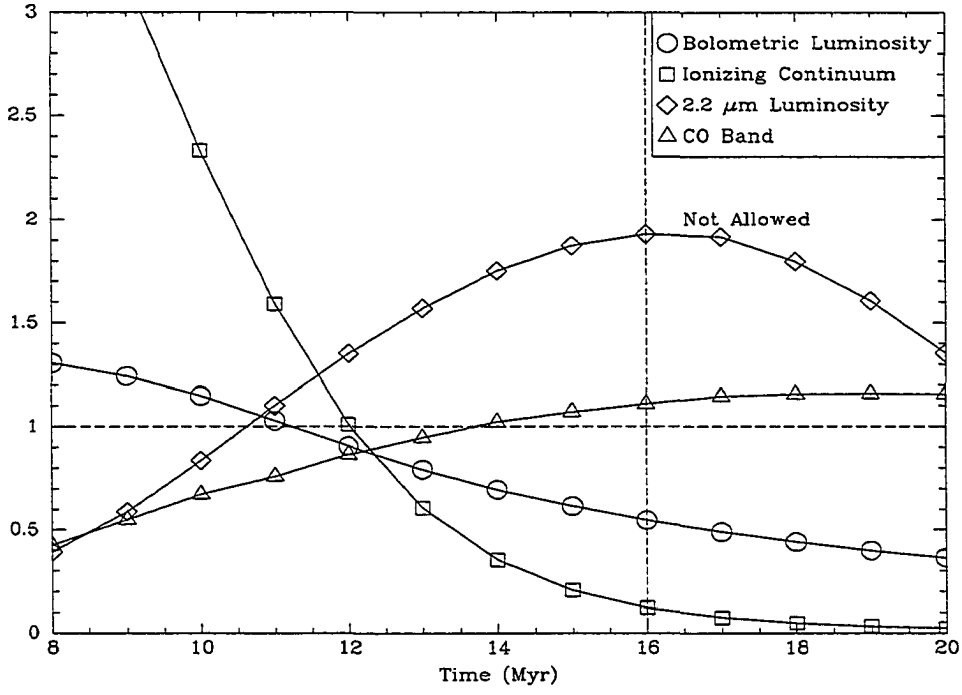

The best fitting model for the stellar population of NGC 1614. This model was created using IMF # 8 and a very short burst of star formation. This model has a mass of 7.4×10^8 $M_\odot$. All of the values for the luminosities have been divided by the values observed for the galaxy. Note that the region on the right hand side of the plot is not allowed by the observations because models older than 16 Myr have a mass-to-bolometric luminosity ratio in excess of that observed for the galaxy.

two sources have the same 2.2 μm-to-bolometric luminosity ratio, then a stellar population can be found which fits the properties of NGC 3690 B_1. The best fitting stellar populations are 10 Myr old. The star formation rate has an exponential decay time of 20 Myr or more. Figure 4.2 compares the properties of the stellar population model and NGC 3690 B_1. As in the case of NGC 1614, the model and the object have similar properties for only a short time. Models with short bursts of star formation are not a good fit to the properties of this object. The stellar population requires 20% or less of the mass of this object.

Since the bolometric luminosity of this object is not well determined, the consequences of other choices for the bolometric luminosity were considered. If the bolometric luminosity of NGC 3690 B_1 was under estimated, then stellar population models similar to those considered for NGC 1614 would be preferred to those discussed above. If NGC 3690 B_1 produces less than two-thirds of the bolometric luminosity of the combination of NGC 3690 B_1 and B_2, then this object must contain an AGN.

4.2.3 NGC 6240

NGC 6240 has the largest 2.2 μm-to-bolometric luminosity ratio of all the sample galaxies. The observed CO index is also the largest in the sample. The best fitting models for this galaxy had a very short burst of star formation about 13 Myr ago. However, models with quite different properties are also allowed by the observations. This galaxy might have a stellar population that has an exponentially declining star formation rate with time constant of 50 Myr or greater and an age of about 65 Myr. In the case of the older models, the IMF # 3 models fit the galaxy better than the IMF # 8 models. Figure 4.3 compares the properties of the young

Fig. 4.2.— Stellar Population Model for NGC 3690 B_1

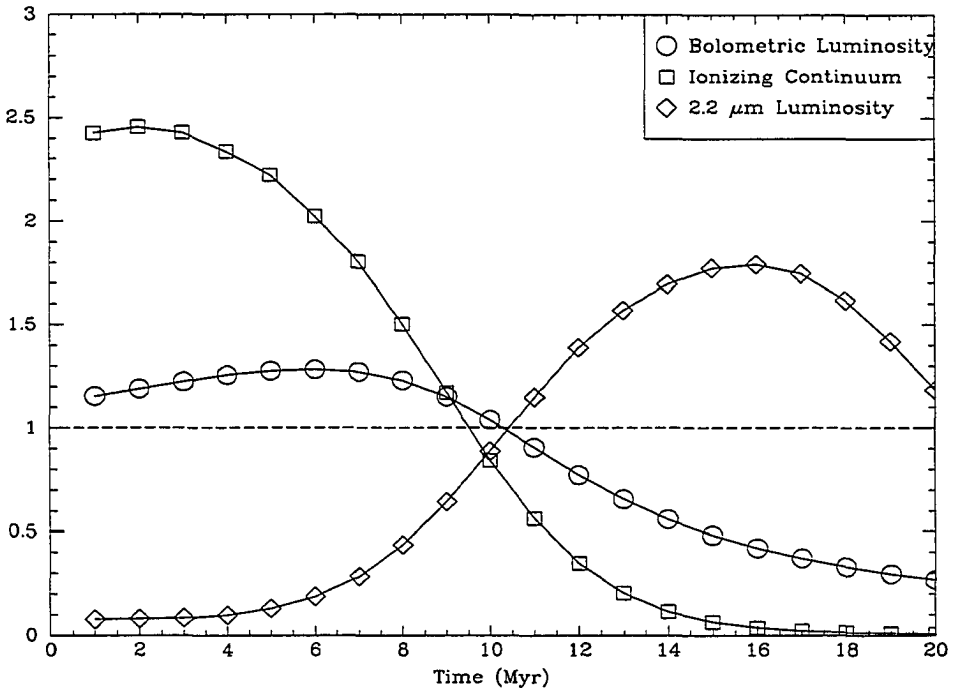

The best fitting model for the stellar population of NGC 3690 B_1. This model was created using IMF # 3 and a star formation rate that declines exponentially with a time constant of 50 Myr. The model has a mass of 5.4×10^8 $M_\odot$. All of the values for the luminosities have been divided by the values observed for the object. Data on the CO index is not included due to the uncertainty of the CO index of the object caused by the fact that the spectrum obtained for NGC 3690 is a composite of the spectra of NGC 3690 B_1 and B_2.

models to those of NGC 6240. All of the young models have properties which change rapidly, and the young model fits the properties of NGC 6240 for only a short period. The properties of NGC 6240 and the older model are compared in Figure 4.4. The properties of the older populations change slowly. Stellar population models with ages between 50 and 85 Myr provide acceptable fits. The tight time constraints on the young stellar population model make it probable that the older model for the stellar population is correct. If the ionizing continuum luminosity were better determined in this galaxy, some of the ambiguity about the stellar population could be removed. In all cases, less than 25% of the mass in the starburst region need be young stars.

4.3 Galaxies with Active Nuclei

4.3.1 Arp 220

There are no stellar population models with properties like those observed in Arp 220. The 2.2 μm-to-bolometric luminosity ratio is inconsistent with any of the stellar population models with ages over 10 Myr. Neither the CO index nor the ionizing continuum luminosity permit such a young age for the stellar population. This galaxy must contain a luminous AGN which generates a large fraction of the bolometric luminosity.

If it is assumed that a hidden active nucleus is contributing to the bolometric luminosity, but not the 2.2 μm luminosity, or the narrow Brα flux, then it is possible to find stellar population models for this galaxy. The best fitting stellar population model produces 8% of the bolometric luminosity. It has exponentially declining star formation rates with a time constant of 50 Myr and an age of 73 Myr.

Fig. 4.3.— Young Stellar Population Model for NGC 6240

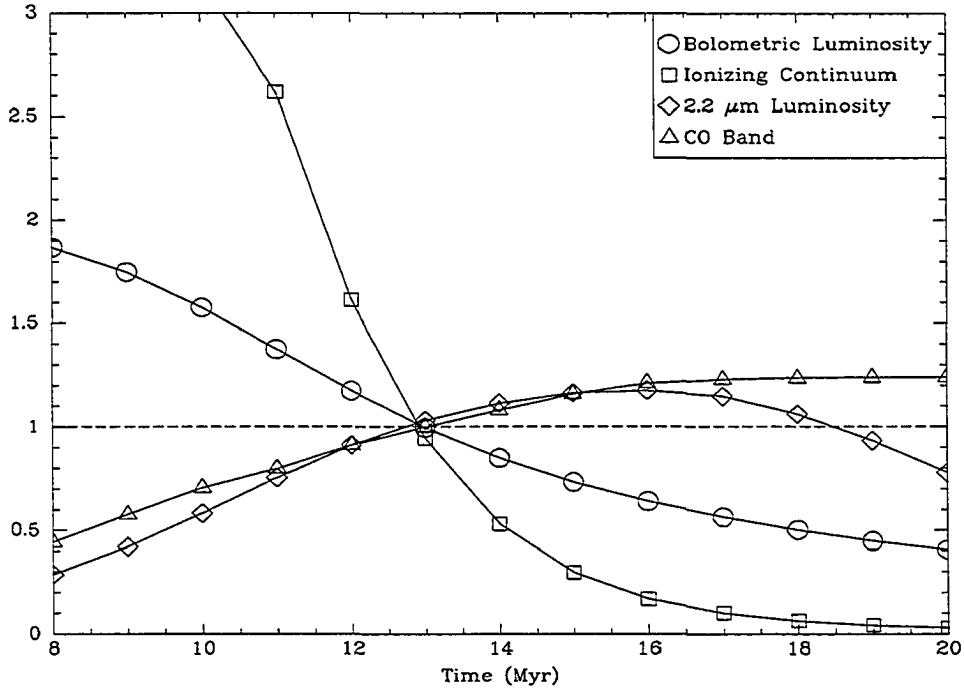

The best fitting model for the stellar population of NGC 6240. This model was created using IMF # 3 and a very short burst of star formation. This model has a mass of 2.2×10^9 $M_\odot$. All of the values for the luminosities have been divided by the values observed for the galaxy.

Fig. 4.4.— Older Stellar Population Model for NGC 6240

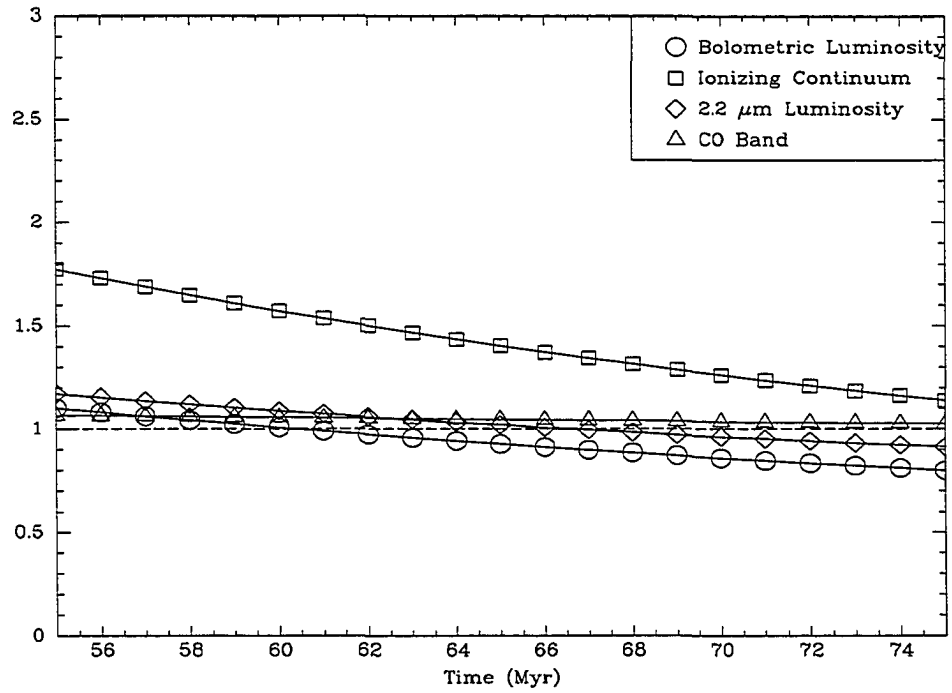

An alternate model for the stellar population of NGC 6240. This model is also allowed by the observations. The ionizing continuum flux for the model at 65 Myr is smaller than the upper limit set in Section 3.2.2. This model was created using IMF # 3 and a of star formation rate that declines exponentially with a time constant of 100 Myr. This model has a mass of 6.2×10^9 $M_\odot$. All of the values for the luminosities have been divided by the values observed for the galaxy.

The IMF # 3 model is a better fit than the IMF # 8 model. Figure 4.5 compared the properties of the model and the galaxy. If some of the observed narrow Brα flux is generated by the AGN, then the stellar population must be older than 73 Myr. The model requires that 72% of the total mass be in the form of stars.

4.3.2 IC 694

The properties of this galaxy are not consistent with the properties of any of the stellar population models. The galaxy does lie near the model tracks in Figures 3.10 and 3.11, but the CO index is much larger than that of any of the population models under 10 Myr. Mixtures of starbursts of different ages failed to reproduce the properties of this galaxy. The CO index requires that the stellar population be older than 12 Myr if the burst of star formation was very short, and older than 15 Myr if the star formation rate has an exponential decay time of 50 Myr or more.

4.3.3 NGC 2623 and Zw 475.056

Neither of these galaxies could be fit with any stellar population model. The ratio of 2.2 μm-to-bolometric luminosity is inconsistent with any stellar population more than 10 Myr old, and the ionizing continuum flux is inconsistent with such a stellar population. Additionally, the CO index of these galaxies is lower than that of any of the models over 10 Myr old. Either of these galaxies could have a stellar population like NGC 1614. If some of the observed emission line flux is produced by the AGN, then the stellar population is older than 10 Myr. Older stellar population models do require that some of the 2.3 μm flux be synchrotron radiation or light from an older or intermediate age stellar population.

Fig. 4.5.— Stellar Population Model for Arp 220

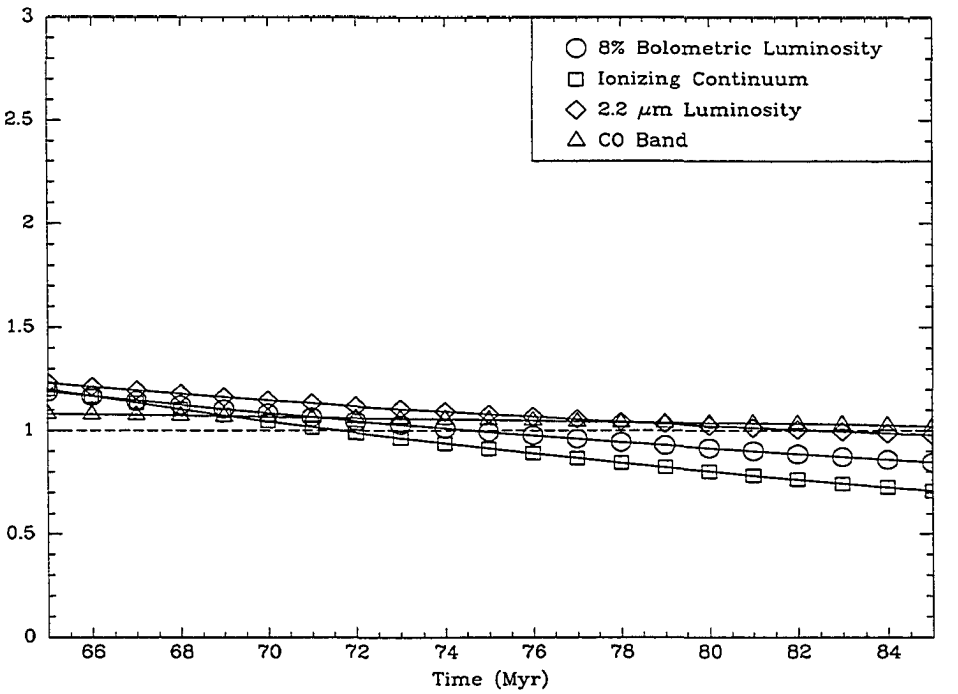

The best fitting model for the stellar population of Arp 220. This model was created using IMF # 3 and star formation rate which declines exponentially with a time constant of 50 Myr. This model has a mass of 3.3×10^9 $M_\odot$. All of the values for the observable parameters except for the bolometric luminosity have been divided by the values observed for the galaxy. The bolometric luminosity of the stars is taken to be 1×11^{10} $L_\odot$, or 8% of the observed bolometric luminosity.

The strong Balmer absorption lines in NGC 2623 led Armus et al. (1987) to suggest that a substantial intermediate age (about 1 Gyr) stellar population is present in this galaxy. However, some of the stars in this galaxy are clearly young. The 2.2 μm luminosity-to-mass ratio will not permit single age stellar populations older than 300 Myr in this galaxy.

4.4 Discussion

The properties of the stellar population in seven very luminous infrared galaxies were investigated. Observations of the galaxies and model stellar populations were compared. Detailed analyses were possible for three starburst galaxies, NGC 1614, NGC 3690 B_1, and NGC 6240. The near-infrared properties of Arp 220 are so dominated by its stellar population that considerable information on the stellar population could be obtained, even though this population produces less than 10% of the bolometric luminosity. Some limits were placed on the properties of the stellar populations in three galaxies with active nuclei. The properties of the stellar populations are summarized in Table 4.1.

The stellar populations have a range of ages. NGC 1614 and NGC 3690 B_1 appear to have very young stellar populations. The conclusion NGC 1614 has a very young stellar population is supported by other evidence. Wolf-Rayet features were discovered in the spectrum of this galaxy (Vacca & Conti 1992). Models of the optical spectra of this galaxy suggest that star formation occurred in a short burst in this galaxy. NGC 6240 and Arp 220 have more mature starbursts than NGC 1614, about 50 - 80 Myr old. Star formation is still occurring in these galaxies. These results are consistent with the stellar population modeling of Arp 220 and NGC 6240 by Rieke et al. (1985). IC 693, NGC 2623 and Zw 475.056 must have

stellar populations older than 10 Myr.

The IMF of the stars in all the very luminous infrared galaxies may be more heavily weighted towards high mass stars than the IMF of the solar neighborhood. NGC 1614 clearly has an IMF unlike that seen locally. If a large fraction of the mass in the center of Arp 220 consists of old stars, or H_2, then the solar neighborhood IMF may not be correct for this galaxy. The solar neighborhood IMF is still allowed in this galaxy if $H_o = 100$ km/s/Mpc, but nearly all of the mass would be required to be in young stars.

Table 4.1: Starburst Model Properties

Galaxy	IMF	SFR	Age Myr	Mass $M_\odot$	% mass in starburst
NGC 1614	# 8	Short Burst	12	7.4×10^8	49
NGC 3690 B_1	# 3	$\tau > 20$ Myr	10	5.4×10^8	20
	# 8	$\tau > 20$ Myr	10	1.9×10^8	7
NGC 6240	# 3	Short Burst	13	2.2×10^9	8
	# 8	Short Burst	13	7.3×10^8	2
	# 3	$\tau = 100$ Myr	65	6.2×10^9	21
Arp 220	# 3	$\tau = 50$ Myr	73	3.3×10^9	72
IC 694	...	Short Burst	> 12	...	...
	...	$\tau > 50$ Myr	> 15	...	...
NGC 2623	...	...	> 10	...	...
Zw 475.056	...	...	> 10	...	...

Chapter 5

COMPARISON OF DYNAMICAL AND MOLECULAR GAS MASSES

5.1 Introduction

Very luminous infrared galaxies also have large luminosities in the ^{12}CO J=1→0 rotation transition which have been interpreted to mean that the galaxies contain enormous amounts of molecular gas, especially in their centers (Sargent & Welch 1993; Scoville et al. 1991). The H_2 mass is usually determined by applying a conversion between ^{12}CO J=1→0 flux and H_2 mass determined from observations of giant molecular clouds in the Milky Way (Young & Scoville 1991). However, there is some controversy about the large inferred H_2 masses because the I_{CO}/M_{H_2} ratio in luminous infrared galaxies, and especially in their centers, may be very different from that in the giant molecular clouds of the Milky Way disk (Maloney

& Black 1988; Aalto et al. 1991; Downes, Solomon & Radford 1993; Aalto et al. 1994).

One obvious limit to the H_2 mass is that it may not exceed the total mass present. The data and techniques described in Chapter 2 were used to measure the dynamical mass of the regions with strong ^{12}CO J=1→0 emission in three luminous infrared galaxies. The three galaxies discussed here - Arp 220, NGC 1614, and IC 694 - were selected on the basis of their high ^{12}CO J=1→0 luminosity and the availability of high-resolution images in the ^{12}CO J=1→0 transition.

The comparison of the total dynamical masses of the three galaxies with their previously deduced H_2 contents provides an observational test of the methods for measuring the H_2 mass. This test is a important step in determining the true molecular gas content of very luminous infrared galaxies.

5.2 ^{12}CO J=1→0 Observations

Interferometer observations have been made of the ^{12}CO J=1→0 rotation transition in NGC 1614, IC 694, and Arp 220 (Sargent & Scoville 1991; Scoville et al. 1991). In each galaxy, a small core of extremely bright emission was found. The flux of the core was used to estimate the molecular gas content of the core.

Sargent & Scoville (1991) observed IC 694 and found strong ^{12}CO J=1→0 emission in the central 2″.7= 500 pc. They used the Galactic I_{CO}/M_{H_2} ratio to infer a H_2 mass of $3.9 \times 10^9 M_\odot$. Observations of NGC 1614 produced an H_2 mass estimate of $6 \times 10^9 M_\odot$ for the inner 2″=1.2 kpc (Scoville et al. 1991). Arp 220 was observed by Scoville et al. (1991). They found a 1″.4 × 1″.9 (500 × 640 pc) core containing an estimated $1.8 \times 10^{10} M_\odot$ of H_2.

5.3 Dynamical Mass

The total mass in the region of strong ^{12}CO J=1→0 emission was computed from the stellar kinematics and tabulated in Table 5.1. These masses were calculated from the velocity dispersions listed in Table 2.5. The procedures used in the calculation were the same as those described in Section 2.6. However, the size of the starburst region, as determined in Section 3.2.1, is not the same as the size of the core of ^{12}CO J=1→0 emission described in Section 5.2, so the masses listed in Table 5.1 differ from those in Tables 2.6 and 2.7.

Table 5.1 demonstrates that the dynamical mass is not significantly affected by the choice of kinematic and structural models for the galaxies. The total dynamical mass, as determined from stellar kinematics, is free from large systematic errors.

5.4 Discussion

The masses derived in Section 5.3 provide an upper limit to the mass of any individual component in the center of the galaxies, including H_2. Therefore, the validity of the use of the Galactic I_{CO}/M_{H_2} ratio (Scoville & Sanders 1987) to measure M_{H_2} in the centers of luminous IRAS galaxies can be tested. In all three

Table 5.1: Dynamical Masses of ^{12}CO J=1→0 Cores

Galaxy	r_{CO}	$M(r < r_{CO})$		
		$\eta = 2$ spheroid	$\eta = 3$ spheroid	disk
	pc	$10^9 M_\odot$	$10^9 M_\odot$	$10^9 M_\odot$
NGC 1614	600	2.1 ± 0.6	2.0 ± 0.6	2.1 ± 0.6
IC 694	250	3.1 ± 1.4	2.7 ± 1.2	2.8 ± 1.2
Arp 220	350	4.4 ± 1.2	2.5 ± 0.7	3.6 ± 1.0

galaxies, the masses obtained from the ^{12}CO J=1→0 flux are larger than the total dynamical mass.

The upper limits on the total molecular gas content become smaller if the contribution of stars to the total mass is considered. The stellar population in all three galaxies is quite luminous, so a significant amount of mass in the centers of each of the galaxies must be in the form of stars and not H_2. The stellar populations of the galaxies are discussed in detail in Chapter 4. Models of NGC 1614 require that at least 50% of the mass be in the form of stars. The models of Arp 220 require that at least 28% of the mass be in the form of stars. Consideration of the stellar mass places upper limits on the H_2 mass of $1.2 \times 10^9 M_\odot$ in the center of NGC 1614, and $1.8 \times 10^9 M_\odot$ in the center of Arp 220.

The reported H_2 masses are larger by a factor of 2 - 10 than the upper limits resulting from subtraction of the mass of the stars from the total kinematic masses. The molecular gas mass estimates and the kinematic mass calculations depend on the assumed distances to the galaxies in differing ways, so their ratio goes as $1/H_o$. Even if H_o is 100, the reported molecular gas masses are larger than the dynamical masses in NGC 1614 and Arp 220 by a factor of 8.

Detailed modeling of the molecular line emission in NGC 1808 by Aalto et al. (1994) led to the conclusion that the molecular gas mass in the center of that galaxy is also smaller than the mass estimated from the ^{12}CO J=1→0 flux and the standard I_{CO}/M_{H_2} conversion factor. The modeling of the line emission suggested that high pressure at the center of NGC 1808 galaxy leads to molecular cloud envelopes that are smaller and denser than their Milky Way counterparts. This difference in the physical state of the gas leads to a I_{CO}/M_{H_2} conversion factor which is different from that observed in Milky Way giant molecular clouds.

5.5 Conclusion

Masses have been determined for the central regions of IC 694, NGC 1614 and Arp 220 using stellar dynamics. In all three galaxies, the total dynamical mass of the ^{12}CO J=1→0 core is less than the H_2 mass inferred from the ^{12}CO J=1→0 flux and the standard I_{CO}/M_{H_2} conversion factor. Consideration of the likely mass of the stellar populations in the galaxies places even lower limits on the molecular gas mass. The conversion factor found for Milky Way GMCs is evidently not correct for these luminous infrared galaxies. The true H_2 content of these galaxies and the gas mass fraction must be determined by more detailed observations and modeling of the state of the molecular gas.

Chapter 6

CONCLUSIONS

The power source, stellar population, and molecular gas content of seven very luminous galaxies were examined. The mass of each of the nuclei of the galaxies was measured from the stellar velocity dispersion. The spectra used to determine the velocity dispersion were also used to measure the CO index. The bolometric, 2.2 μm, and ionizing continuum luminosity of the galaxies was determined. These properties of the galaxies were compared to the properties of stellar population models to determine if a galaxy could powered entirely by stars or by a mixture of stars and an AGN. The age and star formation rate of the stellar population were determined. The dynamical masses of three galaxies were compared to the claimed molecular gas mass to test whether the molecular gas mass measurements are accurate.

Many of the techniques previously developed for the study of galaxies and stellar populations must be modified for use in infrared galaxies. The extinction in the galaxies is quite large, and difficult to model. Observations at infrared wavelengths are less affected by extinction, and thus provide more accurate

information on the state of infrared galaxies. The gas kinematics may be affected by a variety of nongravitational forces, so stellar kinematics must be used for mass determinations.

Dynamical masses were measured for the centers of seven galaxies using a combination of new and traditional techniques. Stellar velocity dispersions were measured from the 2.3 μm overtone bands of ^{12}CO. The cross-correlation method pioneered by Tonry & Davis (1979) was used to measure the velocity dispersion. New techniques had to be developed for continuum subtraction due to the unusual shape of galaxy spectra near 2.3 μm. New models for the structure of kinematically hot galaxies (Tremaine et al. 1993) were used to convert the stellar velocity dispersions into dynamical masses. It was shown that extinction, mass-to-K band light ratios and differences in kinematic models for the galaxies have minimal impact on the derived masses. The CO index was measured from the spectra as well, using the methods of Kleinmann & Hall (1986).

The 2.2 μm luminosity of the galaxies was determined from K band images and near-infrared colors. The K fluxes were corrected for hot dust emission. The foreground screen model was used to determine the extinction to the stars. The distances were inferred from the redshift of the galaxies, using H_o=75 km/s/Mpc.

The ionizing continuum luminosity and the bolometric luminosity of each galaxy studied were determined from previously published data. Hydrogen recombination line fluxes were used to determine the extinction to the gas and the ionizing continuum luminosity. The bolometric luminosity was assumed to be nearly the same as the far-infrared luminosity measured by IRAS.

The properties of a suite of starburst stellar population models were compared to the observed properties of the galaxies to determine the nature of the power

source and stellar populations of these galaxies.

It was found that four of the seven galaxies – Arp 220, IC 694, NGC 2623, and Zw 475.056 – must contain active nuclei. The active nuclei in each of these galaxies provides more than 60% of the bolometric luminosity but less than 35% of the observed 2.2 μm luminosity. The other three galaxies in the sample may be modeled as pure starburst populations.

NGC 1614, IC 694, and Arp 220 are known to have small cores with bright ^{12}CO J=1$\rightarrow$0 emission. The H_2 mass inferred from the ^{12}CO J=1$\rightarrow$0 flux and the standard I_{CO}/M_{H_2} conversion factor was compared to dynamical masses for the core region determined from stellar velocity dispersions. In all three galaxies, the total dynamical mass of the ^{12}CO J=1$\rightarrow$0 core is less than claimed H_2 mass. Some of the mass in the centers of these galaxies must be in the form of stars, so the upper limit on the H_2 content is lower than that obtained from the velocity dispersion alone.

The I_{CO}/M_{H_2} conversion factor found for Milky Way GMCs is evidently not correct for some very luminous infrared galaxies. The true H_2 content of these galaxies and the gas mass fraction must be determined by more detailed observations and modeling of the state of the molecular gas.

There is no requirement that all very luminous infrared galaxies contain luminous active nuclei, nor is there any evidence that all of the very luminous infrared galaxies will eventually become AGN. The infrared galaxies can have many possible fates, as suggested by Neff & Hutchings (1991). The galaxies with AGN, like Arp 220, may evolve into optically selected AGN as supernovae and the central engine remove the obscuring dust from the circumnuclear regions, as was described by Sanders et al. (1988). The infrared galaxies with luminous AGN may

be galaxies which had a massive black hole before a starburst occurred. A nuclear starburst creates conditions in which a black hole with a mass greater than 10^6 $M_\odot$ can rapidly accrete matter (Norman & Scoville 1988).

The galaxies which do not have AGN will become normal galaxies as the starburst fades. Numerical simulations of galaxy mergers suggest that the remnant becomes an elliptical galaxy. The techniques developed here for kinematic examination of the stellar population in infrared galaxies will be important in the refinement of the stellar dynamical models of merging galaxies. Further information on the fate of the very luminous infrared galaxies may be obtained by study of morphologically selected post-merger galaxies, and their stellar populations.

It is likely that all of the the ultraluminous ($L > 10^{12}$ $L_\odot$) galaxies contain AGN, and derive most of their luminosity from that central engine. None of the stellar populations in Table 4.1 are capable of producing more than 6×10^{11} $L_\odot$ at any point in their evolution. The value of L_* for starburst galaxies may be higher than the value of 3×10^{11} $L_\odot$ for normal galaxies, but it is likely less than 10^{12} $L_\odot$. The value of L_* for starburst galaxies can be determined through stellar population modeling of a larger sample of very luminous and ultraluminous galaxies.

Some of the conclusions of this thesis could be strengthened if limits could be placed on the mass of the pre-starburst stellar population. Detailed modeling of the structure and kinematics of the very luminous infrared galaxies can provide information on the total mass, and likely stellar mass of the infrared galaxies before they interacted strongly. Estimates of the pre-starburst stellar mass would allow tighter limits to be placed on the initial mass function of the starburst, particularly in Arp 220. Knowledge of the pre-starburst stellar mass would also allow better estimates of the molecular gas mass to be made, which could lead to a better

understanding of the temperature, density and filling factor of this interstellar medium component.

REFERENCES

Aalto, S., Black, J. H., Johansson, L. E. B., & Booth, R. S. 1991, A&A, 249, 323

Aalto, S., Booth, R. S., Black, J. H., Koribalski, B., Weilebinski, R. 1994, A&A, 286, 365

Anantharamaiah, K. R., Zhao, J.-H., Goss, W. M., & Viallefond, F. 1993, ApJ, 419, 585

Antonucci, R. 1993, ARA&A, 31, 473

Armus, L., Heckman, T. L., & Miley, G. K. 1989, ApJ, 347, 727

Barnes, J. E. & Hernquist, L. E. 1991, ApJ, 370, L65

Basu, S. & Rana, N. C. 1992, ApJ, 393, 373

Beck, S. C., Turner, J. L., & Ho, P. T. P. 1986, ApJ, 309, 70

Beck, S. C., Turner, J. L., & Ho, P. T. P. 1990, ApJ, 359, 57

Binney, J. & Tremaine, S. 1987, Galactic Dynamics (Princeton, NJ: Princeton University Press)

Bushouse, H. A. 1986, AJ, 91, 255

Bushouse, H. A. & Gallager III, J. S. 1984, PASP, 96, 273

Cardelli, J. M., Clayton, G. C., & Mathis, J. S. 1989, ApJ, 345, 245

Carico, D. P., Sanders, D. B., Soifer, B. T., Matthews, K., & Neugebauer, G. 1990, AJ, 100, 70

Condon, J. J., Huang, Z. P., Yin, Q. F., & Thuan, T. X. 1991, ApJ, 378, 65

Depoy, D. L., Becklin, E. E., & Geballe, T. R. 1987, ApJ, 315, L63

Depoy, D. L., Becklin, E. E., & Wynn-Williams 1986, ApJ, 307, 116

Downes, D., Solomon, P. M., & Radford, S. J. E. 1993, ApJ, 414, L13

Doyon, R., Joeseph, R. D., & Wright, G. S. 1994, ApJ421, 101

Doyon, R., Puxley, P. J., & Joseph, R. D. 1992, ApJ, 397, 117

Doyon, R., Wells, M., Wright, G. S., Joseph, R. D., Nadeau, D., & James, P. A. 1994, ApJ, 437, L23

Eales, S. A., Becklin, E. E., Hodapp, K.-W., Simons, D. A., & Wynn-Williams, C. G. 1990, ApJ, 365, 478

Elston, R. & Maloney, P. 1990, ApJ, 357, 91

Fischer, J., Smith, H. A. & Glaccum, W. 1991 in Astrophysics with Infrared Arrays ASP Conference Series vol. 14 ed. R. Elston, (San Francisco: Astronomical Society of the Pacific) 63

Forbes, D. A., Ward, M. J., Depoy, D. L., Boisson, C., & Smith, M. S. 1992 MNRAS, 254, 509

Frogel, J. A., Persson, S. E., Aaronson, M., & Matthews, K. 1978, ApJ, 220, 75

Gaffney, N. I., Lester, D. F., & Doppmann, G. 1995, PASP. 107, 68

Gaffney, N. I., Lester, D. E., & Telesco, C. M. 1993 ApJ, 407, L57

Gehrz, R. D., Sramek, R. A., & Weedman, D. W. 1983, ApJ, 267, 551

Graham, J. R., Carico, D. P., Mathews, K., Neugebauer, G., Soifer, B. T., & Wilson, T. D. 1990, ApJ, 354, L5

Hernquist, L. 1993 ApJ, 409, 548

Hutchings J. B. & Neff, S. G. 1991, AJ, 101, 434

Joy, M., Lester, D. F., Harvey, P. M., Telesco, C. M., Decher, R., Rickard, L. J., & Bushouse, H. 1989, ApJ, 339, 100

Joy, M. & Harvey, P. M. 1987, ApJ, 315, 480

Keel, W. C. 1984, ApJ, 282, 75

Keel, W. C., Kennicutt, R. C., Hummel, E., van der Hulst, J. M. 1985, AJ, 90, 708

Kleinmann, S. G., & Hall, D. N. B. 1986, ApJS, 62, 501

Keto, E., Ball, R., Arens, J., Jernigan, G., Meixner, M. 1992, ApJ, 387, 117

Lake, G. & Dressler, A. 1986, ApJ, 310, 605

Larsen, N., Nørgaard-Nielson, H. U., Kjærgaard, P.,& Dickens, R. J. 1983, A&A, 117, 264

Lester, D. F. & Gaffney, N. I. 1994, ApJ, 413, L13

Lester, D. F., Harvey, P. M., & Carr, J. 1988, ApJ, 329, 641

Lonsdale, C. J., Smith, H. E., & Lonsdale, C. J. 1993, ApJ, 405, L9

Maeder, A. & Meynet, G. 1988, A&AS, 76, 411

McAlary, C. W. & Rieke, G. H. 1988, ApJ, 333, 1

Maloney, P. & Black, J. H. 1988, ApJ, 325, 389

Moorwood, A. F. M., & Oliva, E. 1988, A&A, 203, 278

Nakagawa, T., Nagata, T., Geballe, T. R., Okuda, H., Shibai, H., & Matsuhara, H. 1989, ApJ, 340, 729

Norman, C., & Scoville, N. 1988, ApJ, 322, 124

Osterbrock, D. E. 1989, Astrophysics of Gaseous Nebulae and Active Galactic Nuclei (Mill Valley, CA: University Science Books)

Prestwich, A. H., Joseph, R. D., & Wright, G. S. 1994, ApJ, 422, 73

Ridgway, S. E., Wynn-Williams, C. G., & Becklin, E. E. 1994, ApJ, 428,609

Rieke, G. H. 1988, ApJ, 331, L5

Rieke, G. H., Cutri, R. M., Black, J. H., Kailey, W. F., McAlary, C. W., Lebofsky, M. J., & Elston, R. 1985, ApJ, 290, 116

Rieke, G. H. & Lebofsky, M. J. 1985, ApJ, 288, 618

Rieke, G. H., Loken, K., Rieke, M. J., & Tamblyn, P. 1993, ApJ, 412, 99

Rieke, M. J., Rieke, G. H., Green, E. M., Montgomery, E. F., & Thomson, C. L. 1993, Proc. SPIE, 1946, 179

Rix, H.-W. 1993, PASP, 105, 999

Roche, P. F., Aitkin, D. K., Smith, C. H., & Ward, M. J. 1991, MNRAS, 248, 606

Rowan-Robinson, M. & Crawford, J. 1989, MNRAS, 238, 523

Sanders, D. B., Soifer, B. T., Elias, H. J., Madore, B. F., Matthews, K. Neugebauer, G., & Scoville, N. Z. 1988, ApJ, 325, 74

Sargent, A. I & Scoville, N. Z. 1991, ApJ, 366, L1

Sargent, A. I. & Welch, W. J. 1993, ARA&A, 31, 294

Sargent, W. L. W., Young, P. J., Boksenberg, A., Shortridge, K., Lynds, C. R., & Hartwick, F. D. A. 1978, ApJ, 221, 731

Scoville, N. Z. & Sanders, D. B. 1987, in Interstellar Processes, eds. D. Hollenbach & H. A. Thoronson (Dordrech:Reidel), 21

Scoville, N. Z, Sargent, A. I., Sanders, D. B., & Soifer, B. T. 1991, ApJ, 366, L5

Soifer, B. T., Sanders, D. B., Madore, B. F., Neugebauer, G., Danielson, G. E., Elias, J. H., Lonsdale, C. J., & Rice, W. L. 1987, ApJ, 320, 238

Thronson, H. A., Jr., Majewski, S., Descartes, L., Hereld, M., 1990, ApJ, 364, 456

Toomre, A. & Toomre, J. 1972, ApJ, 178, 623

Tonry, J. & Davis, M. 1979, AJ, 84, 1511

Tremaine, S., Richstone, D. O., Byun, Y.-I., Dressler, A., Faber, S. M., Grillmair, C., Kormendy, J., & Lauer, T. R. 1994, AJ, 107, 634

Vacca, W. D., & Conti, P. S. 1992, ApJ, 401, 543

Veilleux, S., Kim, D.-C., Sanders, D. B., Mazzerella, J. M., Soifer, B. T. 1995, ApJS preprint

Veilleux, S. & Osterbrock, D. E. 1987, ApJS, 63, 295

Williams, D., Thompson, C. L., Rieke, G. H., & Montgomery, E. F. 1993, Proc. SPIE, 308, 482

Wright, R. S., James, P. A., Joseph, R. D., & McLean, I. S. 1990, Nature, 344, 417

Wynn-Williams, C. G. & Becklin, E. E. 1993, ApJ, 412, 535

Wynn-Willams, C. G., Eales, S. A., Becklin, E. E., Hodapp, K.-W., Joseph, R. D., McLean, I. S., Simons, D. A., & Wright, G. S. 1991, ApJ, 377, 426

Young, J. S., & Scoville, N. Z. 1991, ARA&A, 29, 581

Zenner, S. & Lenzen, R. 1993, A&AS, 101, 363

Zhou, S., Wynn-Williams, C. G., & Sanders, D. B. 1993, ApJ, 409, 149

This manuscript was prepared with the AAS LaTeX macros v3.0.